

**THE UNIVERSITY OF NOTTINGHAM
DEPARTMENT OF ELECTRICAL AND
ELECTRONIC ENGINEERING**

**Modeling and Optimization of Microwave Ring
Resonator filters using CST software**

by Zhongdao Zhu, BEng.

Supervised by Dr. Ana Vukovic

**Thesis submitted to University of Nottingham for the degree of
Master of Science (by Research) in Electromagnetic Design**

September 2013

Abstract

The thesis reports on modeling two types of bandpass microwave filters that use dielectric resonator for filtering of the signal. The instance modeling is done using a commercial CST software package. The thesis introduces the CST software package and outlines the approach of modeling of two filters. Then tested CST meshing properties and simulation results. The first model is a dielectric ring loaded on substrate excited by microstrip lines. The second model has two dielectric rings loaded in a metal box which is filled with foam.

The impact of different mesh sizes is investigated on the convergence of S-parameters, in particular their characteristics at centre frequency. Many simulations have been done to find out the relationship between physical parameters, such as the radius of the outer ring, and the S-parameters. The CST software is also used to optimize characteristics of filters by changing the critical parameters. The patterns of e-field and h-field are been compared and analyzed to modify the structure of the dielectric ring resonator filter. The newly developed CST's Perfect Boundary Approximation (PBA) and FPBA solver is tested to prove their quality. Based on simulation data, a guess is proposed to revise the simulation result to get better accuracy.

Acknowledge

The author wishes to thank Dr Ana Vukovic for her guidance throughout last year in all aspects especially in this study project, and also Dr Steve Greedy, for his help on installing CST software and other arrangement.

Dr Ana's encouragement and guidance changed my negative attitude. I was confusing about many things, so I just hoped to finish work assigned to me as soon as possible. Dr Ana showed me an elegant way to live and think. To me, the most important value of this thesis is that Dr Ana trained me to be more than myself, this experience is a lifelong treasure. I enjoyed the process of writing this thesis.

List of figures

Fig. 1.1 TE ₁₀ surface currents distribution of the rectangular waveguide with slots on the narrow walls.	4
Fig. 1.2 Fundamental mode fields for three dielectric-resonator configurations. 7	
Fig. 1.3 Unit cell of the dielectric SRR [12].	8
Fig. 1.4 Structure of the DSR.	8
Fig. 1.5 Top view of the microstripline coupled rectangular aluminium cavity.	9
Fig. 1.6 (A) E-field pattern of the microstripline fed dielectric ring resonator mounted inside the aluminium cavity. (B) H-field pattern distribution showing the high intensity at the input feed and low intensity at the output microstrip line (Simulated using AnsoftHFSS).	10
Fig. 1.7 The simulated return loss and transmission characteristics using FEM method [14].	10
Fig. 1.8 shows the measured return loss (S ₁₁) and transmission characteristics (S ₁₂) of the band pass filter [14].	11
Fig. 1.9 Configuration of a band-pass filter employing dielectric ring resonators.	12
Fig. 1.10 Measured response of the band-pass filter, (a) transmission and return loss; (b) spurious modes performance [15].	12
Fig. 2. 1 Overviews of structured and Unstructured grid.	14
Fig. 2. 2 A Delaunay triangulation in the plane with circumcircles shown	15
Fig. 2. 3 Advancing-front approaches mesh generation.	16
Fig. 3. 1 Grid approximations of rounded boundaries:	19
Fig. 4. 1 section drawn for 2.4GHz band pass filter simulation model version1. 21	
Fig. 4. 2 coaxial cable part of version 1 model	23

Fig. 4. 3 the section drawn for 2.4GHz version2, with extended shielding part..	23
Fig. 4. 4 the coaxial cable and the linkage of the port and micro strip of version3	24
Fig. 4. 5 different combinations of different parameters for meshing properties.	26
Fig. 4. 6 S11 and S21 peak magnitude of different maximum frequency.....	27
Fig. 4. 7 Peak frequency of different frequency range.....	28
Fig. 4. 8 S11 and S21 magnitude for maximum frequency =10GHz	29
Fig. 4. 9 S11 and S21 magnitude for maximum frequency= 15GHz	29
Fig. 4. 10 S11 and S21 peak magnitude of different w	31
Fig. 4. 11 S11 and S21 peak frequency of different w	31
Fig. 4. 12 peak frequency of different w	32
Fig. 4. 13 S11 and S21 peak magnitude for different w	33
Fig. 4. 14 Simulation results for different lines per wavelength.	34
Fig. 4. 15 numerical value for 6GHz test.	35
Fig. 4. 16 numerical value for 10GHz test.	35
Fig. 4. 17 S11 and S21's peak magnitude and frequency of different ratio limit.	36
Fig. 4. 18 Mesh cells for different R. (a) mesh property is R=30, (b) R=20, (c) R=10	37
Fig. 4. 19 Mesh cells of different CST parameters. (a) is set as 30-30-30, (b) is set as 60-60-60 (c) is set as 10-10-20	38
Fig. 4. 20 S11 and S21 peak frequency and magnitude of different substrate thickness.	39
Fig. 4. 21 S11 and S21 magnitude of substrate thickness=4mm	40
Fig. 4. 22 S11 and S21 peak frequency and magnitude of different distance	41
Fig. 4. 23 S11 magnitude of different distance	41
Fig. 4. 24 S21 magnitude of different distance	42
Fig. 4. 25 Mesh cells of dis=0.01mm. The mesh boundaries around the gap are boldfaced.	42

Fig. 4. 26 S11 and S21 magnitude of dis=0.01mm.....	43
Fig. 4. 27 S11 magnitude of different microstrip thickness	43
Fig. 4. 28 S21 magnitude of different micro strip line	44
Fig. 4. 29 the z axis cutplane mesh view of 0mm thickness microstrip lines.	44
Fig. 4. 30 S11 and S21 magnitude of mt=0mm and mt=0.1mm.....	45
Fig. 4. 31 peak frequency and magnitude of different microstrip width.....	47
Fig. 4. 32 S11 and S21 magnitude of mwid=0.5 mm	47
Fig. 4. 33 Original shape optimization CST parameters set as 30-30-20	48
Fig. 4. 34 Change Subt to 2.5 to get the first peak as the pass band.....	49
Fig. 4. 35 peak frequency of different height.....	50
Fig. 4. 36 Peak magnitude of different height	50
Fig. 4. 37 S11 magnitude of different height.	51
Fig. 4. 38 S21 magnitude of different h.....	51
Fig. 4. 39 S11 and S21 magnitude of height=8.	52
Fig. 4. 40 S11 and S21 magnitude of outer radius =8.	53
Fig. 4. 41 S11 and S21 magnitude of outer radius =10	53
Fig. 4. 42 Peak frequency and magnitude of different outer radius.....	54
Fig. 4. 43 s11 magnitude of different outer radius	54
Fig. 4. 44 s21 magnitude of different outer radius	55
Fig. 4. 45 Peak magnitude and frequency of different inner radius	56
Fig. 4. 46 S11 magnitude of different inner radius	56
Fig. 4. 47 S21 magnitude of different inner radius	57
Fig. 4. 48 S11 and S21 magnitude against frequency.	58
Fig. 4. 49 optimized model.....	58
Fig. 4. 50 S-parameters of changed model	59
Fig. 4. 51 S-parameters for one ring loaded on substrate ($\epsilon=41$) without a dielectric cylinder inside the ring.....	60
Fig. 4. 52 (a) the H-field of the changed model at $f=2.6\text{GHz}$ plotted in dB. (b) the H-field of the one ring model at its first peak $f=3.3\text{GHz}$	60

Fig. 4. 53 (a) the e-field of the changed model at $f=2.6\text{GHz}$ plotted in dB. (b) the e-field of the one ring model at its first peak $f=3.3\text{GHz}$.	61
Fig. 5. 1 Section drawn for dielectric ring resonators loaded in waveguide.	62
Fig. 5. 2 S11 and S21 peak magnitude for different lines per wavelength	62
Fig. 5. 3 peak frequency for different lines per wavelength	63
Fig. 5. 4 S11 magnitude of different port length	65
Fig. 5. 5 S21 magnitude of different port length	65
Fig. 5. 6 S11 magnitude of different cable length	66
Fig. 5. 7 S21 magnitude of different cable length	66
Fig. 5. 8 S11 and S21 magnitude	67
Fig. 5. 9 S11 and S21 magnitude for different cable length	68
Fig. 5. 10 Cross-section draw of the optimized model.	69
Fig. 5. 11 S11 magnitude for short length and normal length of the cable	69
Fig. 5. 12 S11 magnitude for short length and normal length of the cable	70
Fig. 5. 13 (a) e-field ($f=4.58\text{GHz}$) of extended model. (b) h-field ($f=4.58\text{GHz}$) of extended model. (c) e-field ($f=4.1\text{GHz}$) of shorter model (d) h-field ($f=4.1\text{GHz}$) of shorter model.	70
Fig. 5. 14 S11 and S21's magnitude of shorter model with different cable length	71
Fig. 5. 15 S11 and S21 magnitude of different length of l1.	71
Fig. 6. 1 Accumulated S11 and direct S11 magnitude.	72
Fig. 6. 2 Accumulated S11 and S21 magnitude.	73
Fig. 6. 3 Direct S11 and S21 magnitude	73
Fig. 6. 4 Accumulated result of two rings model	74
Fig. 6. 5 Direct result of two rings model	74
Fig. 6. 6 PBA S-parameters with CST parameters set as 15-15-10.	75
Fig. 6. 7 (a) h-field $f=2.646\text{GHz}$ using FPBA (b) h-field $f=2.646\text{GHz}$ using PBA	76

List of Tables

Table 4. 1 peak value and frequency of different versions	24
Table 4. 2 Peak frequency and magnitude of coaxial cable with different radius of the inner conductor.	25
Table 4. 3 Peak frequency and magnitude of coaxial cable with different radius of the shielding part.....	25
Table 4. 4 simulation results of different frequency with same mesh cell number	30
Table 4. 5 Simulation results of maximum frequency set to 10GHz.....	34
Table 4. 6 Different thickness and material of the microstrip lines.....	46
Table 5. 1 Lower mesh limit simulation result	63
Table 5. 2 Mesh line ratio limit simulation result	64
Table 5. 3 Different port length simulation result.....	65
Table 5. 4 S11 and S21 peak frequency and magnitude of different length of cable.....	66
Table 6. 1 Comparisons of FPBA and PBA	75

Contents

Abstract.....	i
Acknowledge.....	ii
List of figures.....	iii
List of Tables.....	vii
Chapter 1 Introduction.....	2
1.1 Previous study of microwave filters.....	2
1.2 Dielectric ring resonators.....	5
Chapter 2 Different types of meshing.....	13
2.1 Cartesian grids.....	13
2.3 Triangle meshes.....	15
Chapter 3 Simulation software packages.....	16
3.1 Simulation software and meshing properties.....	16
3.2 CST meshing property.....	18
Chapter 4 Dielectric ring resonator band pass filter for 2.4GHz.....	20
4.1 CST model parameters.....	20
4.3 Mesh properties accuracy test.....	27
4.4 Parameters of the dielectric ring test.....	39
4.5 Plausible optimization.....	48
Chapter 5 Dielectric Ring Resonators Loaded in waveguide.....	61
5.1 Mesh properties accuracy test.....	62
5.2 physical parameters test.....	64
5.3 Optimization.....	67
Chapter 6 Conclusions.....	72
6.1 Errors caused by maximum frequency.....	72
6.2 PBA and FPBA test.....	75
6.3 A guess for algorithm refinement.....	76
Bibliography.....	77

Chapter 1 Introduction

This chapter introduces previous studies and theories about microwave filters and dielectric resonators.

1.1 Previous study of microwave filters

This section will discuss studies about microwave filters and their major properties and theories. Filters are the most fundamental of signal processing circuits using energy storage elements such as capacitors, inductors, and transmission lines to obtain frequency-dependent characteristics. Microwave filter is widely used in high-frequency wireless communication systems. At radio frequency, a filter can consist solely of lumped elements, solely of distributed elements, or comprise a mix of lumped and distributed elements. The distributed realizations can be transmission line-based implementations of the components of lumped-element filter prototypes or, make use of particular frequency characteristics found with certain distributed structures. For example, coupled lines have particular frequency selective characteristics that can be exploited. Loss in lumped elements, particularly above a few gigahertz, means that the performance of distributed filters nearly always exceeds that of lumped-element filters. However, since the basic component of a distributed filter is a one-quarter wavelength long transmission line, distributed filters can be prohibitively large at a few gigahertz and lower in frequency [1].

For the requirements of smaller, higher performance and lower cost, the filter design encountered many challenges, and then derived from that, there are many different kinds of microwave filters. In communication, radar and data storage systems, filter is always one of the most important parts. It is vital to improve the quality of signal in wireless communication as in recent years, the electromagnetic environment has become very complicated and the frequency spectrum becomes much more crowded. During the past 50 years, wireless communication expanded to high frequency and microwave frequency, that makes filter's structure changed from

lumped element resonator to distributed component resonator, such as coaxial resonator, micro strip resonator and waveguide resonator.

The classic chebyshev filter theory is well developed, the general chebyshev filter theory concerns about finite transmission zero. Especially in band pass, band reject, multimode, multi pass filter [2]. The presence of the transmission zero can be explained as a critical frequencies where signal transmission between input and output is stopped. Filters uses the transmission zero frequencies together with the passband edge frequencies and passband ripple to form the transfer function between the input and output, and for shaping the response of the filter. Transmission zeros must always be placed in the stopband(s) of a filter.

The passive (LC) filters work quit well at frequency up to a few hundred megahertz [3]. Beyond this range, components deviate significantly from anything close to ideal. Parasitics start to dominate, and components values become impractical, while capacitors become inductors and vice versa. Distances between components turn important, and traces on a PC board introduce unwanted capacitance and inductance. The methodology concerns using PC board traces to create transmission lines by controlling their properties, and then configuring these transmission lines into an architecture resulting in filters. The resulting filters are then based on distributed parameters rather than lumped inductors and capacitors. At submicrowave frequencies (1-300MHz), this approach is not feasible since the dimensions based on fractions of a wavelength become impractical.

For low-power applications, stripline and microstrip filters are extensively used because of their low cost and repeatability. A microstrip transmission line consists of a strip conductor and a ground plane separated by a dielectric medium [4]. The dielectric material serves as a structural substrate upon which the thin-film metal conductors are deposited. Conductors are usually gold or copper. In our case, the metal conductors will actually be the copper tape. For high-power requirements, waveguide structures are utilized. Rectangular Waveguide become the dominant waveguide structure largely because high-quality components could be designed

using it. One of the main issues was its narrow bandwidth due to the cut-off frequency characteristic. Ridge Waveguide offered a step in that direction, having one or more longitudinal internal ridges that serve primarily to increase transmission bandwidth by lowering the cut-off frequency. Coaxial Line was very suitable, since it possessed a dominant mode with zero cut-off frequency, providing two important characteristics: very wide bandwidth, and the capability of miniaturization. The lack of a longitudinal component of field, made it more difficult to create components using it [5].

Meanwhile, with the development of material science, the structure of filters has changed a lot. From 1970s and 80s, with the tremendous development of ceramic which has high Q and temperature stability, dielectric ring has been widely used in radio frequency communication and microwave communication.

In recent years, some new technology and new materials also accelerated the development speed of filter, which includes: high temperature superconducting, low temperature co-fired ceramic, monolithic microwave integrated circuit, micro electro mechanical system, and micro machining technology. The structure of filters also extended from traditional circular polarized wave into substrate integrated waveguide [6].

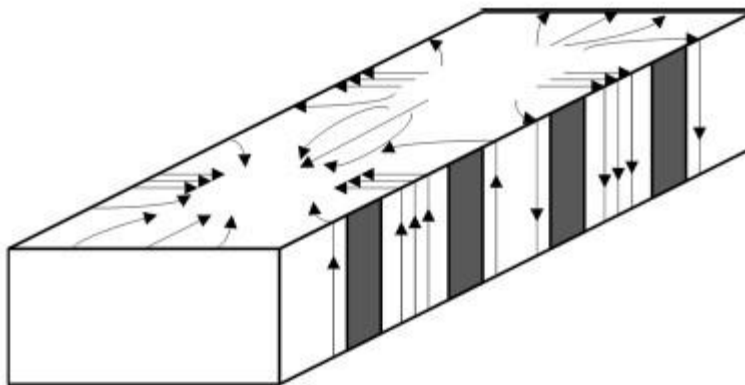


Fig. 1.1 TE_{10} surface currents distribution of the rectangular waveguide with slots on the narrow walls.

The SIW structures have similar properties as the conventional rectangular

waveguides as is shown in Fig. 1.1, the differences between them are also obvious. First, the SIW is a sort of periodic (or discrete) guided-wave structures, and it may lead to an electromagnetic bandstop phenomenon. Second, the SIW structures are subject to a potential leakage problem due to the periodic gaps. Therefore, the modes or waves traveling in the SIW circuits are different from those in the normal waveguides and there exists a certain type of leakage wave [6].

In microwave applications two types of resonators are available, namely cavity metal resonators (which can be circular or rectangular cross section) and dielectric resonator. A cavity resonator stores energy in the electric and magnetic fields for any particular mode pattern. In practical cavity the walls have a finite conductivity (a nonzero surface resistance), and the resulting power loss causes a decay of the stored energy. For the resonant cavity to operate efficiently the loss needs to be small. The measure of stored energy is given by a quality factor, Q . Q factor is a dimensionless parameter that describes how under-damped an oscillator or resonator is [8], or equivalently, characterizes a resonator's bandwidth relative to its center frequency [9]. Higher Q indicates a lower rate of energy loss relative to the stored energy of the resonator; the oscillations die out more slowly. A pendulum suspended from a high-quality bearing, oscillating in air, has a high Q , while a pendulum immersed in oil has a low one. Resonators with high quality factors have low damping so that they ring longer.

1.2 Dielectric ring resonators

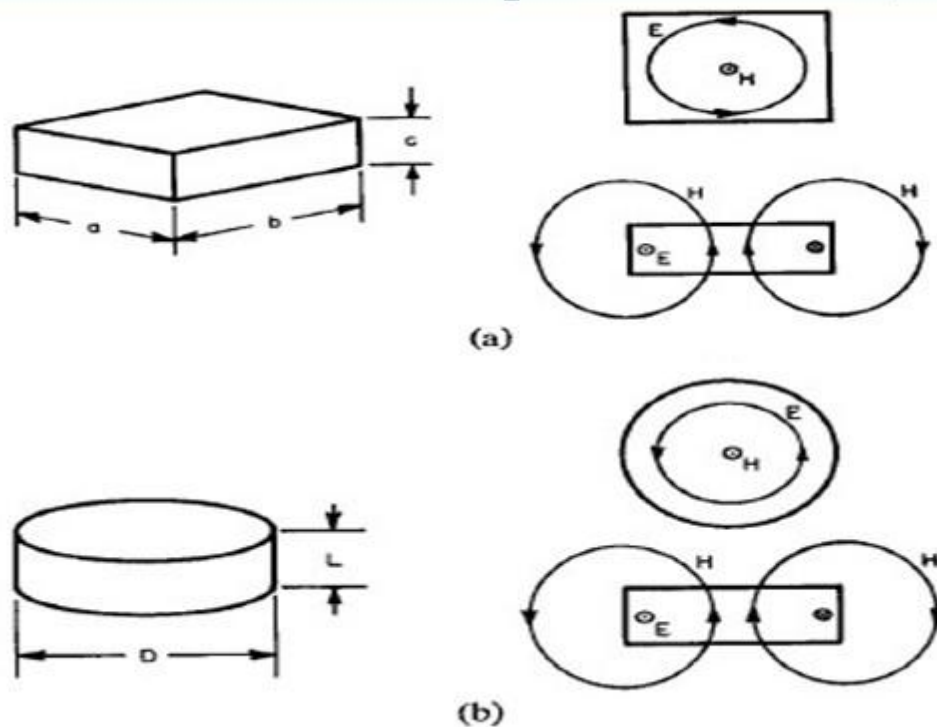
This section introduces properties of dielectric resonators and their advantages. A dielectric material is a more or less insulating material, A dielectric material is a substance that is a poor conductor of electricity, but an efficient supporter of electrostatic field. It has high resistivity and a band gap of a few eV, that is polarizable, in which electrostatic dipoles exist or form under the influence of an electric field. If the flow of current between opposite electric charge poles is kept to a minimum while the electrostatic lines of flux are not impeded or interrupted, an electrostatic

field can store energy. This property is useful in capacitors, especially at radio frequencies. Dielectric materials are also used in the construction of radio-frequency transmission lines. Dielectric material is characterized with a dielectric constant ϵ which is by definition

$$(1)$$

where ϵ_0 is the dielectric constant of the vacuum [$\epsilon_0 = 8.854\ 187\ 817\dots \times 10^{-12}$ farads per meter (F·m⁻¹)] and ϵ_r is the relative dielectric constant.

In 1968, Cohn proposed the theory to use the dielectric resonator to build band pass microwave filters and calculated the coefficient of a cylinder dielectric resonator and its dominant TE₀₁₀ mode [7]. These filters have a significant advantage that they can change the coupling coefficient by adjusting the distance between dielectric resonator and micro strip lines without changing the distance between the resonators. So it is much easier to design and adjust the filter.



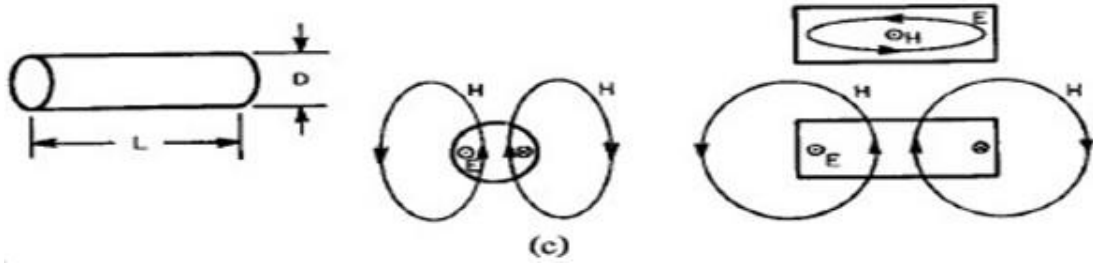


Fig. 1.2 Fundamental mode fields for three dielectric-resonator configurations.

(a) Rectangular resonator, a and $b > c$. (b) Cylindrical resonator, $L < D$. This case is preferable for most filter applications. (c) Cylindrical resonator, $L > D$ [7].

Fig. 1.2 is referenced from cohn's paper, which is mentioned above. There are three convenient shapes for a dielectric resonator as are shown in Fig. 1_1. The most practical is usually a cylindrical disk whose length L is less than its diameter D . With this shape the lowest-frequency resonant mode has a circular electric-field distribution, as shown in Fig.1_1 (b). The magnetic field is strongest on the axis of the disk and at a sufficient distance outside the disk the field resembles that of an axial magnetic dipole. For L greater than D [Fig. 1_1 (c)], the fundamental mode has an equivalent magnetic dipole moment transverse to the axis [7].

There are several new type dielectric ring resonators, since they are not used in this paper, only brief introductions are presented

SRRs are subwavelength magnetic resonant structures built from nonmagnetic conducting sheets [10]. They provide negative permeability in the vicinity of the resonance frequency and their applications in filters using waveguides have been demonstrated. In order to realize more compact devices, printed-circuit technology is used in SRR design [11]. SSR consist of a pair of concentric metallic rings etched on a dielectric substrate, with slits etched on opposite sides. The shapes of dielectric SRRs are removed from the metal ground plane via a milling process using an LPKF machine, leaving only dielectric in the shape of the SRRs. The fact that the SRRs are made of dielectric instead of a conducting metal helps to ensure a better coupling with the electric field coming from the conducting strip. Dielectric SSR has an

advantage of easy fabrication and the device is very compact [12]. Fig. 1.3 is the shape of the dielectric SSR.

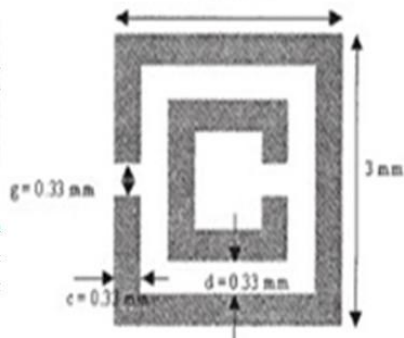


Fig. 1.3 Unit cell of the dielectric SRR [12].

Fig. 1.4 shows the structure of the newly developed dielectric split ring (DSR). It is composed of ring-shaped ceramics with metalized film and tuning capacitor which connects to both ends of a resonator conductor [12].

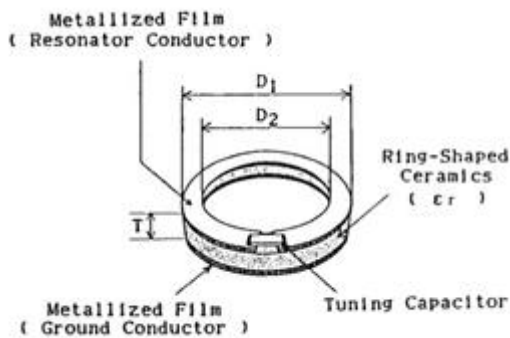


Fig.1.4 Structure of the DSR

The dominant resonance mode is TEM. The resonance frequency can be calculated from the electric parameters of the resonator, such as the resonator length, characteristic impedance and tuning capacitance, the same as for the microstrip-line split-ring resonator [13].

1.3.1 Dielectric ring resonator band pass filter for 2.4GHz

In this section all data are referenced from the original paper [14].

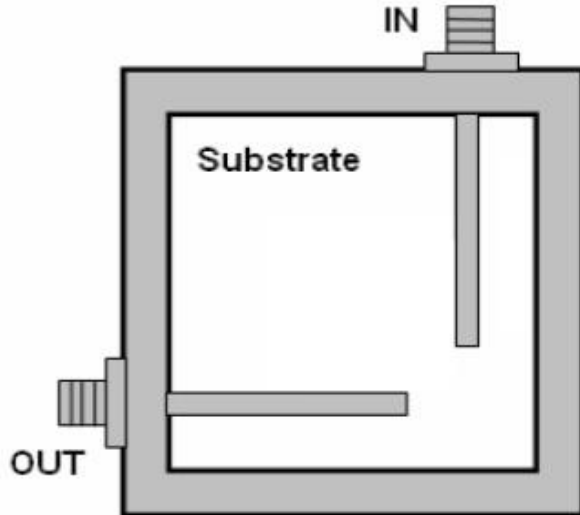


Fig. 1.5 Top view of the microstripline coupled rectangular aluminium cavity.

The ring resonator is excited by an input coupling coaxial probe which couples to a microstripline of dimensions 3 mm x 60 mm and has impedance of 50 ohms. The filtered signal is extracted by an out-put coupling microstrip line (3mm x 60mm) which is designed perpendicular to the input microstripline as shown in Fig. 1.5. The whole system is enclosed within a rectangular aluminum box of dimensions 82 mm, 82 mm, 25 mm. The dimensions of the dielectric ring resonator are as follows: height 10 mm, outer diameter 20 mm and inner diameter of 12.5 mm, with a relative dielectric constant $\epsilon_r = 69$. The resonant frequency of the ring resonator is determined by height, outer and inner diameters, and dielectric constant of the material. The E-field and H-field patterns are computed and optimized using Ansoft HFSS software and are shown in Fig.1.6 (A,B). The filter is modeled using the FEM method and the return loss (S11) and transmission characteristics (S21) are shown in Fig.1.7. Fig.1.7 is clearly wrong as S11 and S21 are not aligned at the centre frequency.

The S-parameters are also measured with Agilent 8714 ET network analyzer and are shown in 1.7 [14]. Fig.1.8 shows that the filter exhibits a large loss at the centre frequency.

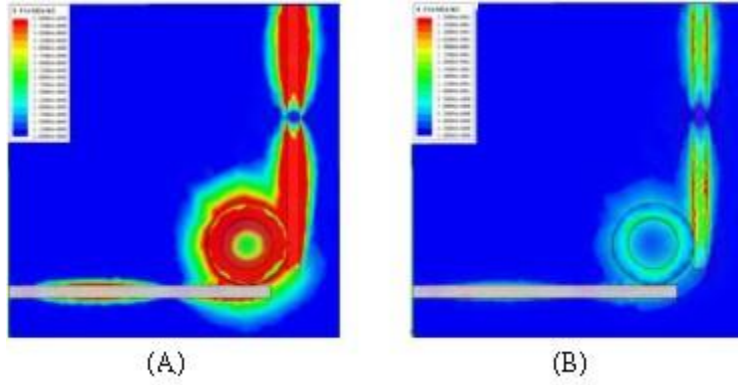


Fig. 1.6 (A) E-field pattern of the microstripline fed dielectric ring resonator mounted inside the aluminium cavity. (B) H-field pattern distribution showing the high intensity at the input feed and low intensity at the output microstrip line (Simulated using AnsoftHFSS).

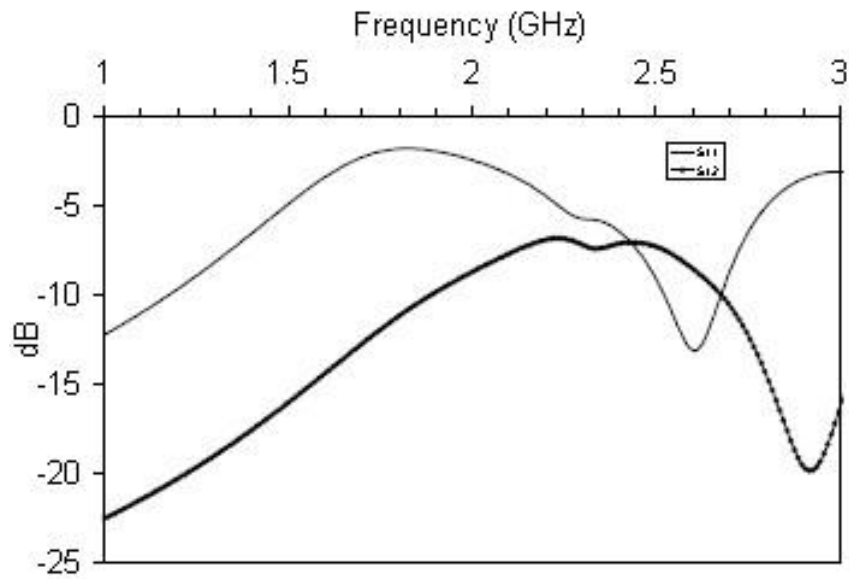


Fig. 1.7 The simulated return loss and transmission characteristics using FEM method [14].

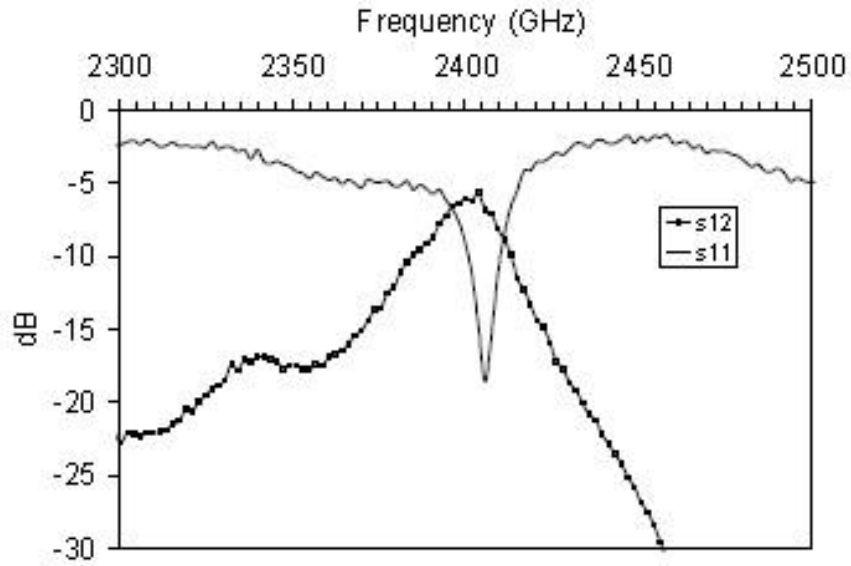


Fig. 1.8 shows the measured return loss (S11) and transmission characteristics (S12) of the band pass filter [14].

1.3.2 Dielectric Ring Resonators Loaded in waveguide

This section overviews another example of microwave filter that uses dielectric resonator which is originally given in [15].

The schematic of the bandpass filter that uses two coupled cavities with dielectric rings is given in Fig.1.9, dimensions are: $2a = 0.25$ in, $2b = 0.8$ in, $2c = 1.2$ in, $2d = 0.8$ in, $l_1 = 0.71$ in, $l_2 = 0.28$ in, $l_3 = 0.29$ in, $l_t = 0.18$ in, and dielectric constant of the ring is 36.

Chapter 2 Different types of meshing

A variety of modeling techniques are used for modeling of microwave filters such as [16-20]. The main difference between them is how they solve Maxwell's equations and the type of meshing they use to discretize the object. In terms of meshing there are two types of meshes – cubical meshes that are aligned to the Cartesian grid and unstructured meshes (triangular meshes for two-dimensional structures and tetrahedral meshes for three-dimensional structures).

This chapter will discuss modeling methods that use different meshing strategies.

2.1 Cartesian grids

This section overviews methods based on Cartesian grids which is the simplest meshing method and is widely used.

Computation electromagnetic field in time domain usually mainly uses mainly two modeling approaches namely: Finite Difference and Finite Volume method. Yee [18] introduced Finite Difference Time Domain (FDTD) method in which a second-order central difference scheme is used to discretize the Maxwell equations in time and space. Since it is a time-domain method, FDTD solutions can cover a wide frequency range with a single simulation run.

Holland and Kunz & Lee [19-20] applied Yee's algorithm to electromagnetic environment to solve problems. Holland introduced finite difference scheme for non-orthogonal curvilinear coordinates. Because Maxwell equations have the same mathematic characteristic as Euler equations in hydromechanics, Taflov and Umashankar [21-22] began to use finite volume method of computational fluid dynamics in solving problems about electromagnetic scattering and radiation. They developed the first FDTD electromagnetic wave scattering models computing sinusoidal steady-state near-fields, far-fields, and radar cross-section for two- and

three-dimensional structures. Zheng, Chen, and Zhang [23-24] introduced the first three-dimensional alternating-direction implicit FDTD algorithm with provable unconditional numerical stability. They use a finite volume time domain method based on unstructured Cartesian grids to solve the scattering problem of Computational electromagnetics, with second order time and special accuracy.

Most software uses FDM, because of its meshing simplicity that relies on cubes. There are mainly two kinds of Cartesian grids as are shown in Fig. 2.1: 1. Structured Cartesian grids, which use rectangular grids in 2D or rectangular hexahedron in 3D to mesh the object. The 2D cartesian grids consist of cells aligned with a rectilinear coordinate system. Each cell center or grid node can have a unique elevation. The grid can also be rotated about the Z axis if desired. 2. Unstructured Cartesian grids, unlike structured grid, it do not have definite data structure. Its elements are usually triangular or tetrahedral that gives a lot of flexibility in mesh generation. Unstructured solvers are more expensive than structured solvers and getting high order of accuracy is more difficult [25].

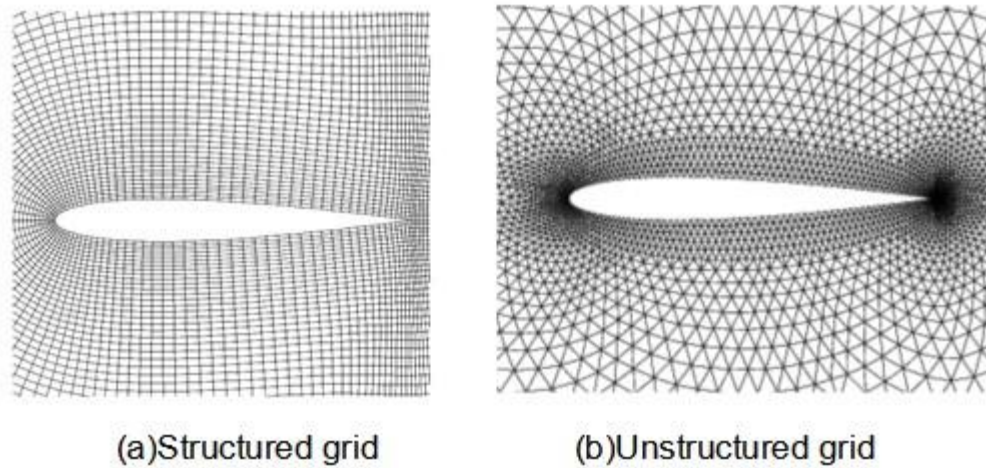


Fig. 2. 1 Overviews of structured and Unstructured grid.

There are two kinds of methods to generate boundary grids. The first is the CutCell Cartesian grids that using different geometric figures to simulate the real boundary, it could have several different figures combined together and has complex topology [26]. The second approach is adaptive viscous Cartesian grid, with three

different approaches namely, immersed boundary, embedded boundary and projection boundary [27-29].

2.3 Triangle meshes

This section introduce a brief information on triangle meshes that are typically used to model two-dimensional objects. Automatic mesh generation for finite element analysis of electromagnetic field has been widely researched and has been developing to maturity in many areas. The most popular mesh generation methods are Delaunay based methods [30] and advancing front technique[31] for generation of two dimensional unstructured grids of high quality.

Delaunay triangulations maximize the minimum angle of all the angles of the triangles in the triangulation; they tend to avoid skinny triangles as is shown in Fig 2.2.

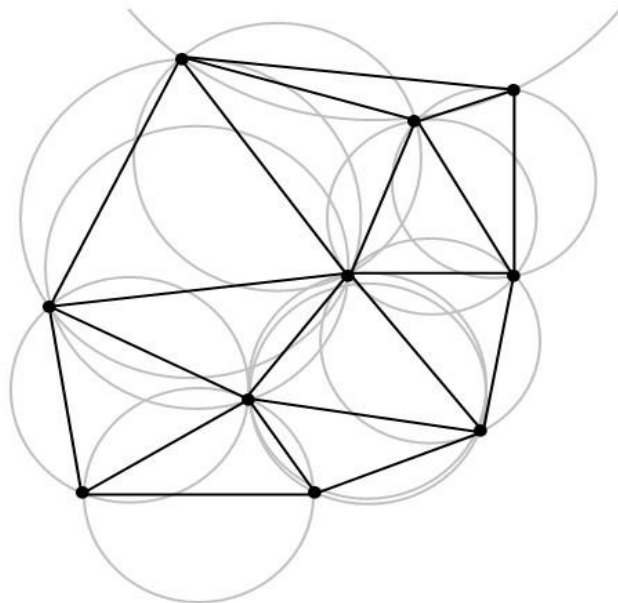


Fig. 2. 2 A Delaunay triangulation in the plane with circumcircles shown

Classical advancing-front approaches start from a discretization of the domain boundaries as a set of edges in two dimensions or a set of triangular faces in three dimensions. The name of this class of methods refers to a strategy that consists of creating the mesh sequentially, element by element, creating new points and

connecting them with previously created elements, thus marching into as yet unmeshed space and sweeping a front across the domain [31]. Depending on the strategy the front can have multiple components as is shown in Fig. 2.3.

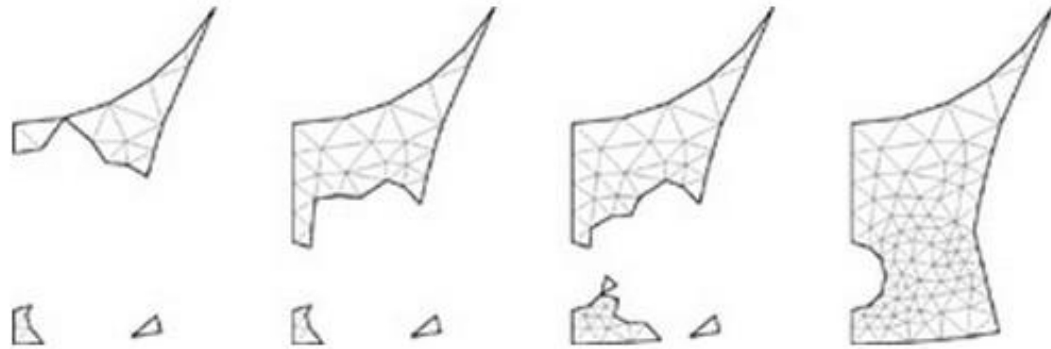


Fig. 2. 3 Advancing-front approaches mesh generation.

Finite difference method using unstructured grids is used in meshing resonators, which is designed originally for finite element calculations. Unstructured grids can be easily adapted to complicated problem geometries. Results show considerable advantages over the standard FD method, when applied to a problem not conforming to a rectangular grid. The methodology can easily be adopted to a regular FD algorithm having unstructured mesh only locally [32].

Chapter 3 Simulation software packages

This chapter discuss differences between different commercial software packages which are widely used by engineers nowadays. Which include AWR Microwave office, WIPL-D Microwave, ANSYSY, CST. As CST software is used in this thesis the major parameters that affect its accuracy are explained.

3.1 Simulation software and meshing properties

In this section four commercial softwares namely AWR,WIPL-D, ANSYS and CST are compared in terms of their characteristics about modeling types of solvers and special algorithm.

AWR Microwave Office (MWO) is very comprehensive software for designers of

all types of RF and microwave circuits, from integrated microwave assemblies to MMICs[33]. MWO use Automatic Circuit Extraction (ACE™) which using layout-based models for circuit extraction, ACE dramatically reduces the time required to initially model complex interconnects by automatically identifying transmission lines from the layout and partitioning them into existing models. APLAC RF harmonic balance for large-scale and highly nonlinear design, its solvers include transient-assisted harmonic balance, multi rate harmonic balance, and transient time-domain. MWO has a task-specific tools for lumped and distributed filter synthesis (iFilter™), thermal management (CapeSym SYMMIC), and antenna design (Antenna Magus) [34].

WIPL-D Microwave software package serves as a fast and accurate design and simulation tool for projects involving microwave circuits, components, and antennas. Seamlessly integrated with WIPL-D Pro 3D EM solver and WIPL-D Optimizer, it enables easy inclusion of 3D models into the circuit as well as their optimization from within the circuit. The current version is v2.3. WIPL-D Microwave add-ons, Filter Designer and Array Designer, allow automatic synthesis of microwave filters and antenna arrays. It is also possible to simulate and optimize various antennas by combining the circuit and 3D-EM solver, such as: Microstrip antennas embedded in finite lossy dielectric/magnetic materials; Horn-type feeds for reflector antennas; Phased arrays along with their matching circuitry, and Handset antenna in the vicinity of human head [35].

ANSYS offers a comprehensive software suite that spans the entire range of physics, providing access to virtually any field of engineering simulation that a design process requires. Organizations around the world trust ANSYS to deliver the best value for their engineering simulation software investment [36]. The ANSYS suit includes capabilities for:

1. Modeling, analysis, simulation and design optimization of antennas, radar cross section (RCS), filters, diplexers, power amplifiers, RF packaging and microwave circuits
2. Harmonic balance, circuit envelope, transient, and Agilent's X-Parameter

simulation with direct integration with 3-D EM simulators (including FEM, method of moments, integral equation, and transient solvers.

3. Thermal and stress analysis based on electrical performance by linking to other products in the ANSYS multiphysics suite [36].

CST offers a wide range of EM simulation software to address design challenges across the electromagnetic spectrum, from static and low frequency to microwave and RF, for a range of applications, including EDA & electronics, EMC & EMI and charged particle dynamics. CST MWS enables the fast and accurate analysis of high frequency (HF) devices such as antennas, filters, couplers, planar and multi-layer structures and SI and EMC effects [37].

CST software package is one of the most widely used Electromagnetic simulation software, it streamlines the difficult and complex simulation process without compromising on its power and flexibility. It has a friendly user -interface, a range of powerful tools and features, it's up to date solver technology has been optimized for many years, definitely suitable for complex systems, can simulate object with faster speed and higher accuracy than former generations.

CST microwave studio possess many solvers: Transient solver, TLM solver, Frequency domain solver, Eigenmode solver, Resonant solver, Integral Equation solver and Asymptotic solver [38]. In addition to its time domain solver featuring the Perfect Boundary Approximation (PBA)[®], modules based on methods including FEM, MoM, MLFMM and SBR are available each offering distinct advantages in their own domains.

3.2 CST meshing property

Perfect Boundary Approximation is a newly developed theory. In CST software, the official guide book recommends time-domain solver using Finite PBA (FPBA) with enhanced accuracy. The differences between conventional boundaries and PBA is shown in Fig. 3.1.

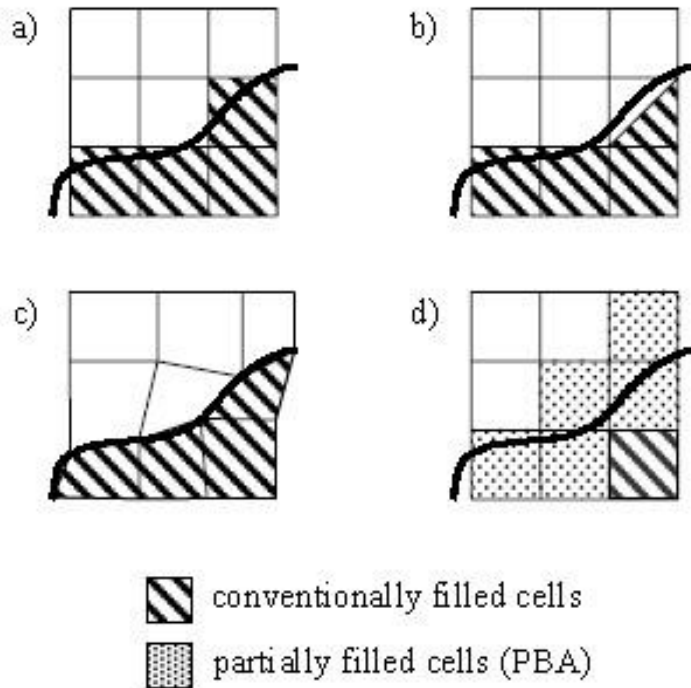


Fig. 3. 1 Grid approximations of rounded boundaries:

Standard (a), triangular (b), non-orthogonal (c), PBA (d)

Recent study shows that the Finite Integration Theory, combined with newly developed Perfect Boundary Approximation Technique, is able to model structures with very fine geometric details with high accuracy. The application especially of the PBA-technique to typical accelerator devices demonstrates the high efficiency of the method compared to conventional FD- or FE-approaches [39].

There are many parameters which are controlling the properties of meshing in CST software. Most of them are set as default for there is no need to adjust them. The CST MWS has 3 main parameters that define the mesh quality which are:

Line per wavelength: MWS takes the dielectric into account. 10 lines per wavelength means minimum of ten lines at the shortest wavelength inside a dielectric. It greatly change the number of mesh. The Lines per wavelength parameter describes the spatial sampling rate of the field. A Lines per wavelength setting of 10 means that a plane wave propagating along one of the coordinate axes is sampled at least 10 times. The reduction of the wavelength when propagating

through dielectric materials is taken into account here. And the wavelength is also determined by maximum simulation frequency. Line per wavelength parameter is suitable for Electrically Large structures.

Lower mesh limit : This setting allows you to define the maximum mesh step to be used for the mesh creation, regardless of the setting in Lines per wavelength. The maximum step width of the mesh is determined by dividing the smallest face diagonal of the bounding box of the calculation domain by this number. It can be understood as the smallest number of mesh cells on the shortest diagonal of the model. The number of total mesh cells increase with this value, but slower than the first one. This parameter is suitable for Electrically Small structures, which means physical size is smaller than $1/10$ wavelength.

Mesh line ratio limit/smallest mesh step: It determines the ratio of the largest mesh step and the smallest mesh step, smallest mesh step' defines the limitation.

Chapter 4 Dielectric ring resonator band pass filter for 2.4GHz

This chapter tested a model which has one dielectric ring loaded on a substrate and two micro strips. I will firstly represent the original data, then list the parameters of my model. Some fixed parameters will be tested before the mesh test began. With all these parameters chosen, then I will test the three mesh property parameters. After finding out a suitable combination of mesh parameters, I will change some physical parameters which will change the test model to find their relationship with the S-parameter and peak frequency and peak magnitude. In the final part I will optimize these parameters to get a better model.

4.1 CST model parameters

In this section overviews some fixed parameters which are used in the CST

simulation models. All these parameters remain the same in following tests but they will be revisited in the optimization section. There are three versions of simulation model for the 2.4GHz band pass filter.

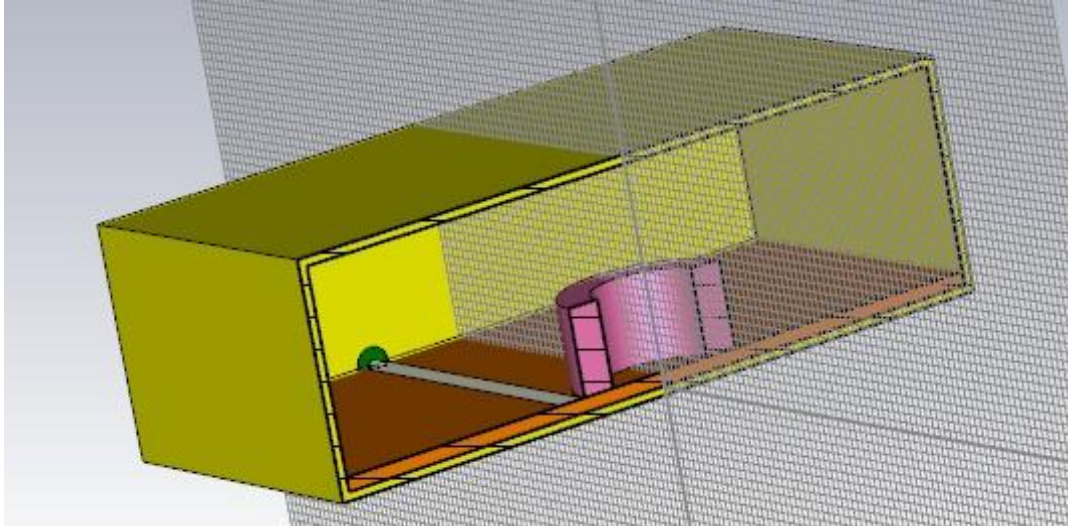


Fig. 4. 1 section drawn for 2.4GHz band pass filter simulation model version1.

All dimensions given in the paper [14] are obtaining in the model which is simulated in CST2013 based on the time-domain hexahedral, enhance Finite Perfect Boundary Approximation (FPBA) accuracy.

In the Special time domain solver (Time domain solver Parameters→specials→waveguide) parameters, the option line impedance adaptation before solver run is unchecked. Simulation is set so that normalization is set to fixed impedance of 50 ohms, accuracy is set to -30dB, source type is set to "all ports" and the mode is set to "All" S-parameter symmetries are also used.

The original paper omitted to specify several important parameters, which are:

The of substrate and coaxial cable which are defined as ϵ_{sub} and ϵ_{coax} .

The thickness of substrate which is defined as *subt*.

The length of the micro strip line exceeds the center point of the dielectric ring, the length of coaxial cable merged into the micro strip line. The merged part is set to 2mm, the length of the micro strip line is 45mm, so there is 7mm length of the microstrip line that exceeds the center point of the ring.

The gap between microstrip line and dielectric ring.

- Full specification of the coaxial cable dimensions and dielectric constant.

In this model all units are set as Dimensions=mm, Temperature= Kelvin, Frequency=GHz, Time=ns.

In defining the model the parameters are set as

The size of the metal box container is set to $box=82$

The distance between the micro strip and the dielectric ring is set to $dis=0.1$

of the dielectric ring is set to $ering=69$

of the substrate is set to $esub=4.5$

The height of the dielectric ring is set to $h=10$

id means inner diameter but CST use radius to define a cylinder, so the diameter is divided by 2 which is set to $id=12.5/2$

The real length of micro strip line, not including the length of port is set to $mle=45$

The thickness of the micro strip line, since its material is PEC, it does not need thickness is set to $mt=0$

The width of the micro strip line is set to $mwid=3$

In the original paper out diameter is 20, so its radius is 10, $od=10$

The thickness of substrate is set to $subt=1.6$

The width of the box is set to $w=25$, the outer length of the metal box in y direction and the outer length of the metal box in x and z direction equal to box which is set to 41mm. The thickness of the box is 1mm.

of the coaxial cable is set to 2.4.

Radius of the metal port is set to 0.3mm

Radius of the coaxial cable is set to 1.6mm

The material of the metal box is aluminum and all other metal are PEC.

There are three version of the 2.4GHz filter, the model was changed to get a better result and lower lose. The difference between them are:

Version1:

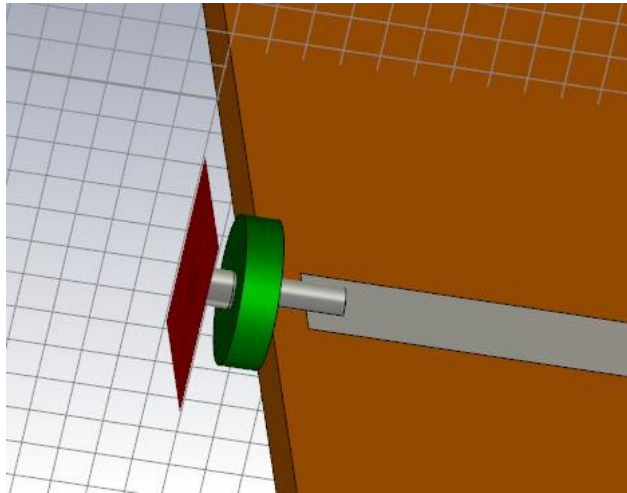


Fig. 4. 2 coaxial cable part of version 1 model

Fig.4.2 hided the metal box to get a clear inside view. Version1 have short shield part of the coaxial cable which is just the thickness of the metal box equals to 1mm as is shown in Fig.4.2. The green cylinder is the shielding part. The inner conductor of the port is merged into the substrate and micro strip line for its center is fixed to the thickness of the substrate.

Version2:

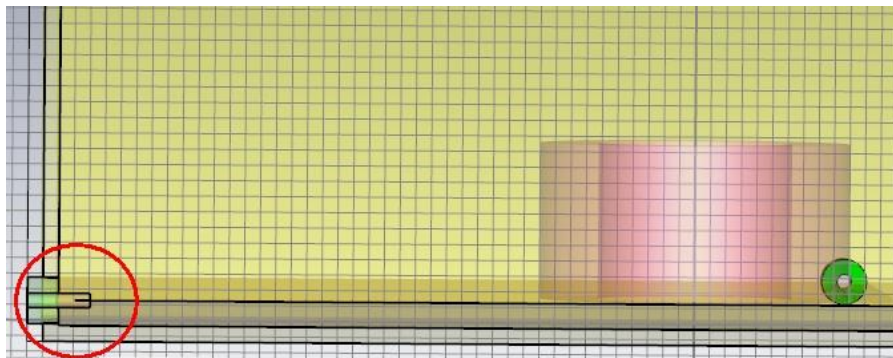


Fig. 4. 3 the section drawn for 2.4GHz version2, with extended shielding part.

The coaxial cable shielding part is extended to the same length of the metal port, and the port is still merged inside the substrate as shown in Fig. 4.3. The circle highlight the changed part.

Version3:

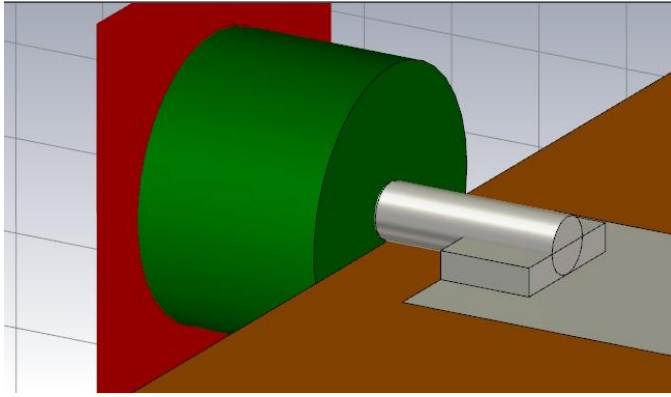


Fig. 4. 4 the coaxial cable and the linkage of the port and micro strip of version3

In version 3, the improvement including longer shielding part and the metal port is above the micro strip, and they are connected by a 2mm PEC cuboids, which make the micro strips have zero thickness and merged into the port possible. Version3 take longer solving time than first and second version. In version 3, the material of metal box is changed to PEC.

	V1	V2	V3
S11F	2.244	2.244	2.652
S11V	-6.54538	-6.76662	-9.13172
S21F	2.238	2.244	2.67
S21V	-5.59777	-5.45154	-4.28499

Table 4. 1 peak value and frequency of different versions

In table 4.1, S11F means the position of the first peak frequency of S11 in GHz, S11V means the peak magnitude for S11 in dB, and similarly for S21F and S21V. From table 4.1 it can be seen that version 1 and version 2 do not show significant differences. The peak frequency in version 3 becomes larger than version 1 and 2 but the loss in S21 becomes smaller. That means version 3 has better structure and it is more stable than version 1 and 2. All tests will be made using the Version3, but some important parameters will be tested in both Version 2 and Version3.

Because of the structure is too large that it take too long to run simulations, the

optimized parts will be tested in a smaller and similar environment. That will not only accelerate the speed but also enhance the simulation accuracy.

R_Pole	0.1	0.3	0.6
S11F	2.658	2.652	2.64
S11V	-8.10438	-9.13172	-11.6145
S21F	2.67	2.67	2.652
S21V	-4.6932	-4.28499	-2.81662

Table 4. 2 Peak frequency and magnitude of coaxial cable with different radius of the inner conductor.

R_cable	0.91	1	1.5	2	RG141A/U	RG141A/U+
S11F	2.652	2.652	2.652	2.652	2.64	2.64
S11V	-9.63505	-9.63746	-9.13172	-9.14782	-12.2073	-14.1061
S21F	2.67	2.664	2.67	2.664	2.64	2.64
S21V	-3.87104	-3.66716	-4.28499	-4.11866	-3.22337	-2.65207

Table 4. 3 Peak frequency and magnitude of coaxial cable with different radius of the shielding part.

The last two is tested with real stander coaxial cable parameters, they have better performance than 0.3mm model. The radius of metal indeed affect the simulation result, there is a tendency that the larger the radium is the less loss for S21would be. The larger pole also reduce the peak frequency. It seems that the size of the dielectric part does not affect the outcome since the magnitude and frequency do not change with the radius. In all tests radius of the metal pole remained 0.3mm and the radius of the cable is 1.6mm, which is the standard size for RG-179B/U coaxial cable. But in reality this kind of cable has 75 Ohm resistance while in the simulation there is only 500hm resistance. I use the parameter of RG-179B/U coaxial cable in optimized models, which has a 0.95mm inner conductor and 2.95mm shielding cable with 500hm resistance. RG141A/U and RG141A/U+ are the type of the real coaxial cable, their standard dimensions are used in the simulation. As shown in table 4.3 their results are better than previous one.

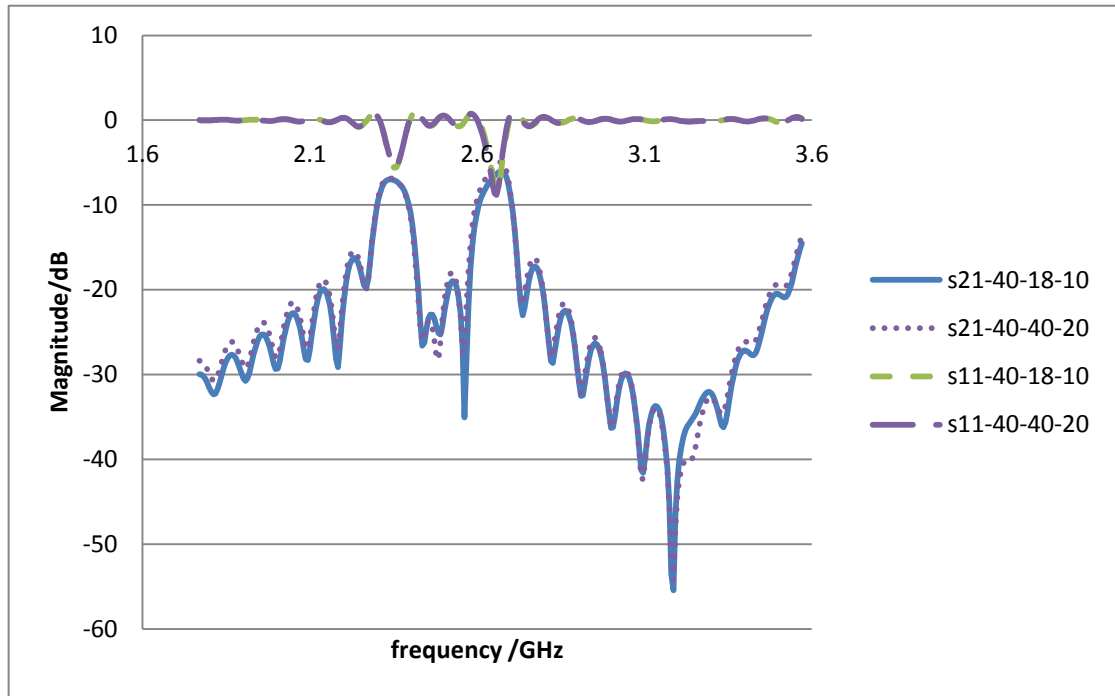


Fig. 4. 5 different combinations of different parameters for meshing properties.

Fig. 4.5 based on version 3, the last three number in legend means the three value for mesh definition. Take S21-40-40-18-10 as an example, S21 means this curve represents S21's magnitude. The first 40 means the parameter in Mesh properties-Hexahedral, whose name is lines per wavelength, is set to 40. The second 40 represents lower mesh limit is set to 40, the parameter below lines per wavelength. The final 20 means mesh line ratio limit.

Some CST introduction books set lines per wavelength the same value as the lower mesh limit while some do not. To verify the difference between them, the tests of different combinations are necessary. As can be seen from Fig. 4.5 the simulation results of 40-40-20 and 40-18-10 do not have obvious difference. They are almost the same. So both definition are acceptable, they will not introduce great difference in the final simulation results.

Compared with 40-18-10 combination, the 40-40-20 has less loss at S21peak. So I choose to set same value to the first and second parameter.

4.3 Mesh properties accuracy test

4.3.1 Frequency

In this section I will change maximum frequency to find out its effect on simulation result.

To find out how frequency effect the result, the maximum frequency changed from 6 to 25 GHz, with these data I could continue the test with a reasonable frequency.

Version 1 frequency test:

All tests are set as 10-18-10 for the three CST parameters mentioned in Chapter 3.2. This is the lowest requirement to get the solver running.

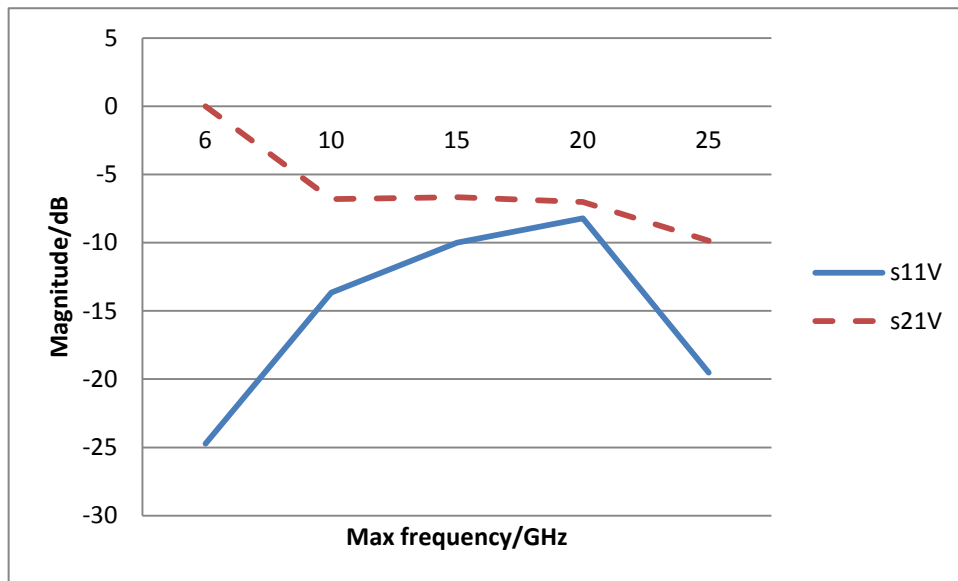


Fig. 4. 6 S11 and S21 peak magnitude of different maximum frequency.

In Fig.4.6 Max frequency means the maximum frequency set for the simulation, S11V means the peak magnitude for S11, which also means the lowest value. S21V means the peak magnitude of S21, which is the highest value. As is shown in Fig.4.6 the difference between S11 and S21 becomes smaller as the peak frequency increased, that means the pass band become vague rather than sharp. At the point that maximum frequency = 25GHz, it seems that the difference began to increase,

but when plot S11 and S21 together the pass band at 2.4GHz has already disappeared, this is the second pass band.

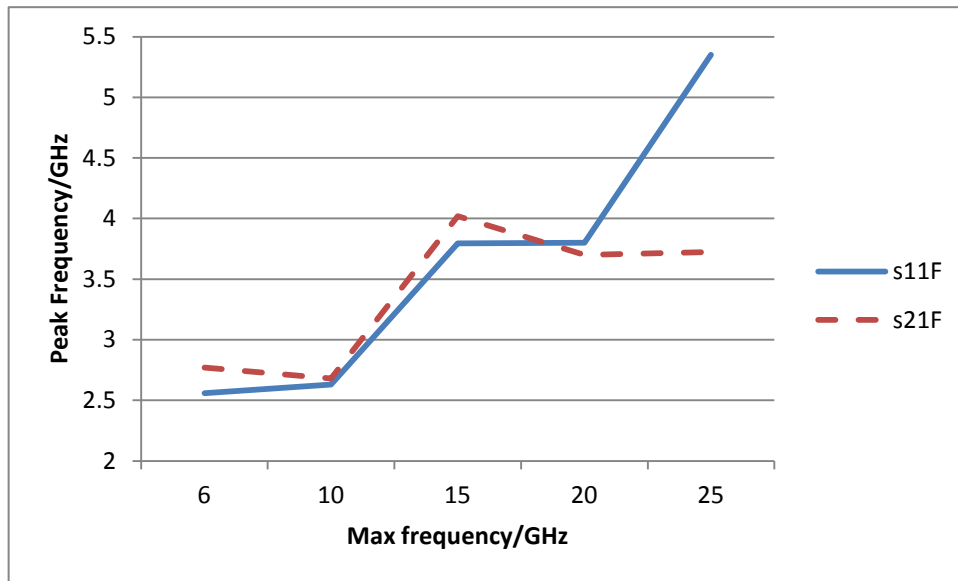


Fig. 4. 7 Peak frequency of different frequency range

As can be seen from figure 4.7 the first peak for S11 and S21 is almost the same when the maximum frequency range is set below 20GHz, but it does not mean there is a pass band. Based on Fig. 4.7 if there is supposed to be a peak lower than 4GHz, the test frequency shouldn't larger than 20GHz.

In Fig. 4.6, the peak magnitude become similar as the simulation frequency increased to 10GHz, that means the pass band is not obvious. So I plotted S11 and S21 value against frequency for 10 and 15GHz.

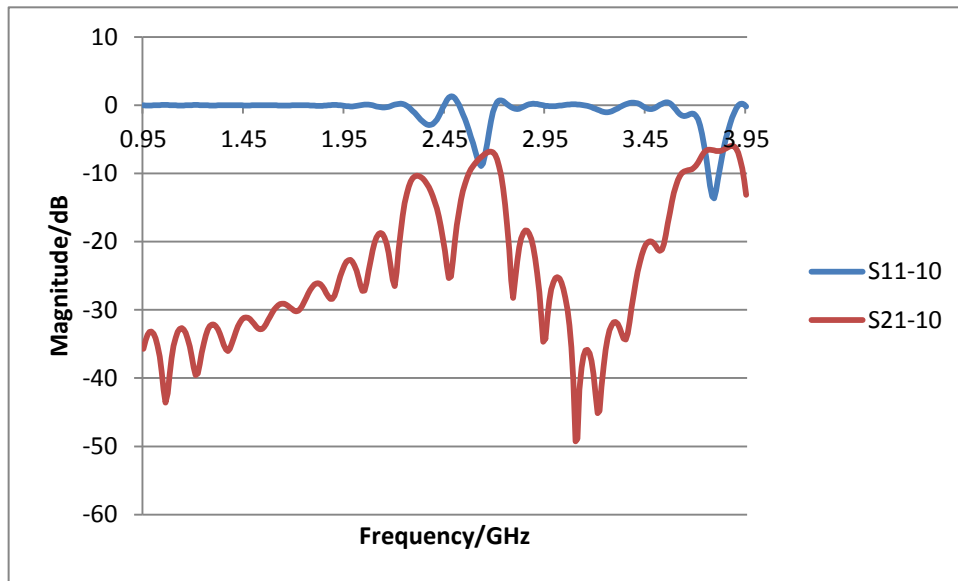


Fig. 4. 8 S11 and S21 magnitude for maximum frequency =10GHz

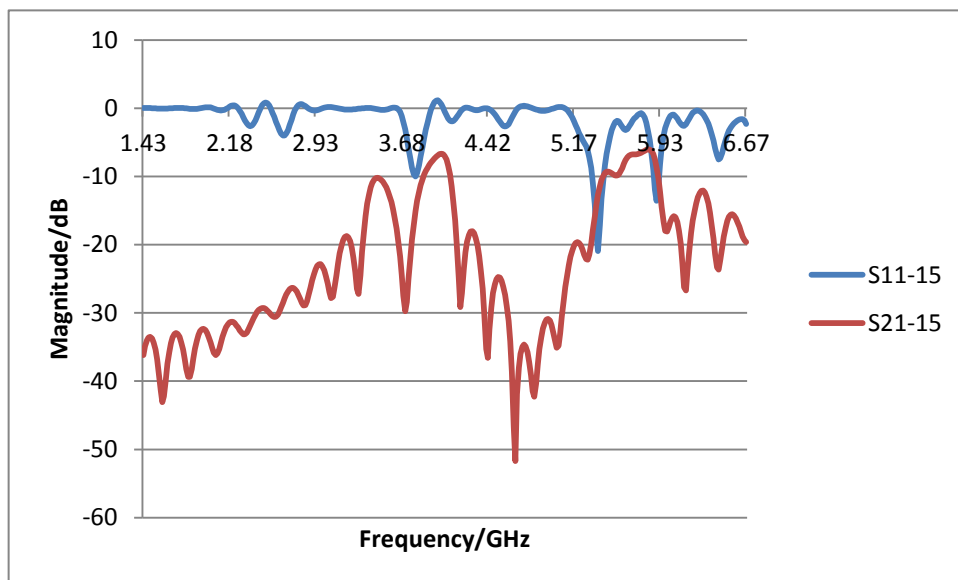


Fig. 4. 9 S11 and S21 magnitude for maximum frequency= 15GHz

Fig. 4.8 shows that at 10GHz there is a pass band at 2.6GHz, but it is not obvious, and when the maximum frequency increased to 15GHz the first peak disappeared. When the maximum frequency increased to more than 15GHz, the first pass band in Fig. 4.9 shifted to higher frequency like 5GHz or higher. So if the real pass band is at 2.6GHz, the simulation frequency should be confined within 10GHz, and even at 10GHz, the result isn't satisfy. So, lower frequency such as 6GHz may be better choice.

Frequency	F6	F7.5
S11F	2.634	2.106
S11V	-16.8351	-14.7741
S21F	2.646	2.118
S21V	-1.3301	-1.74561

Table 4. 4 simulation results of different frequency with same mesh cell number

Table 4.4 is the result of the test designed to prove mesh cell number won't unify test results. The two test are run in different mesh definition but with same total number for mesh: 2166784. The first run is in 6GHz, CST parameters are set as 30-30-10. The second run in 7.5Ghz, with CST parameters set as 24-18-10.

So I will run all the test at 6 GHz. Mesh numbers does not equal to mesh settings and different mesh parameters which have same mesh cell numbers do not have same simulation results.

4.3.2 lines per wavelength

4.3.2.1 6GHz test

To prove that different versions of the models will affect the simulation results, I tested lines per wavelength in all three versions since lines per wavelength is the most important parameter in CST mesh generation.

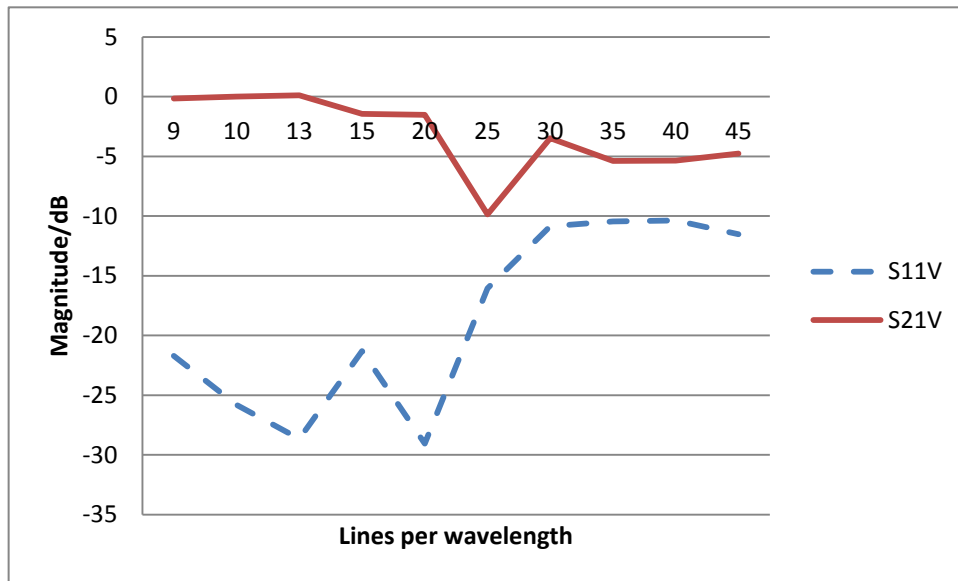


Fig. 4. 10 S11 and S21 peak magnitude of different w

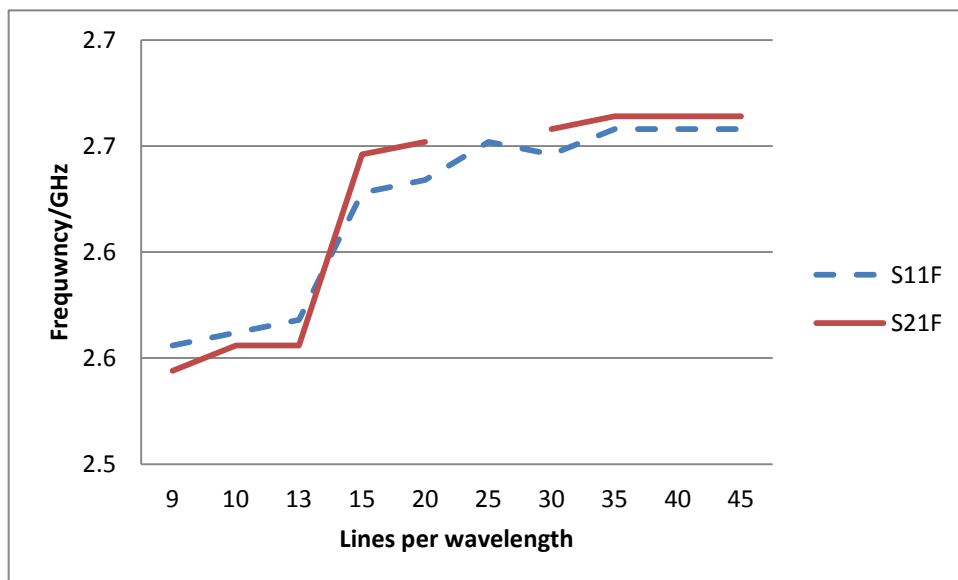


Fig. 4. 11 S11 and S21 peak frequency of different w

In Fig. 4.10 and Fig. 4.11 W means the lines per wavelength; S11V and S11F have same meaning as before. From W= 10 to W=35 is simulated in version 1. As can be seen from the table, when comes to 25 lines per wavelength, there is a odd point. When the w is more than 35, there is a unacceptable large loss for S21, so version2 is adopted. As is shown in Fig 4.10, version 2 did not solve the loss problem.

Fig. 4.11 shows that when w increased from 13 to 20, the peak frequency has an obvious shift. When w is increased to 35 the frequency reached a constant value. The

missing value of S21 at $w=25$ is omitted for it is unusually small. At that odd point S21's peak frequency is 0.9GHz, that means the result is not reliable. In Fig. 4.10 S11 peak magnitude becomes similar after w increased to 35 and S21 has a little shift when w is larger than 40. Maybe the S21 shift at $w=40, 45, 50$ are caused by the model change, so there is another complete test for version3.

Version 3 simulation results report:

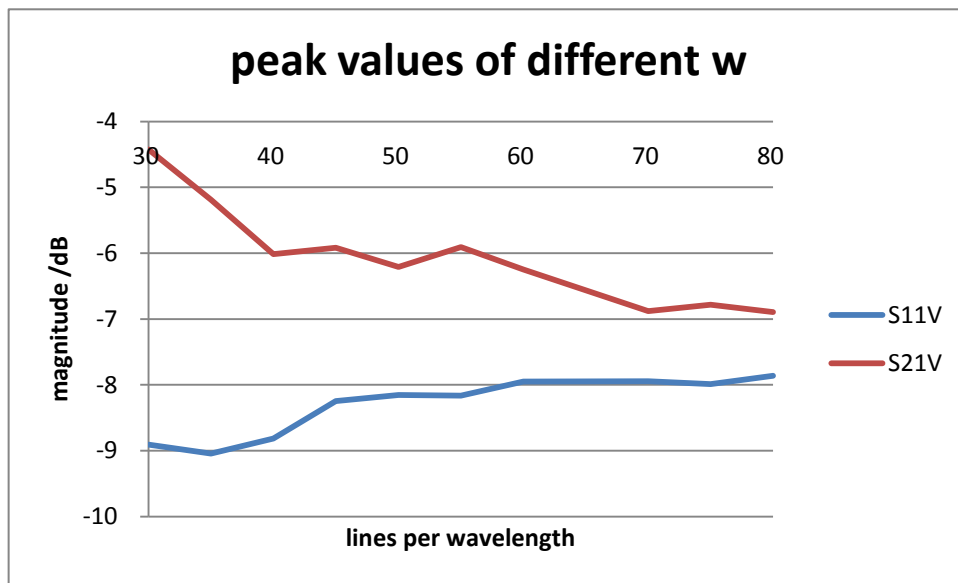


Fig. 4. 12 peak frequency of different w

From Fig 4.12, there is a tendency that when w is over 50, s11 and s21 go stable together. In version 1 and 2 the turning point is at 25 while version 3 is 45. Version 3 has better result for the frequency becomes converged while version 1 and 2 did not.

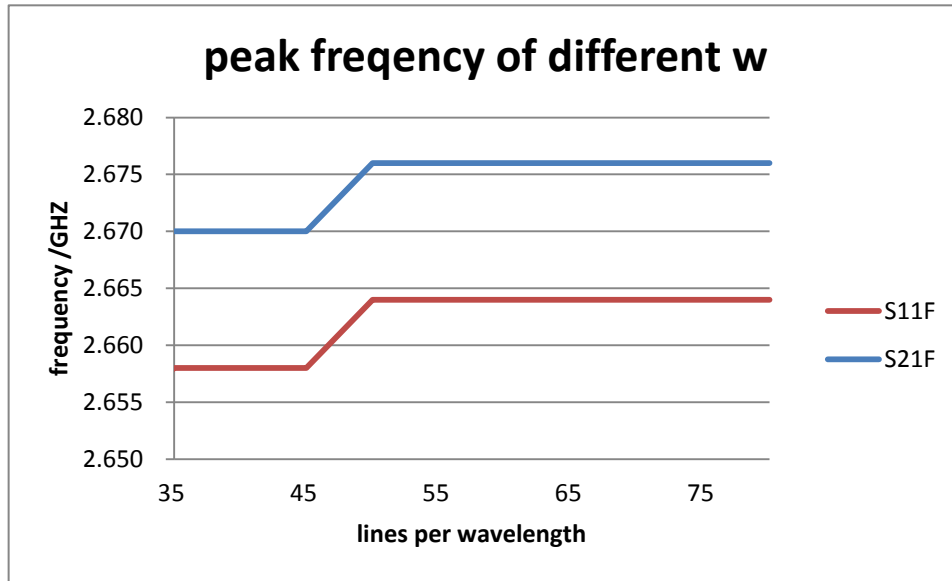


Fig. 4.13 S11 and S21 peak magnitude for different w

From Fig 4.13, S11's values are always stable after 45 while values of S21 changed significantly when w grows larger. There are two smooth stages, the first one is 40-55, the second one is 70-80. I think it does not mean that the higher the better in CST simulation, as was shown in the frequency, higher frequency led to the shift of the first peak. Maybe when the mesh is small enough, there would be some calculation error. As there is no calibrated test result, it is very difficult to tell which value is more accurate.

Compare with the original paper, w=30 is more closer to their measured results. The shift of frequency and loss may be caused by the port which should be thicker than 0.3mm, for the dielectric ring has a larger size. The radius of the cable will not be the only reason, as is said at the start of Chapter 4, many important data are missing in original paper.

4.3.2.2 10GHz test

This section is designed to verify the conclusion made in 4.3.1, that is to prove 10GHz will cause simulation error.

w	10-18	15-18	20-18	20-20	30-30	40-40
S11p	-13.6625	-16.9519	-17.5206	-18.5918	-19.9986	-20.1821

S11F	3.79	3.8	3.8	3.8	3.8	3.8
S21P	-2.61642	-6.02151	-5.76864	-6.86275	0.828848	0.982229
S21F	3.75	3.88	3.89	3.86	2.75	3.92
PBW	0.210001	0.22	0.21	N/A	N/A	N/A

Table 4. 5 Simulation results of maximum frequency set to 10GHz.

In table. 4.5, 10-18 means the lines per wavelength is set to 10, the lower mesh limit is 18, the mesh line ratio limit is fixed to 10. When w (lines per wavelength) is lower than 20, there is still a narrow pass band at around 2.6GHz, but when w grows to more than 20, the pass band disappeared.

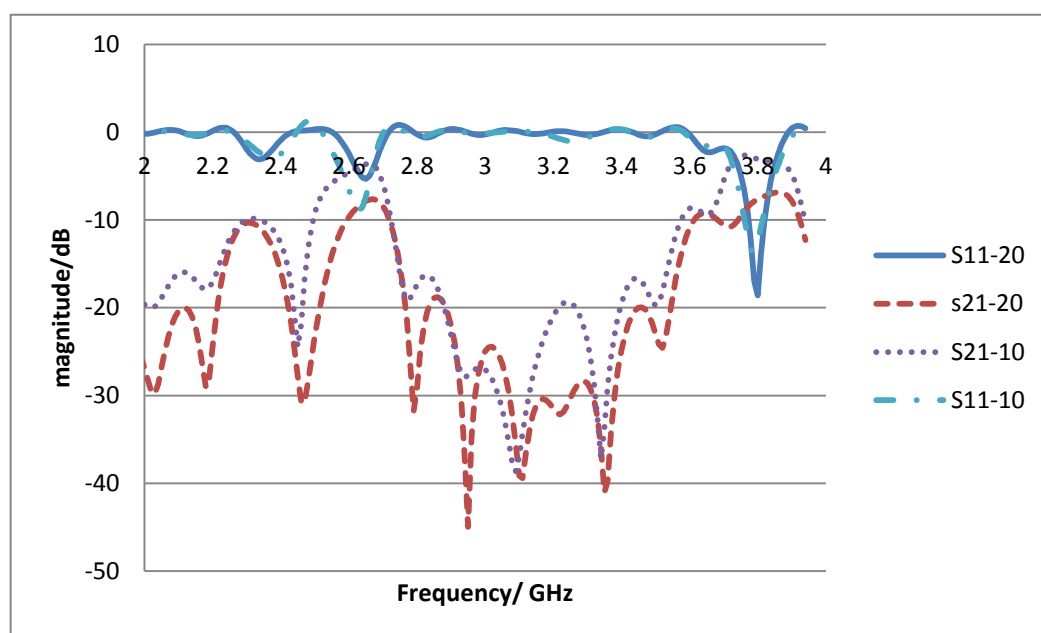


Fig. 4. 14 Simulation results for different lines per wavelength.

As is shown in Fig. 4.14, the first pass band at 2.6GHz disappeared when mesh steps become smaller. It is plausible that when the mesh step is too small, the simulation result tends to have more and more loss than the real condition. The default parameters are set as 10,10,10, under that mesh density, the result has a pass band at 2.6GHz.

Maximum frequency of 6GHz gives better than 10GHz as higher maximum frequency will cause simulation error.

4.3.3 Lower mesh limit

In this section the second parameter will be tested, other parameters remains the same.

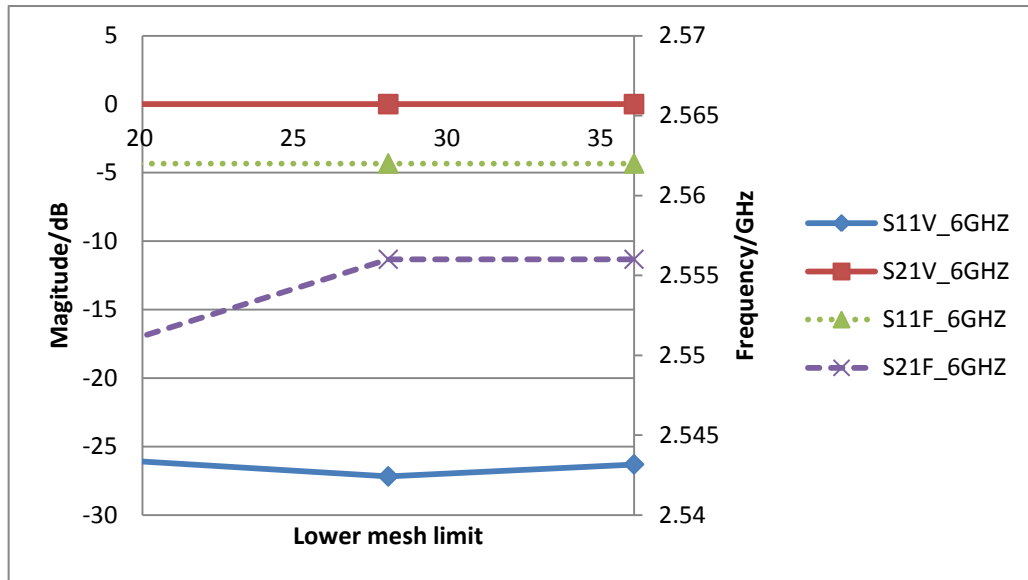


Fig. 4. 15 numerical value for 6GHz test.

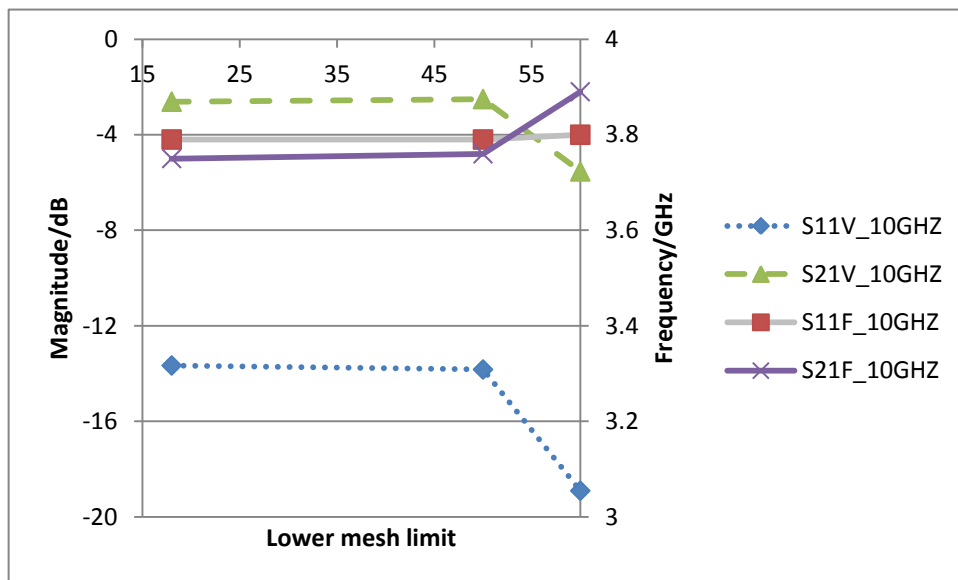


Fig. 4. 16 numerical value for 10GHz test.

S11V means the peak magnitude of S11, S11F means the peak frequency of S11. All peaks are the first pass band peak. In official guide, Lower mesh limit is suitable

for smaller size object, as can be seen from the Fig.4.15 and Fig. 4.16, this CST parameter does not have significant affect on both magnitude and frequency. Fig 4_15 demonstrates that L (lower mesh limit) almost do not have any effect on the simulation result when it is less than 40. Fig. 4.16 shows that if L increased to 60, there would be more loss. At 10GHz, when increase this parameter to 60, there is an obvious change in values. As this gap has also been spotted in the simulation process of the lines per wavelength, it might be caused by the algorithm.

In this model Lower mesh limit does not have great affect on the simulation result distinctly.

4.3.4 Mesh line ratio limit

This section test the mesh line ratio limit parameter. It is the last CST parameter. All the data is tested in version 3.

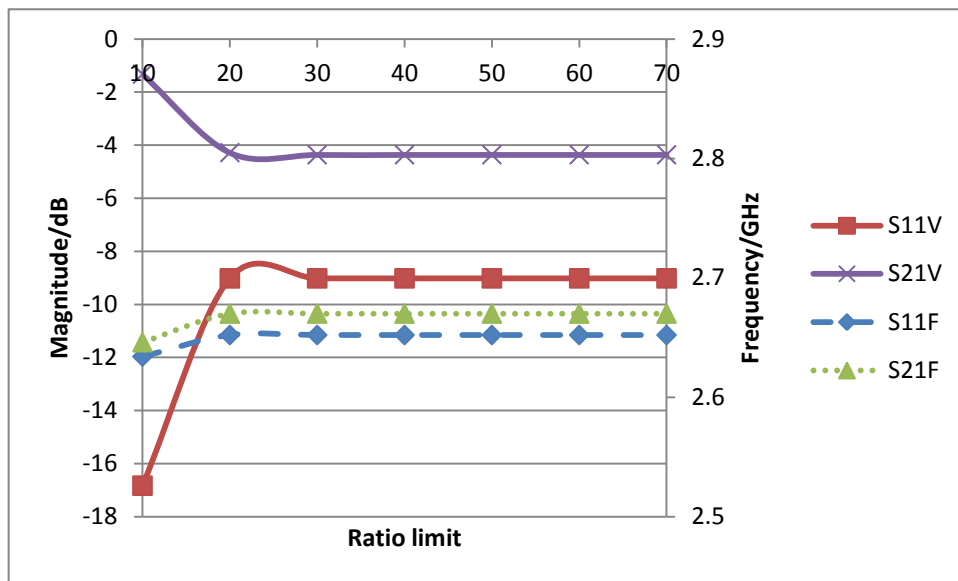


Fig. 4. 17 S11 and S21's peak magnitude and frequency of different ratio limit

It can be seen from Fig. 4.17 that the frequencies of S11 and S21 have links, they rise and down simultaneously. R (ratio limit)= 10 have better result than other values, that means $w = 30$ and $l = 30$ $r = 10$ is the best combination for CST parameters. But if change r to other values, it won't change the result greatly. If R=10 gives correct

result, that means the largest mesh step divided by smallest mesh step should not larger than 10. It might suits other meshing method as well. Then $R > 10$ will introduce simulation errors, or there is a largest mesh step limit.

As Fig.4.17 shows, when $R > 20$ the simulation results become converged. If $R = 10$ gives wrong result, that means small mesh steps will amplify the simulation error. When large mesh step are introduced in the simulation model, they absorb those errors coursed by small steps.

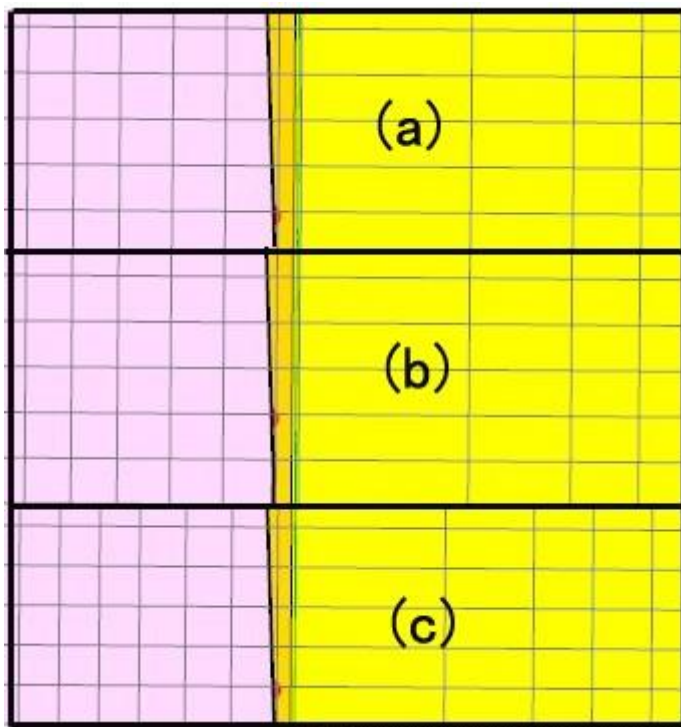


Fig. 4. 18 Mesh cells for different R. (a) mesh property is $R = 30$, (b) $R = 20$, (c) $R = 10$

Fig 4.18 shows the same part of the model. The narrow strip in the middle is the gap between the microstrip line and the dielectric ring. It is the smallest dimension in this model. Fig4.18 clearly showed that when $R > 20$ the mesh is almost the same as $R = 20$. Thus there would be two explanations about the this phenomenon. This first one is confined by the model structure the mesh reached its limitation. The second one is according to the mesh generation algorithm, $R = 20$ reached its limitation in this model. Fig. 4.18 's CST parameters are set as 30-30-R. To solve this question, I

increased W and L , then compare the mesh cells again.

Before compare the screen shots, I adjust the size and position of the original pictures. The narrow gap is exactly the same length and the slope of the dielectric ring is fixed to ensure I compared the same area of the resonators.

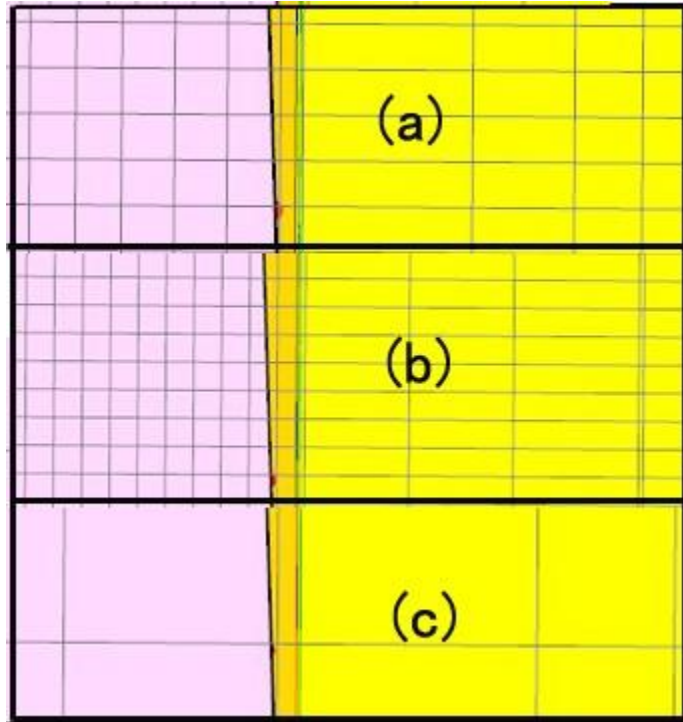


Fig. 4.19 Mesh cells of different CST parameters. (a) is set as 30-30-30, (b) is set as 60-60-60 (c) is set as 10-10-20

Fig. 4.19 (c) proves that when $W=30$ and $L=30$, $R=20$ reached maximum mesh cell, even if $R>20$, the mesh structure will not get any more refinement. Because the mesh cell could become larger than (a). Fig. 4.19 (b) shows another important characteristic, the gap is not one whole mesh cell. I changed R from 8 to 500, the mesh structure did not even changed a bit. When R is smaller than 8, the mesh size structure changed to another one and remains same when $0<R<8$. I then tested $W=70$ to 300 $L=70$ to 300. $R=8$ becomes the changing point in every test. When $W>100$, the smallest cell is smaller than the gap. That means the mesh structure is not determined by the smallest dimension in the model.

In conclusion, the mesh generation algorithm has flaws, when W and L is lower

than 50 (tested result) R will change the mesh structure. When W and L is larger than 50, there would be only 2 kinds of mesh which are $R < 8$ and $R > 8$.

Then I tested CST parameters set as 50-50-20 and 50-50-40, the simulation results have slightly difference. That means the simulation result is not only controlled by the mesh structures. Correct R value is still uncertain.

4.4 Parameters of the dielectric ring test

In this section the missing parameters of the physical structure will be changed to find out their relationship with the S-parameter, peak frequency and magnitude. All tests are simulated with a same CST parameters combination: 30-30-20.

4.4.1 Thickness of the substrate

In this section the thickness of the substrate will be changed.

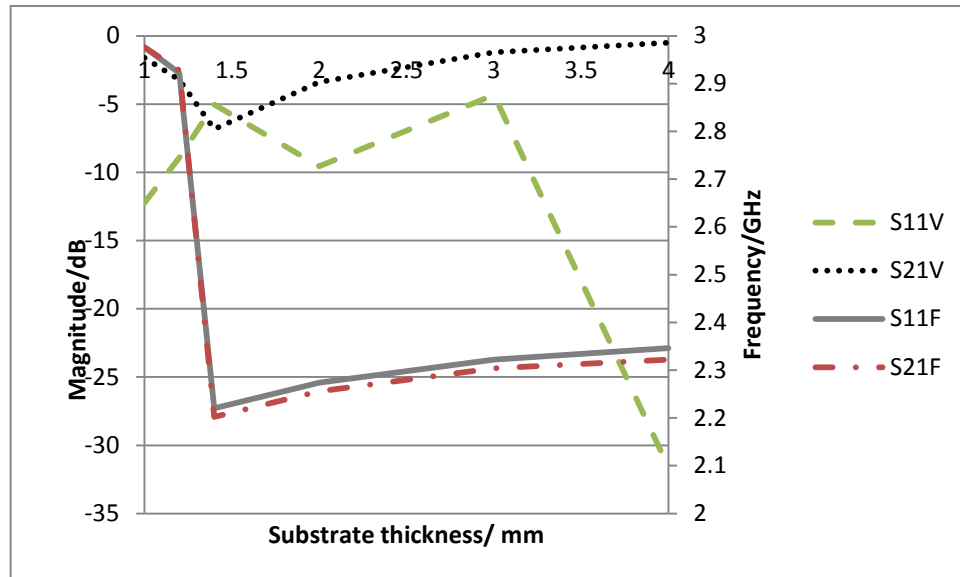


Fig. 4.20 S11 and S21 peak frequency and magnitude of different substrate thickness.

Fig. 4.20 shows strange magnitude of S11 and S21, thickness = 1.5 mm is an odd point. There is a sharp drop in frequency when the thickness increased from 1.2 mm to 1.4 mm. When the thickness is larger than 1.4 mm the peak frequencies have a monotone increasing tendency. It seems that as the substrate becomes thicker the

S11 peak magnitude becomes smaller and S21 becomes higher, but this test focus on 2.4GHz, when the thickness increased to 4mm, there is a pass band at around 1.9GHz as is shown in Fig 4.21.

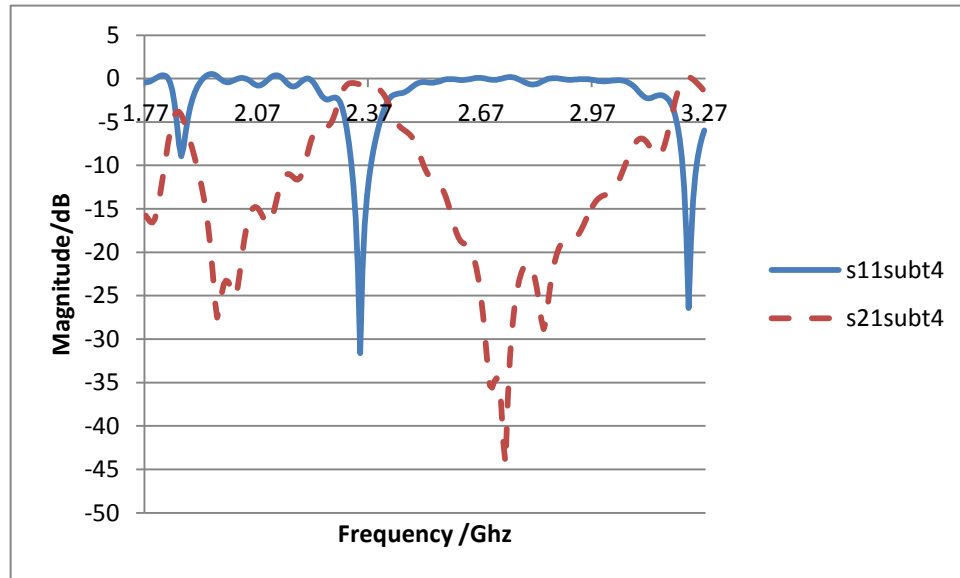


Fig. 4. 21 S11 and S21 magnitude of substrate thickness=4mm

When substrate thickness =1 the first peak is the first pass band, while when subt=2 the first peak is not a pass band and the second peak locates in 2.6GHz.

So, substrate thickness=1 is better than other value.

4.4.5 Length of the gap

In this section the length of the gap between microstrip line and the ring will be changed.

The length of the gap means the distance between the micro strip lines and the dielectric ring. When the gap is larger than 0.3, the pass band becomes smaller as the distance increased.

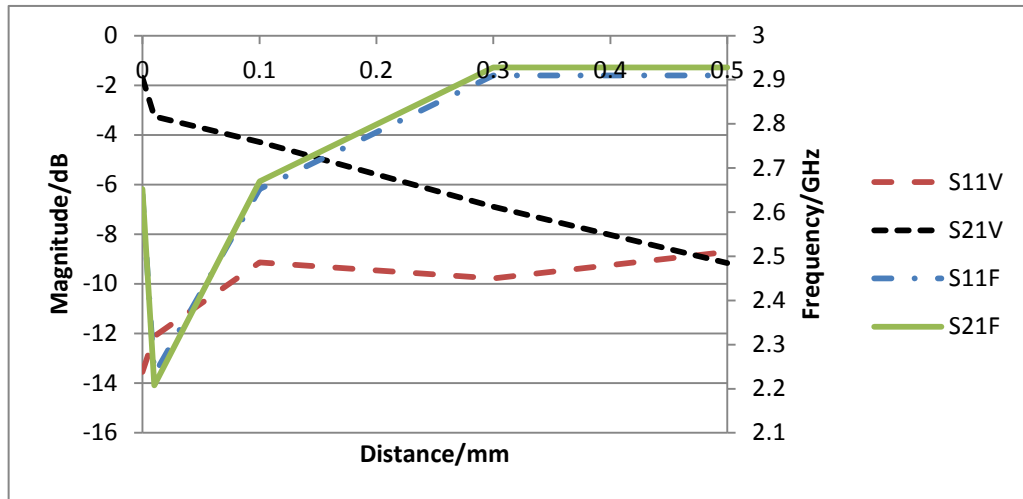


Fig. 4. 22 S11 and S21 peak frequency and magnitude of different distance

There is a great difference between 0 and 0.01 shown in Fig. 4.22, that means a little gap changes the result greatly. Then the frequency continue to grow higher with different slopes. The S11 magnitude has a good linear characteristic while S21 does not.

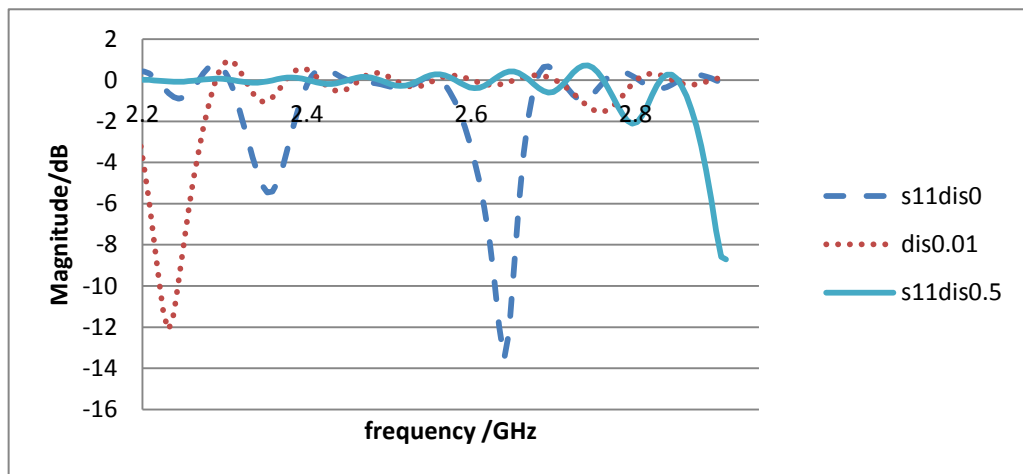


Fig. 4. 23 S11 magnitude of different distance

From Fig. 4.23, there is an obvious distinguish between 0 and 0.01, not only the peak frequency changed but also the magnitude and small ripples. When distance increased to 0.5mm the pass band disappeared.

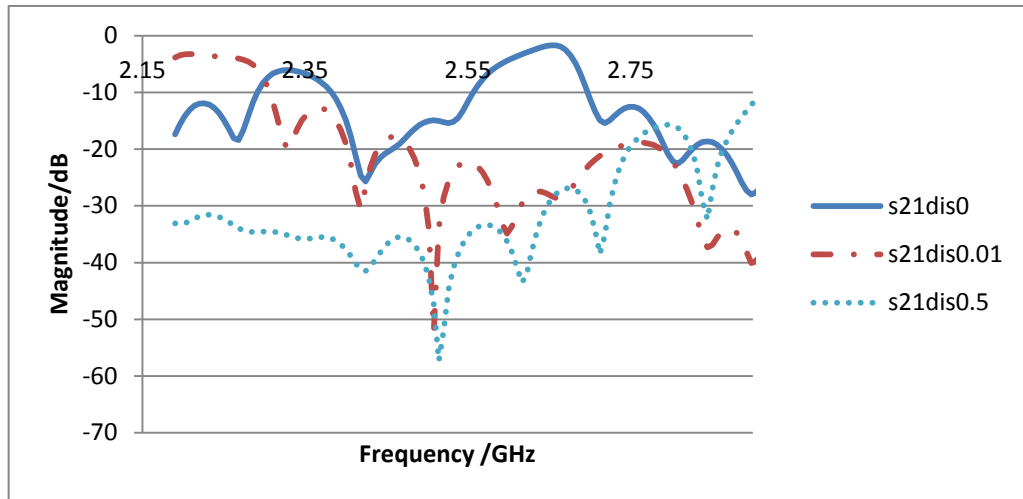


Fig. 4.24 S21 magnitude of different distance

S21 magnitude shows that distance 0 does not have a sharp peak that will add noise to the pass band. So there should be a small gap and less than 0.5mm.



Fig. 4.25 Mesh cells of dis=0.01mm. The mesh boundaries around the gap are boldfaced.

From Fig. 4.22, dis=0.01 is better than 0.1, but the mesh cells show another problem, that is the smallest mesh cell is partially filled with the dielectric ring. That will definitely introduce more error into the result.

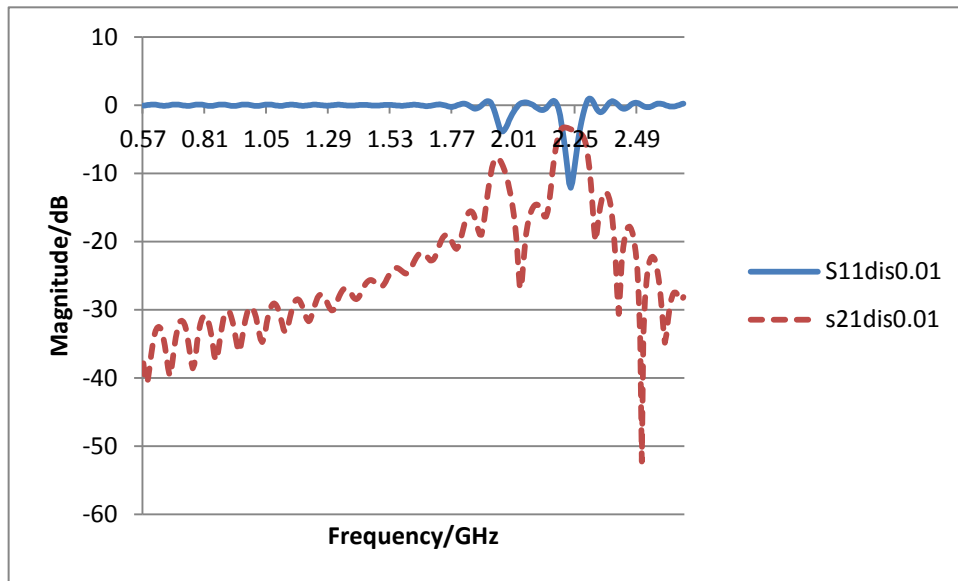


Fig. 4. 26 S11 and S21 magnitude of dis=0.01mm.

Most simulation results show that the first peak is at around 2.6GHz. The first peak in Fig. 4.26 is 2.23GHz, that means even using FPBA enhanced accuracy, partially filled mesh cell still cause error. Thus the dis=0.01 is better choice and the smallest dimension should be larger than 0.1mm, that could reduce partially filled mesh cells.

4.4.6 Microstrip lines thickness

In this section the thickness of the microstrip lines will be changed.

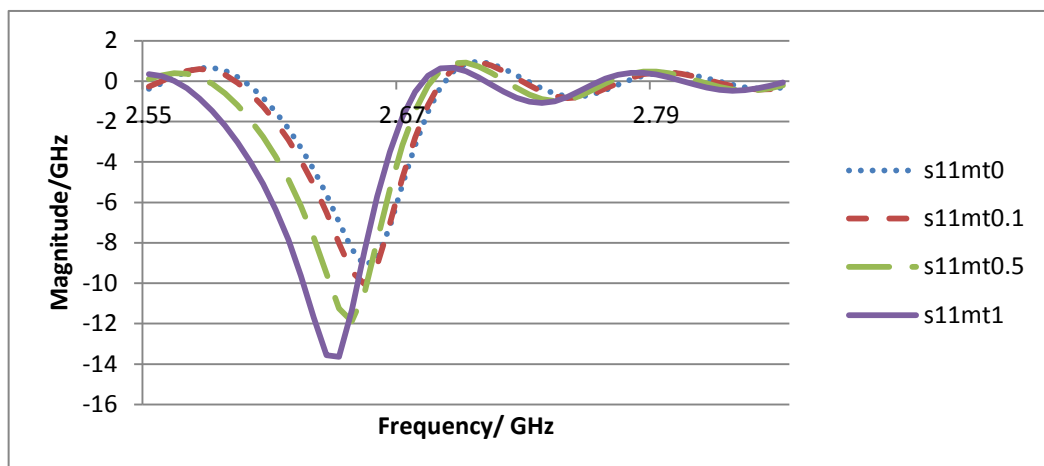


Fig. 4. 27 S11 magnitude of different microstrip thickness

The thickness of micro strip lines have small affect on simulation results and unlike the length of the gap, 0 and 0.1 do not have significant changes. Fig 4.27 shows the peak frequency does not changed too much as the microstrip becomes thicker, but the loss become larger that means the peak becomes more obvious.

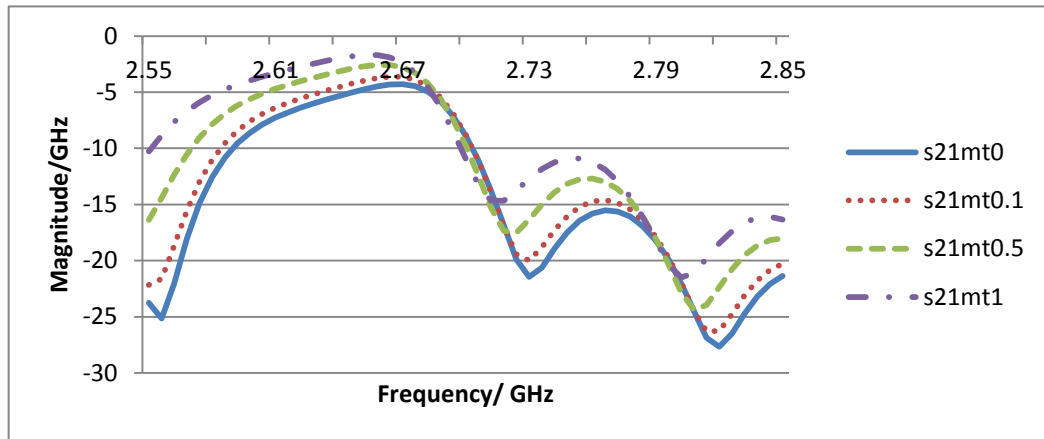


Fig. 4. 28 S21 magnitude of different micro strip line

Higher thickness causes less loss for S21 that means the S21 curve becomes flatter as shown in Fig4.28.

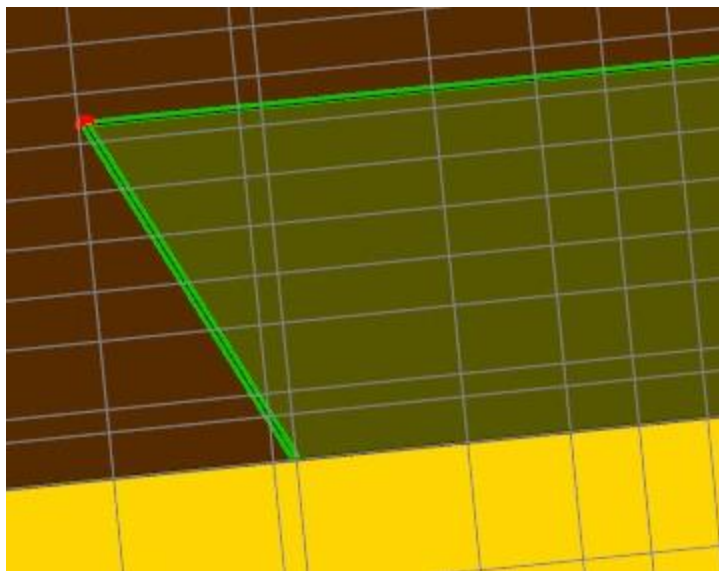


Fig. 4. 29 the z axis cutplane mesh view of 0mm thickness microstrip lines.

The microstrip lines have 0 thickness in Fig 4.29, the mesh type is unknown too.

Thus Fig. 4.30 is needed to prove the difference between $mt=0$ and $mt=0.1$.

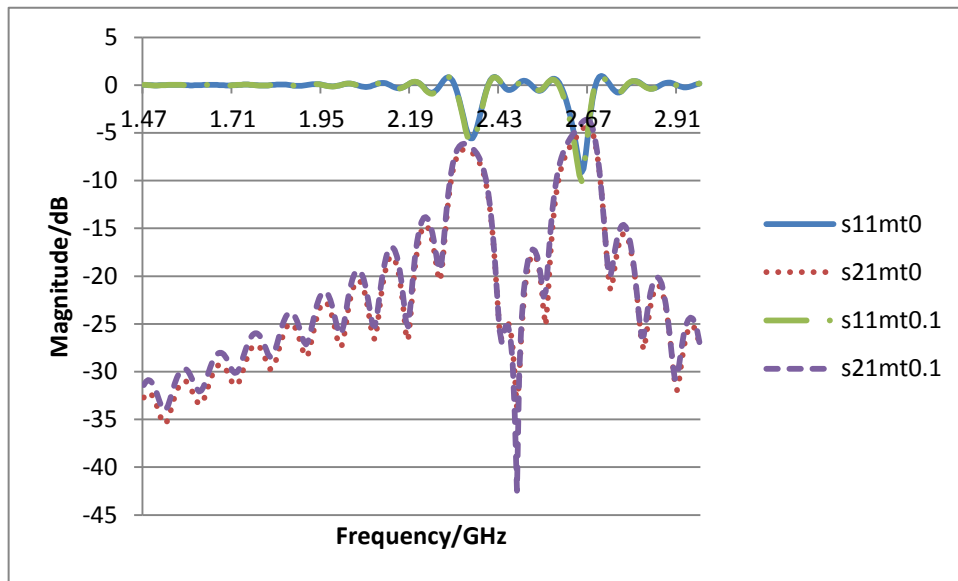


Fig. 4. 30 S11 and S21 magnitude of $mt=0$ mm and $mt=0.1$ mm.

The two curves are almost the same, that means even with 0 thickness the CST solver does not create any simulation errors. In reality, microstrip lines are always made in aluminum or copper, so I replaced PEC to test whether 0 thickness will cause error or not.

W	30	45	W	30	45
PEC	2.6	2.6	PEC	2.6	2.6
S11F	2	58	S21F	7	76
ALUS	2.6	2.6	ALUS	2.6	2.6
11F	2	58	21F	7	76
AMOS	2.6	2.6	AMOS	2.6	2.6
11F	4	547	21F	58	547
PECS	-8.	-8.	PECS	-4.	-5.
11V	9098	2455	21V	423	9168
ALUS	-9.	-8.	ALUS	-4.	-5.
11V	0564	3536	21V	4308	8812
AMOS	-12	-8.	AMOS	-1.	-5.

11V	.319	876	21V	9573	4676
-----	------	-----	-----	------	------

Table 4. 6 Different thickness and material of the microstrip lines

In table 4.6 PECS11F means the S11 peak frequency microstrip lines are made of PEC with a thickness of 0.1mm(0mm is almost the same as 0.1 mm as is shown in Fig. 4.29). ALUS21F means the S21 peak frequency of microstrip lines which are made of aluminum with a thickness set to 0.1mm. AMOS11V means the peak magnitude of S11 of aluminum microstrip lines whose thickness is 0mm. W means lines per wavelength. W=30, CST parameters are set as 30-30-20, W=45, CST parameters are set as 45-45-20.

Table 4.6 proves that PEC has similar simulation results as aluminum with thickness set to 0.1mm. When increase the mesh density, the PEC's peak magnitude changes with aluminum. When apply 0 thickness to aluminum the result changed significant. In summary, 0 thickness PEC almost equals to aluminum or lossy metal with thickness set to 0.1mm. Lossy metal cannot use 0 thickness for that will introduce simulation error.

4.4.7 Microstrip lines width

In this section the width of the microstrip lines will be changed.

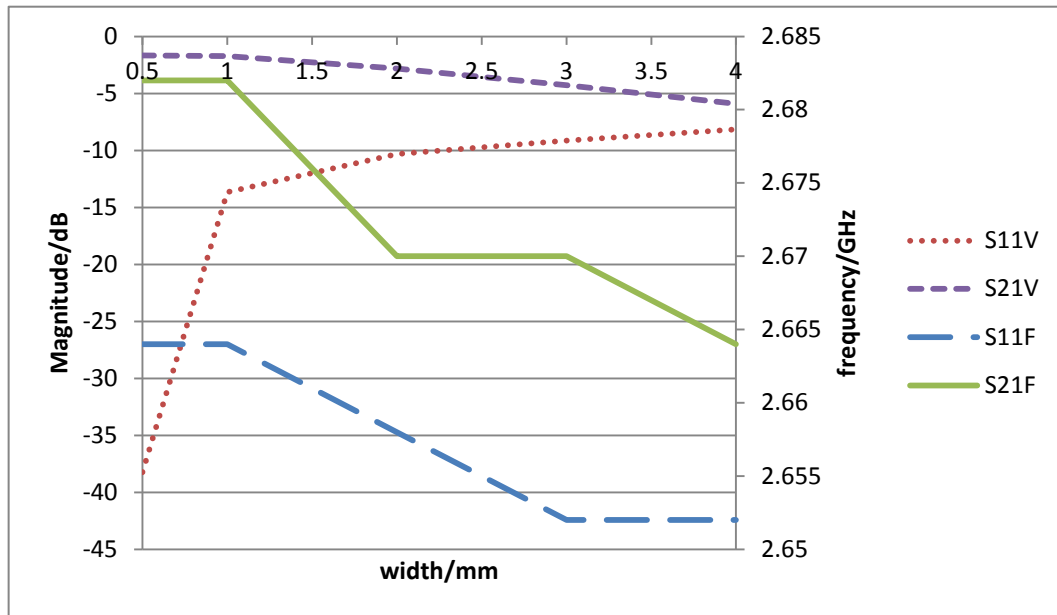


Fig. 4. 31 peak frequency and magnitude of different microstrip width

In Fig. 4.31, when the width of micro strip lines becomes larger, the loss at peak becomes smaller. Narrow micro strip line will get more obvious peak. The peak frequency becomes lower when the width increased, but the shift is very tiny.

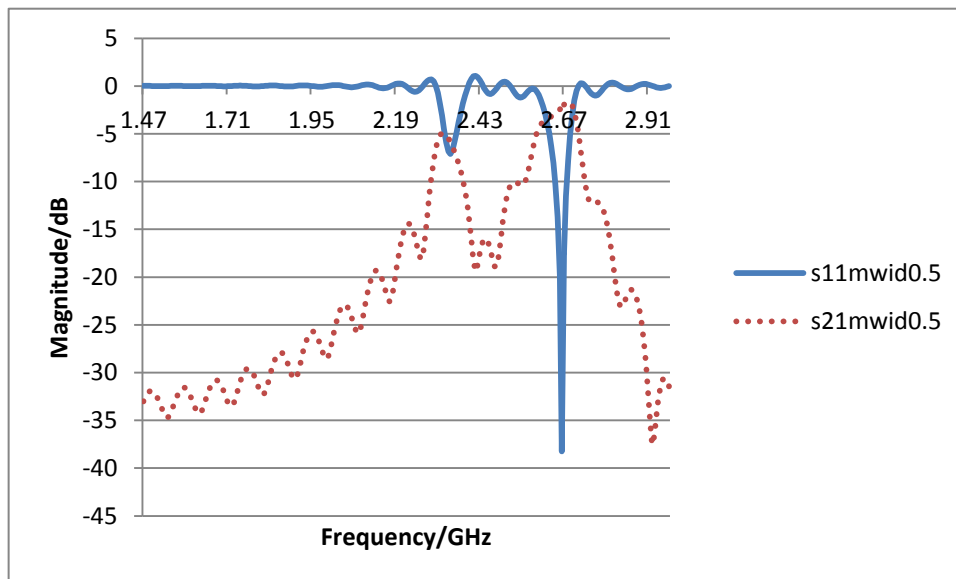


Fig. 4. 32 S11 and S21 magnitude of mwid=0.5 mm

As is shown in Fig. 4.32, the width of micro strip lines is not a crucial parameter until it become smaller than 1. It will greatly affect the magnitude of S11 and S21.

4.5 Plausible optimization

In this section, firstly the missing parameters will be changed to get the desired results. Then a few crucial physical parameters of the original design will be revised and tested based on version 3 model. Then some other model will be tested to get a better result than optimized original design.

4.5.1 Original shape optimization

In this section the height, outer radius inner radius of the ring will remain the same. All the parameters mentioned in the original paper will not change.

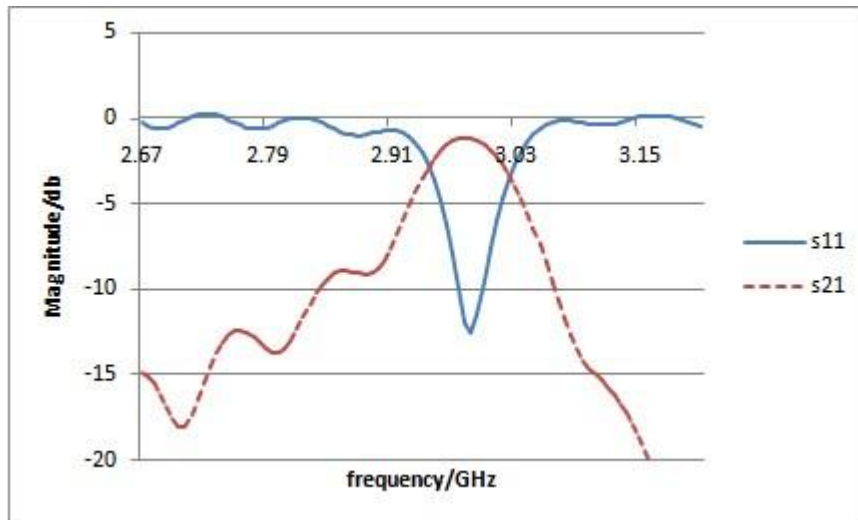


Fig. 4. 33 Original shape optimization CST parameters set as 30-30-20

Other parameters set as: mt (microstrip lines thickness)=0.1, subt (substrate thickness)=1, rpole(radius of the pole)=0.95, oring(radius of the coaxial cable)=2.95.

The S11 peak frequency =2.988, peak magnitude= -12.588869

The S21 peak frequency =2.982, peak magnitude= - 7.89444E-08

Fig. 4.33 shows good simulation results of S11 and S21 magnitude, its peak frequency is 2.982GHz while the original test has a 2.4GHz pass band. More modification is made in Fig. 4.34 to get a lower peak frequency.

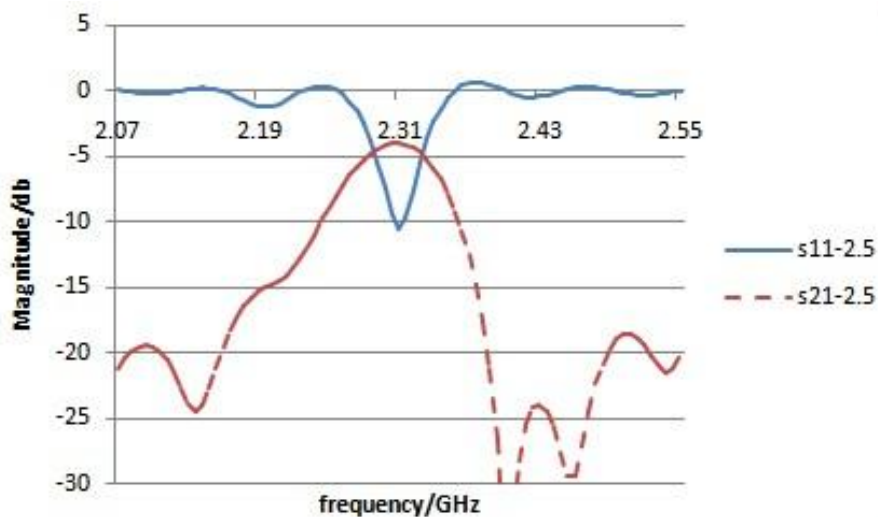


Fig. 4. 34 Change Subt to 2.5 to get the first peak as the pass band

The S11 peak frequency =2.31, peak magnitude= -10.565914

The S21 peak frequency =2.31, peak magnitude= -3.9670516

As is mentioned before, increase the thickness could make the first peak looks very sharp, but it will also make the second peak closer. The original test only plotted a very narrow frequency range, it is uncertain that whether they had the second peak or not. As is mentioned in 4.4.7, to get a sharper peak requires narrow microstrip lines. In this section the width of the microstrip line remains 3mm.

4.5.2 height of the dielectric ring

In this section the height of the dielectric ring will be changed.

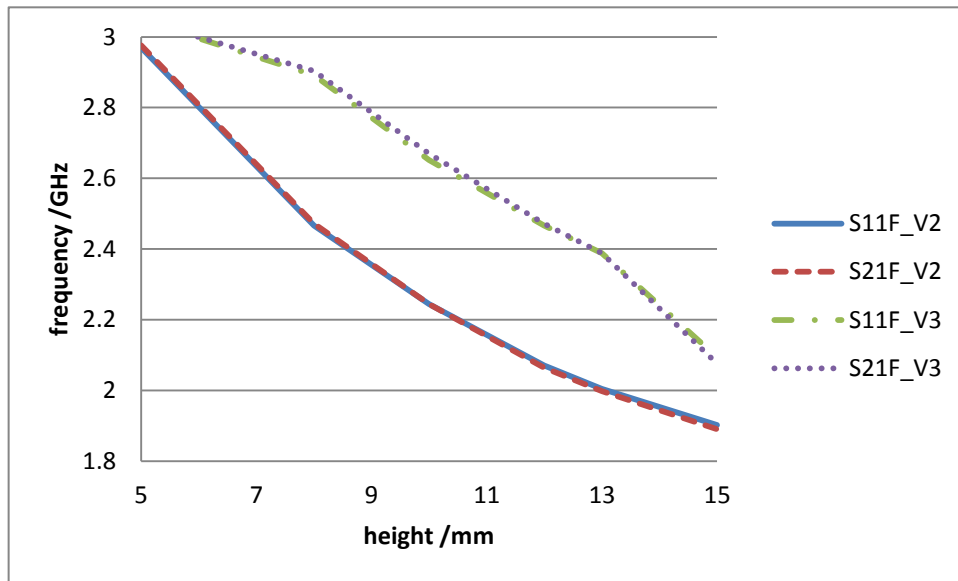


Fig. 4. 35 peak frequency of different height

In Fig. 4.35, S11F_v2 means the peak frequency of S11 in GHz tested in version 2. S21F_V3 means peak frequency of S21 tested in version 3. As the height becomes larger the first peak frequency becomes lower, it also follows the rules in previous tests which version 3 has a higher peak frequency than version 2. It seems that version 2 has a more linear result, both version 2 and version 3's S11 and S21 frequency are almost exactly overlapped.

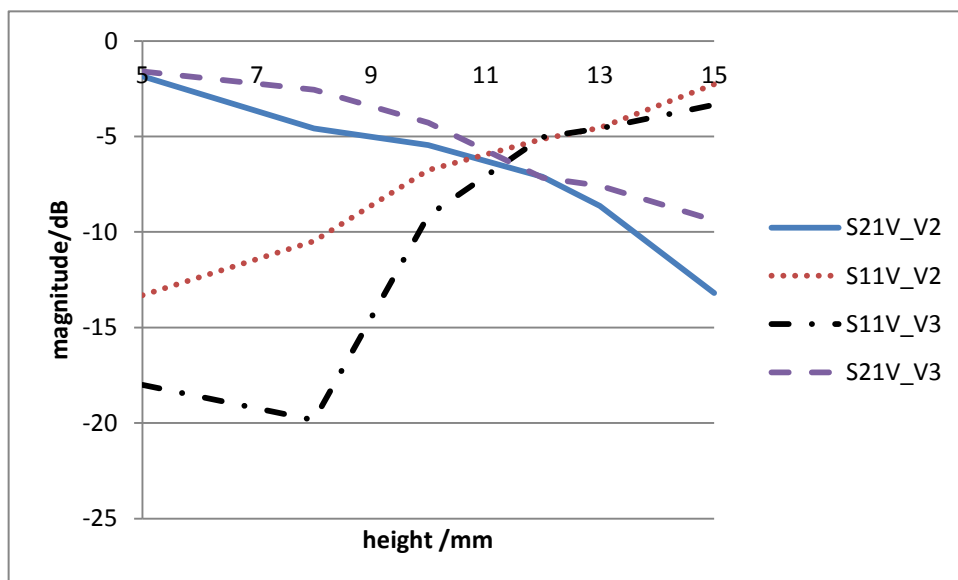


Fig. 4. 36 Peak magnitude of different height

Most S11 value have a tendency to become larger and S21 become smaller in Fig. 4.36, that mean if increase the height of the ring, the first peak will disappear, there won't be a pass band at first peak.

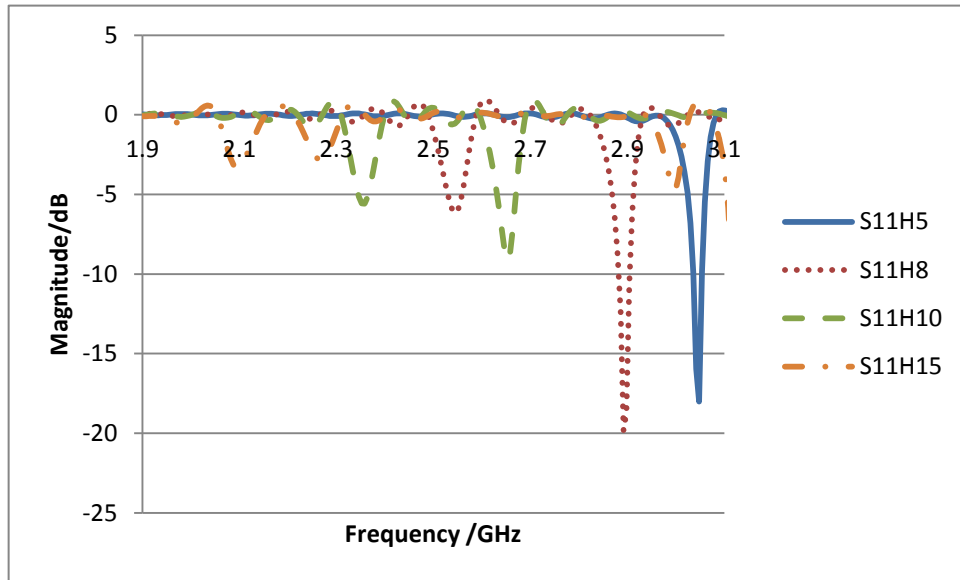


Fig. 4. 37 S11 magnitude of different height.

To simplify Fig. 4.37, only four of them are plotted. When the height is larger than 10, there is no pass band at first peak, they look similar to the curve of $h=15$. $H=5$ has good performance but it has a higher peak frequency than 2.4GHz.

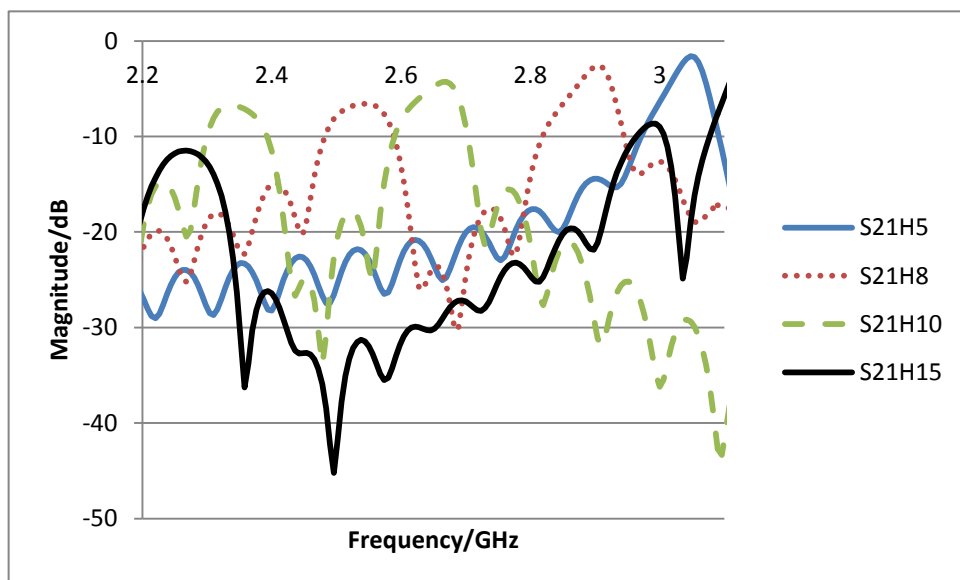


Fig. 4. 38 S21 magnitude of different h

Fig4.38 shows that the original model have two similar peaks which make the stop band very narrow. Increase the height will make peak frequency smaller and more loss. Decrease the height will make peak frequency higher with less loss. Lower height will also increase the distance between the first peak and second peak.

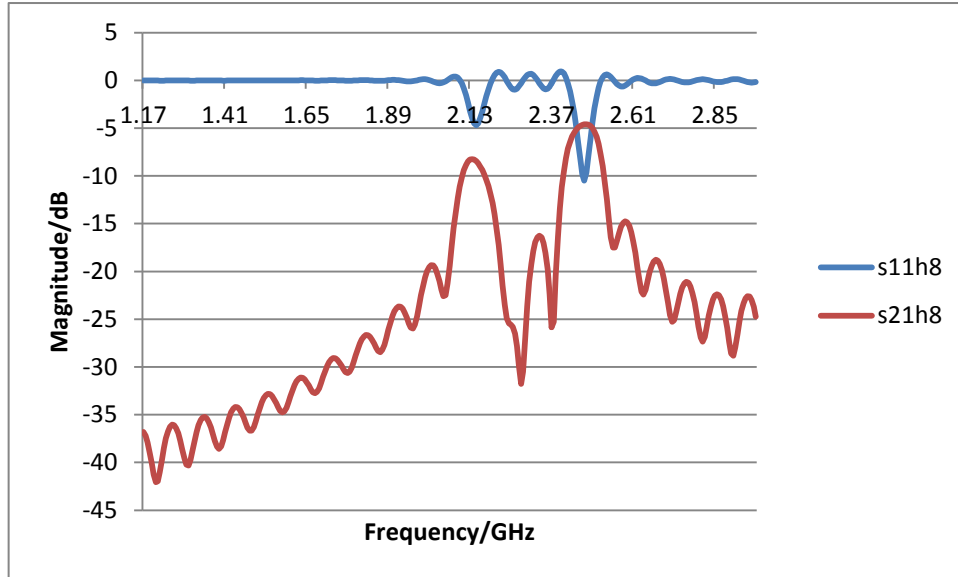


Fig. 4. 39 S11 and S21 magnitude of height=8.

H=8 has a 2.466GHz peak frequency, the pass band is very sharp which meets the requirement in original paper. To get exactly 2.4GHz, the height needs to increase a bit more.

4.5.3 Outer radius of the dielectric ring

In this section the outer radius of the dielectric ring will be changed all tests are run in version 3, 6GHz.

When increase the outer radius the peak frequency becomes smaller, which remind me of the changes of height. Outer radius = 8 seems a better match than the original defined size which is 10.

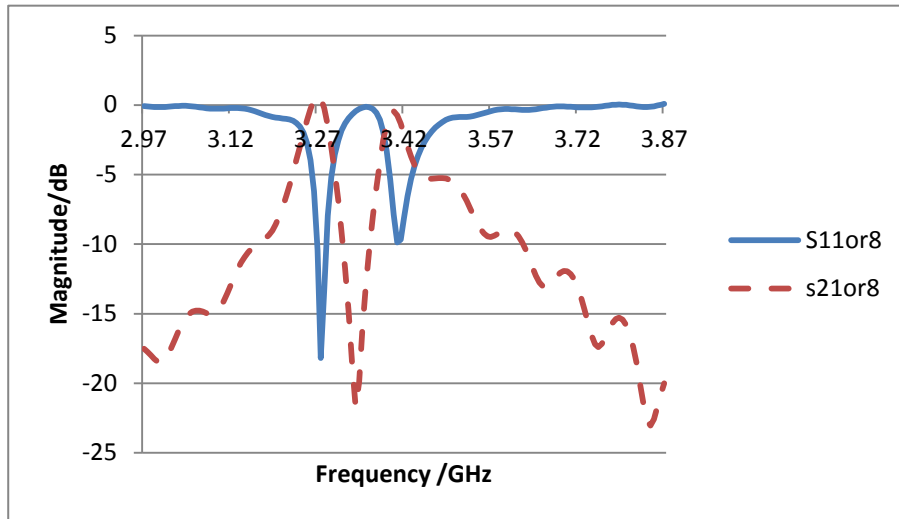


Fig. 4. 40 S11 and S21 magnitude of outer radius =8.

As is shown in Fig. 4.40 the stop band becomes narrow as the radius becomes smaller. The S11 and S21 magnitude reached its peak compared with other outer radius result which is shown in Fig. 4.42.

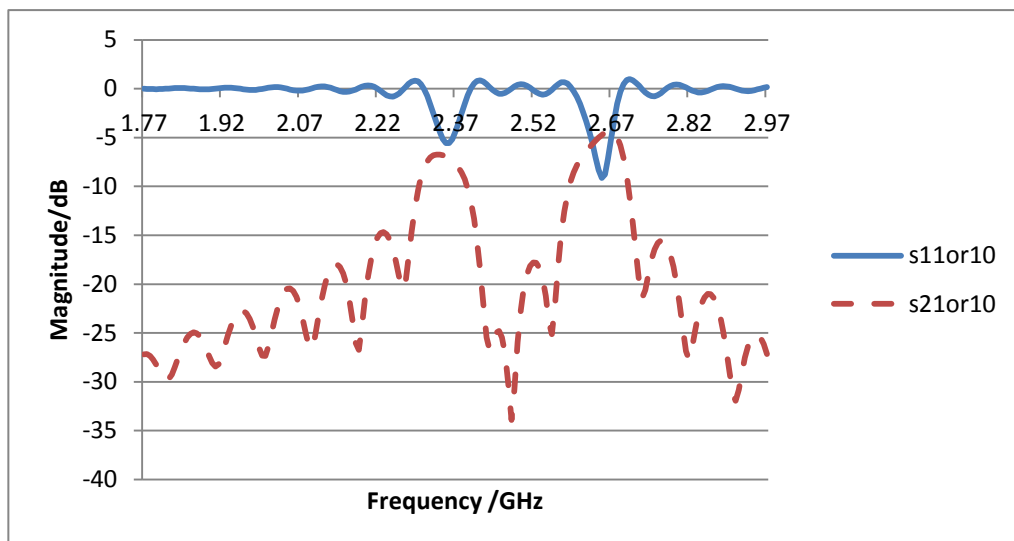


Fig. 4. 41 S11and S21 magnitude of outer radius =10

Compared Fig. 4.39 with Fig. 4.40, they have different peak frequency. Therefore I did not plot them together. Strictly the first pass band of OD=10mm is very lossy while when OD=8mm, the first peak is a pass band. Smaller outer radius has sharper peak, that means to get a good pass band the outer radius should be small.

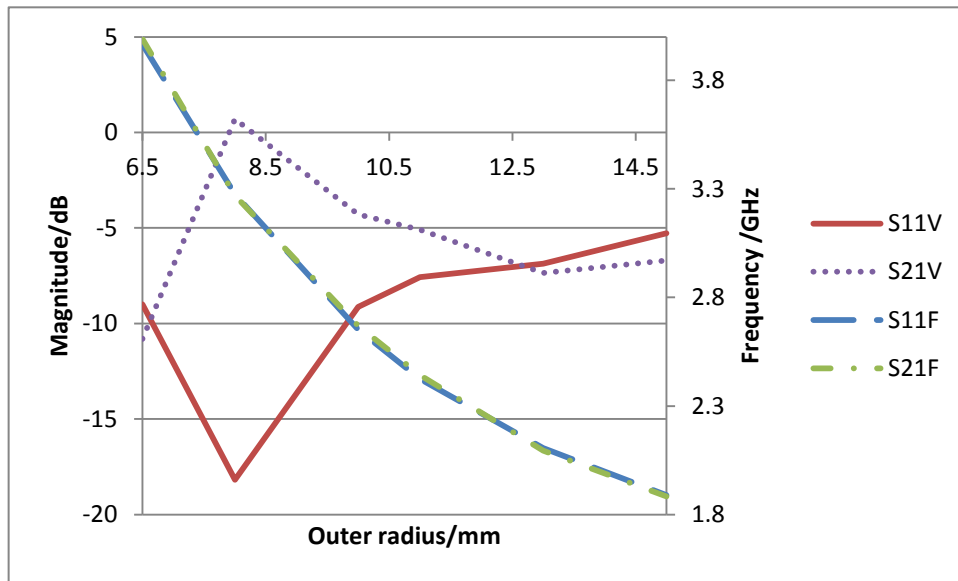


Fig. 4. 42 Peak frequency and magnitude of different outer radius

In Fig. 4.42, the peak frequencies are almost overlapped, it formed a smooth curve while the magnitude of peak values are not that good. At 6.5mm, it means the dielectric ring is very thin, for the inner radius is 6.25mm, it does not possess a pass band at the first peak. When the OD is larger than 12.5mm the pass band at first peak disappeared again, that means the thickness of the dielectric ring shouldn't be too small or too large, outer radius divided by inner radius should remain in 1.1-1.9 ($1.1 < OD/ID < 1.9$) to get a good result.

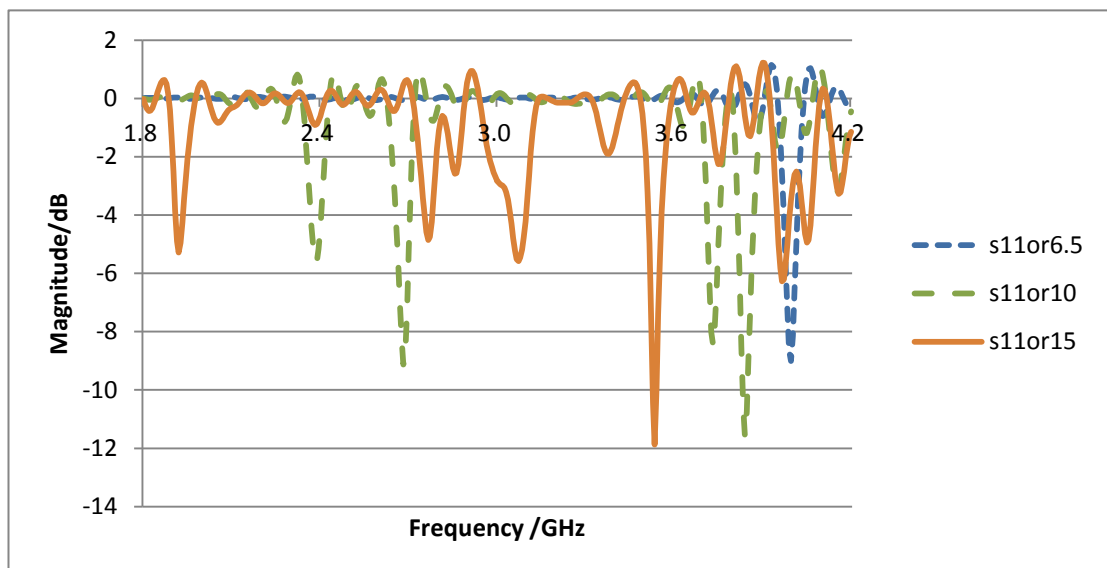


Fig. 4. 43 s11 magnitude of different outer radius

Only 3 lines are plotted in Fig. 4.43 to get a clear view. When OD= 6.5 the peak is obvious, it has less ripples than OD=10 and 15.

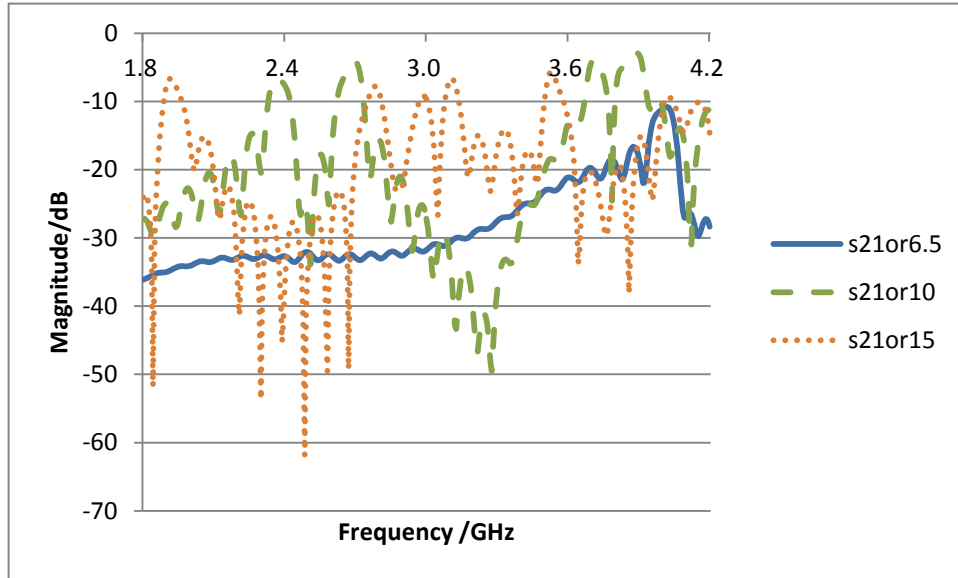


Fig. 4. 44 s21 magnitude of different outer radius

Fig. 4.44 and Fig4.43 show that the higher the outer radius is the more ripples it carries. To get a smooth curve, the outer radius should be lower than 12. In summary the most suitable outer radius is around 8mm.

4.5.4 Inner radius of the dielectric ring

In this section the inner radius of the dielectric ring will be tested.

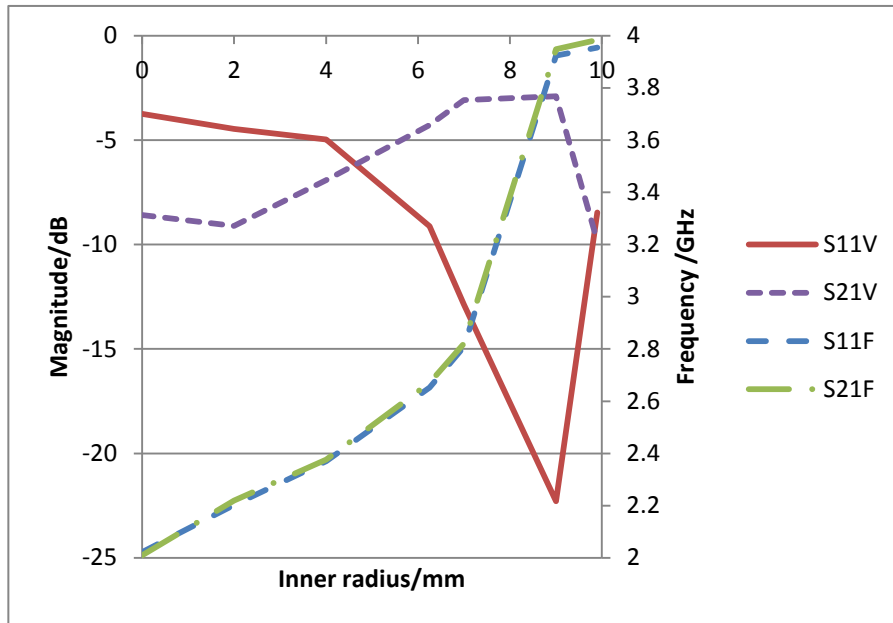


Fig. 4.45 Peak magnitude and frequency of different inner radius

Fig.4.45 shows the first peak rather than first pass band of the S-parameter. IR (inner radius) =0mm means this ring is a cylinder and IR=9.9mm means this ring is very thin for outer radius is 10. The magnitude shows that there are 3 phases, 0-4, 4-9,9-9.9. The boundary value of each phase is a rough estimate rather than exact define.

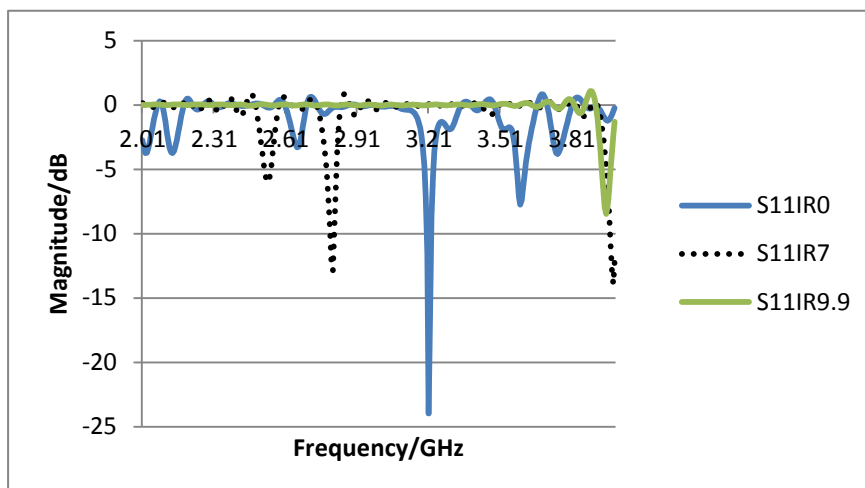


Fig. 4.46 S11 magnitude of different inner radius

IR= 0-4 has a special characteristic, its first peak is not a pass band, but its pass band has the lowest loss. It has ripples, but these ripples are have less loss than

IR=4-9.

IR= 4-9 is what tested as the standard model, they are similar to IR=6.25 which has two close peaks at 2-3GHz and one or two of them become pass band.

IR= 9-9.9 has least ripples but its lowest peak magnitude is higher than IR=4-9.

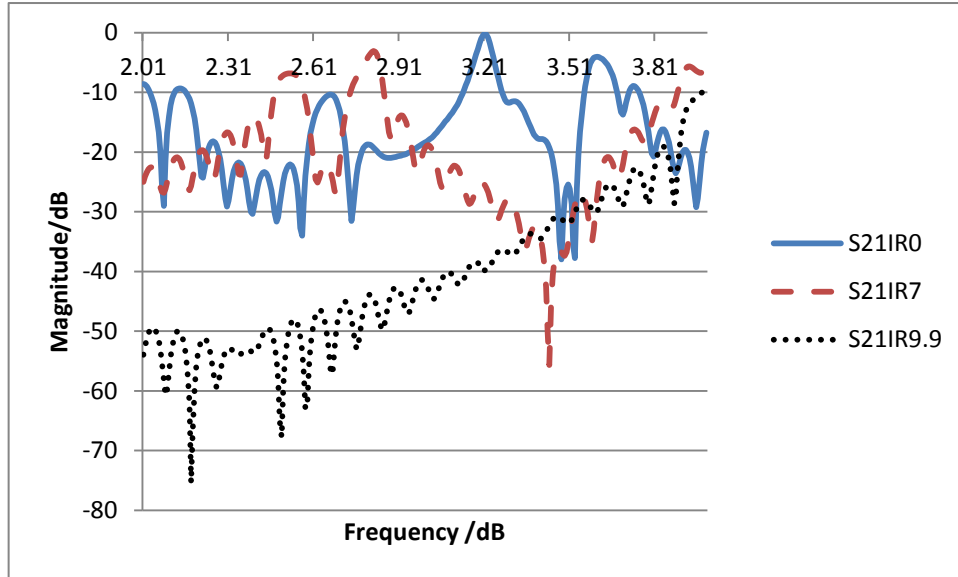


Fig. 4. 47 S21 magnitude of different inner radius

IR=0-4 and IR=4-9 are similar, they all have ripples, but 0-4 has a sharp peak while 4-9 has a narrow stop band between first two peaks. IR=9-9.9 has less noise but it does not even have a pass band at low frequency. It proves again that the dielectric ring should not be too thin, just as what is shown in outer radius.

4.5.4 Other structures

The original model has two peaks, so new structure of the dielectric ring resonator is tested in this section.

Firstly, I changed the missing parameters in original design and the crucial physical parameters of the dielectric ring resonator to get a relatively perfect outcome. The simulation result of new structure will be compared with this final optimization result.

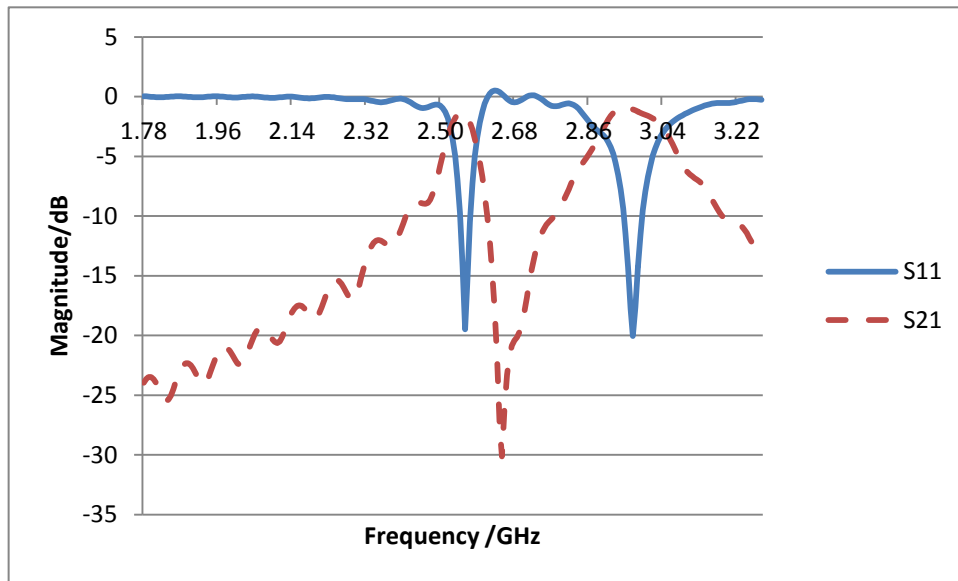


Fig. 4. 48 S11 and S21 magnitude against frequency.

The origin model possess two peaks, it is possible to make the first peak has more loss, so that it won't be a pass band, but that action will shift the pass band to 3GHz as is shown in Fig. 4.32. Fig. 4.48 represents the final optimized version whose height =10mm, inner radius= 6mm, outer radius=10mm, subt=2mm.

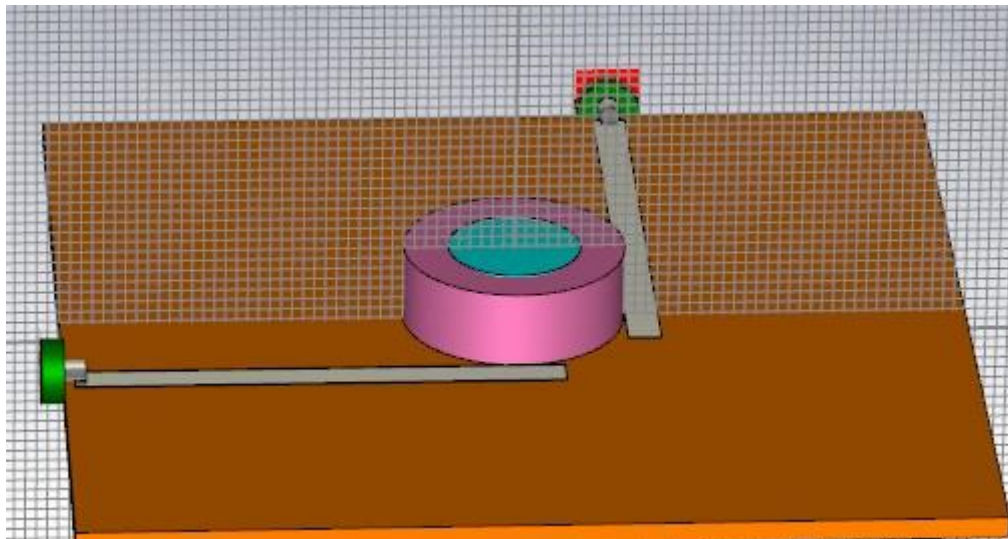


Fig. 4. 49 optimized model

To eliminate the close two peak a new structure is tested. As is shown in Fig. 4.49, I added a dielectric cylinder inside the dielectric ring, try to get more reflection.

The combination of the ϵ of dielectric ring and cylinder affects S-parameter and peak frequency and magnitude.

The epsilon of inner cylinder is fixed to $\epsilon=69$, then change the ϵ of the outer ring from 20-90. After many simulations, I found that when out ring has a ϵ range from 35 to 47, there is only one peak at around 2.6GHZ.

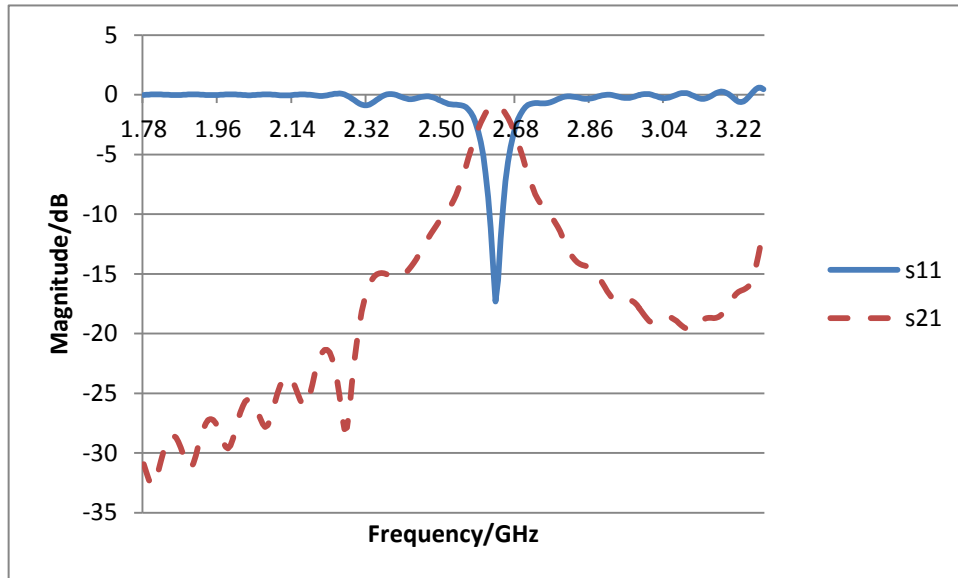


Fig. 4. 50 S-parameters of changed model

Fig. 4.50 shows an obvious peak. Although the outer ring only has an $\epsilon= 41$, it still has a peak frequency as 2.6Ghz. The same peak frequency as using one dielectric ring ($\epsilon=69$) loaded on substrate.

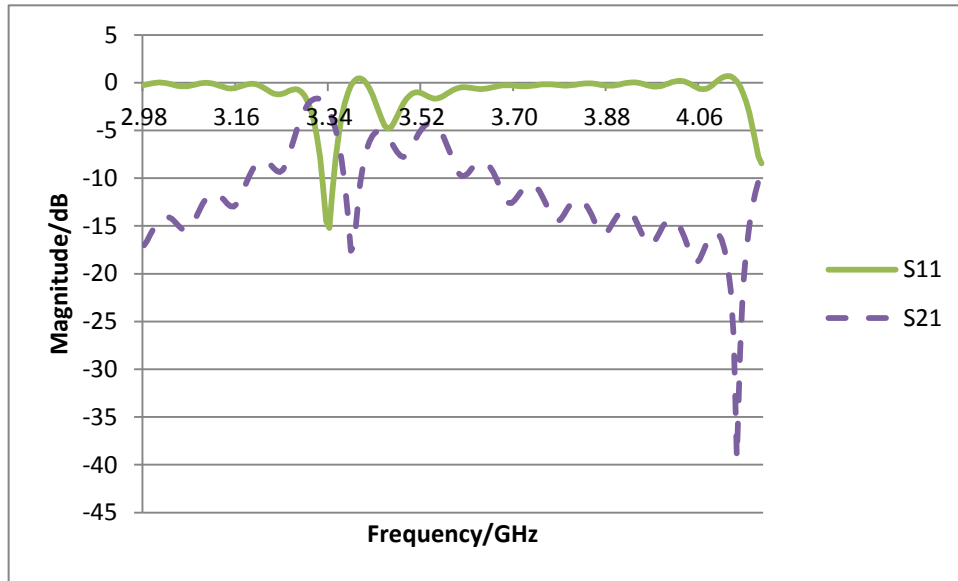


Fig. 4. 51 S-parameters for one ring loaded on substrate ($\epsilon=41$) without a dielectric cylinder inside the ring.

Fig. 4.51 is designed to prove that the inner dielectric cylinder optimized the S-parameters. The only difference between Fig. 4.51 and Fig. 4.50 is the inner cylinder is deleted. Fig. 4.51 shows that without the inner cylinder the peak is not obvious and ripples brings large noise to the pass band. So the inner cylinder can reduce ripples, expand the stop band and change the peak frequency.

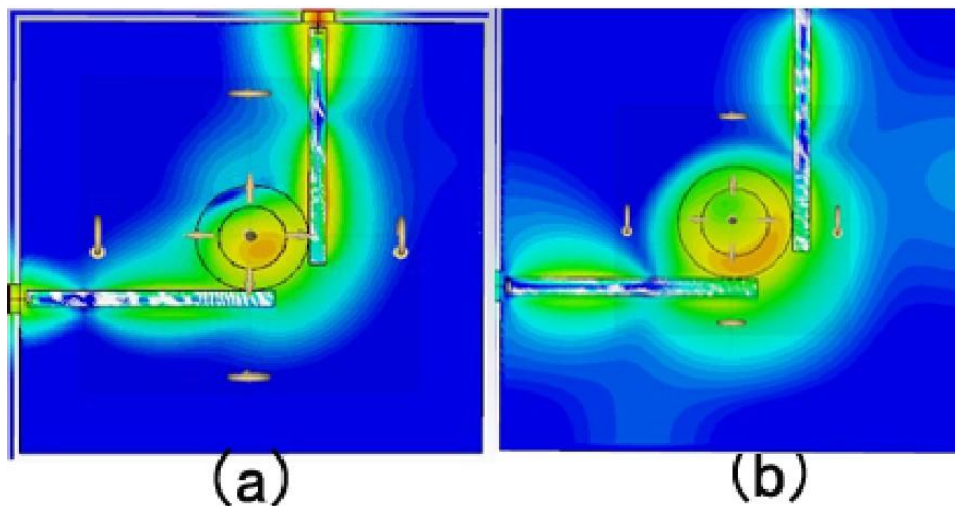


Fig. 4. 52 (a) the H-field of the changed model at $f=2.6\text{GHz}$ plotted in dB. (b) the H-field of the one ring model at its first peak $f=3.3\text{GHz}$.

Fig. 4.52(a) shows that with an extra dielectric cylinder in the center the h-field

becomes more concentrate, it use center cylinder to couple with microstrip lines rather, outer ring becomes a shell to reinforce the effect. Fig. 4.52(b) proves that inner cylinder can prevent h-field leakage.

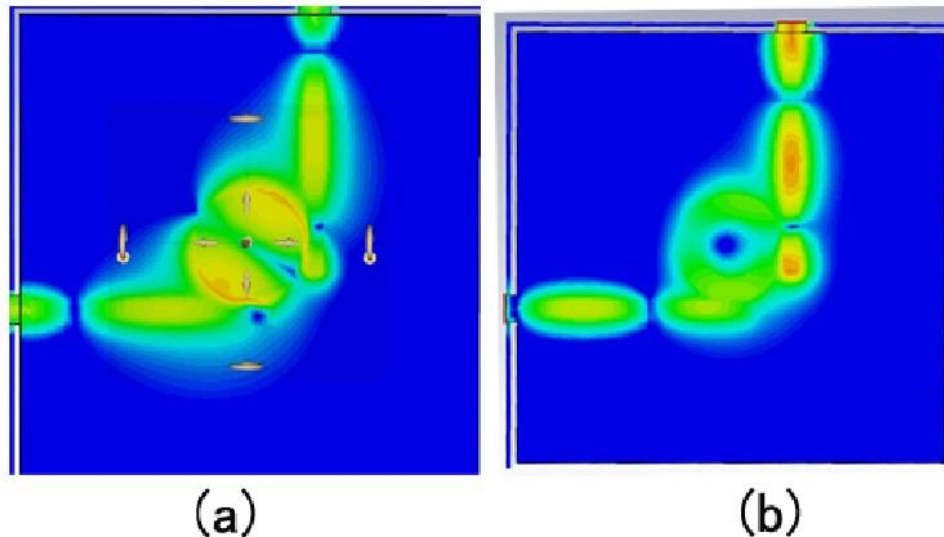


Fig. 4. 53 (a) the e-field of the changed model at $f=2.6\text{GHz}$ plotted in dB. (b) the e-field of the one ring model at its first peak $f=3.3\text{GHz}$.

Fig 4.53 (a) shows that the inner cylinder helps transfer energy while in Fig4.53 (b) part of the income energy stopped at the microstrip line.

In summary after adding a dielectric cylinder in the center, the characteristics of the filter becomes better.

Chapter 5 Dielectric Ring Resonators Loaded in waveguide

In this chapter several missing structure parameters, using same CST mesh parameters proved in chapter 4. The original data is very accurate. The optimization part focus on changing the model to become similar to the original data.

5.1 Mesh properties accuracy test

In previous tests, it proved that the parameter lines per wavelength change the results more than other parameters. Thus in this section mainly overviews lines per wave length.

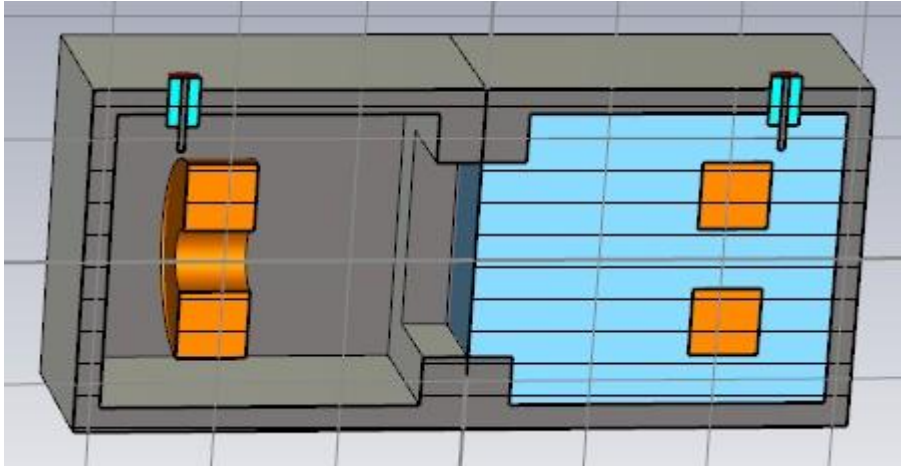


Fig. 5. 1 Section drawn for dielectric ring resonators loaded in waveguide.

I hid the foam in left side to show the dielectric ring, in simulation, the box is filled with foam. Since the original paper gave detail parameters, there is only one version of model. Lines per wavelength test is carried in 8GHz.

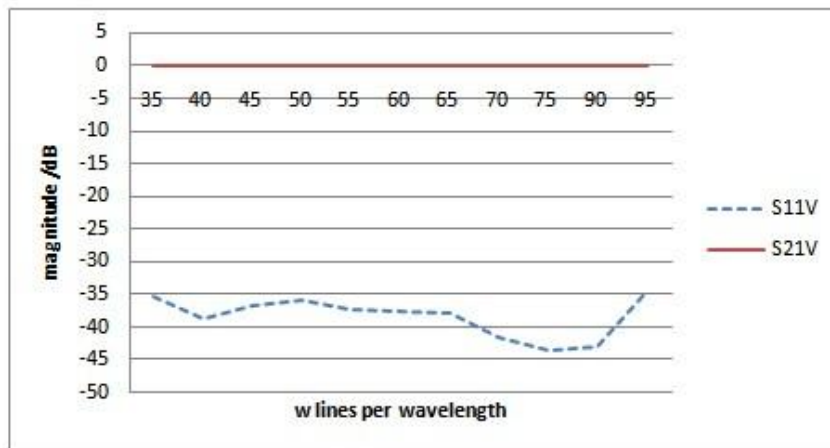


Fig. 5. 2 S11 and S21 peak magnitude for different lines per wavelength

Compared with one ring loaded on substrate, two ring system has a more stable

response. The magnitude of S21 becomes converged but the S11 does not. It proves that the Hexahedral FPBA is not suitable for tiny mesh structures or the mesh generation algorithm is not capable to handle extremely small mesh steps.

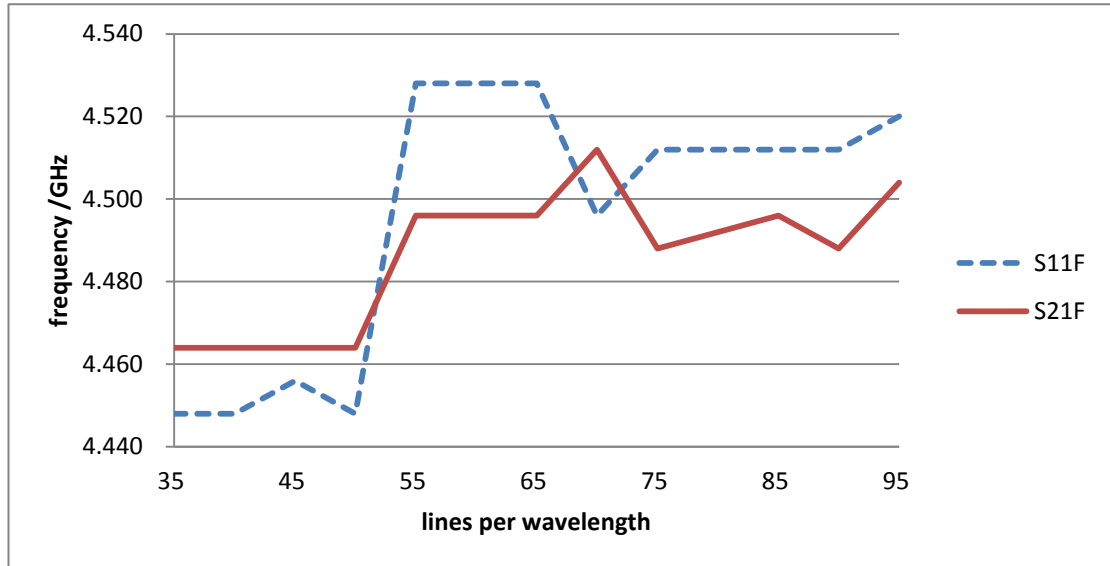


Fig. 5. 3 peak frequency for different lines per wavelength

Although Fig.5.3 shows the many changes of the peak frequency, but the absolute difference is quite small. It seems that at 55-60 and 75-90, there is a tendency that the frequencies for S11 and S21 reached stable platforms but as the mesh numbers become larger, the results have unexpected changes. When the CST parameters are set as 95-95-20, there are 30931264 mesh cells, 55-55-20 have 6471360 mesh cells, 30-30-20 have 1247688 mesh cells. That means 95-95-20 have 25 times mesh cells than 30-30-20, that density might introduce simulation error.

L	15	25	35	45
S11F	4.56	4.56	4.56	4.56
S11V	-20.1608	-20.4302	-19.9757	-19.6515
S21F	4.56	4.56	4.224	4.224
S21V	-0.82294	-0.83679	0.534886	0.518436

Table 5. 1 Lower mesh limit simulation result

When L is larger than W, the simulation result has an obvious change for other

data are almost the same. As can be seen from Table. 5.1 the peak frequency is around 4.5GHz while the original paper has 4GHz. Table 5.1 and Table 5.2's CST parameter as set as 15-15-L, 15-15-R.

R	15	25	35
S11F	4.56	4.56	4.56
S11V	-20.4302	-20.4302	-20.4302
S21F	4.56	4.56	4.216
S21V	-0.83679	-0.83679	0.5592

Table 5. 2 Mesh line ratio limit simulation result

Mesh line ratio limit has the same character as lower mesh limit. The results remain stable when they are lower than w , when they are larger, the S21F and S21V changed to a different one.

In summary W control the major properties, if L and R remain lower than W , there won't be any odd point.

5.2 physical parameters test

In this section several physical parameters will be changed.

Unit are set as in, Kelvin, GHz, ns

In previous tests, the missing parameters were set as the radius of the coaxial cable($r_{coax}=0.0625$), radius of metal port($r_{port}=0.013$) and position(x center = $-l_1-l_2-odring/2$), the length of metal portal($Y_{min}=c-0.15, Y_{max}=c+0.15$) and the length of the cable($Y_{min}=c-0.1, Y_{max}=c+0.15$).

5.2.1 Length of the cable

In this section the length of the metal port and the cable will be changed.

length	0.1	0.15	0.2
S11F	4.56	4.56	4.57599

S11V	-20.3937	-20.4302	-33.3723
S21F	4.56	4.56	4.568
S21V	-0.86817	-0.83679	-0.3608

Table 5. 3 Different port length simulation result

Table 5.3 shows that 0.1 and 0.15 do not have any difference while 0.2 is quite different. 0.2 means the port is almost touching the dielectric ring.

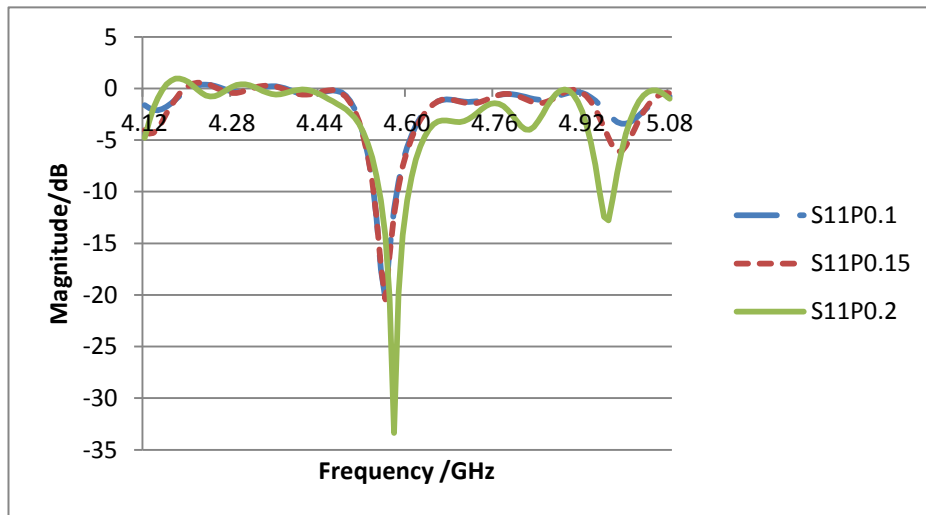


Fig. 5. 4 S11 magnitude of different port length

S11 shows that the longest port has lowest loss in pass band, 0.1in and 0.15in do not have too much difference.

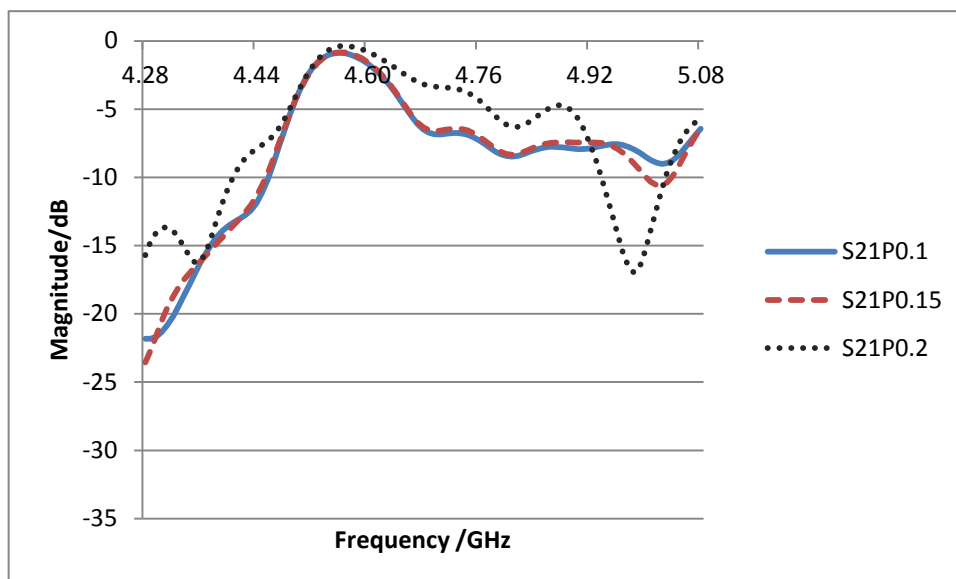


Fig. 5. 5 S21 magnitude of different port length

When the port is near the surface of the ring, S21 becomes flat, it is not good to

have a distinguished pass band. 0.15 or 0.1 has more loss than 0.2, but not too much. Thus, 0.15 is a proper choice.

cable	0.1	0.15	0.2
S11F	4.56	4.568	4.583999
S11V	-20.3937	-24.7488	-23.7743
S21F	4.56	4.569	4.6
S21V	-0.86817	-0.44062	-0.82313

Table 5. 4 S11 and S21 peak frequency and magnitude of different length of cable

Compared Table. 5.4 with Table. 5.3, the magnitude have not change too much, peak frequencies are almost same.

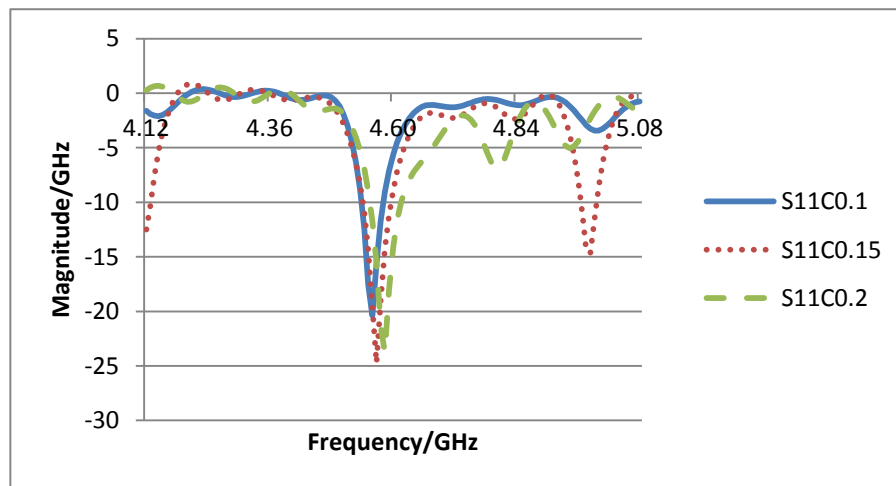


Fig. 5. 6 S11 magnitude of different cable length

The length of cable does not change result too much. 0.15 is better than others.

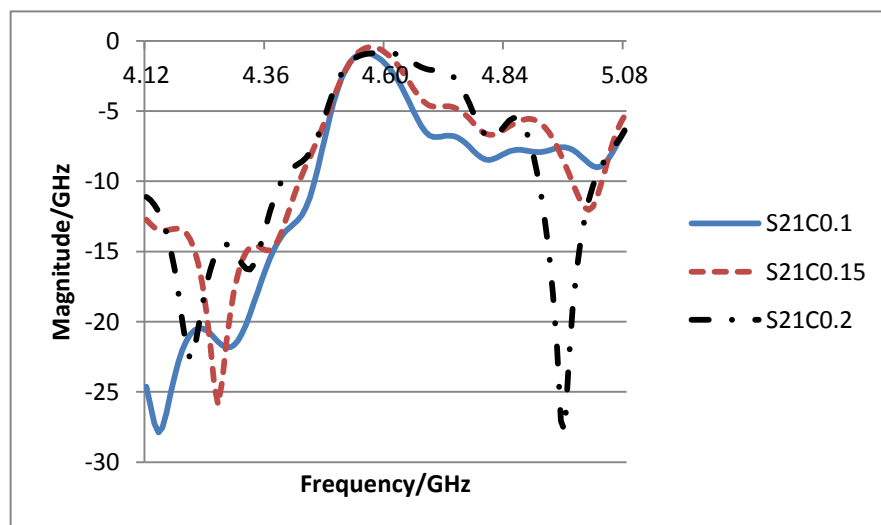


Fig. 5. 7 S21 magnitude of different cable length

Fig. 5.7 is similar to Fig. 5.5, 0.2 cable is too flat to have a stop band. In summary the length of cable will not change the simulation results too much. Thus if increase the cable and inner conduct simultaneously, 0.2in is the best option, if only increase the inner conductor as is shown is the original report 0.15in does not have too much difference compared with 0.2in result.

5.2.2 Position of the cable

In this section the position of the cable will be changed. Shift means the displacement of the cable.

When shift =0 , the center of cable is above the edge of the dielectric ring. S11 and S21's peak frequencies are overlapped at that point. Shift =0 has better magnitude than others too.

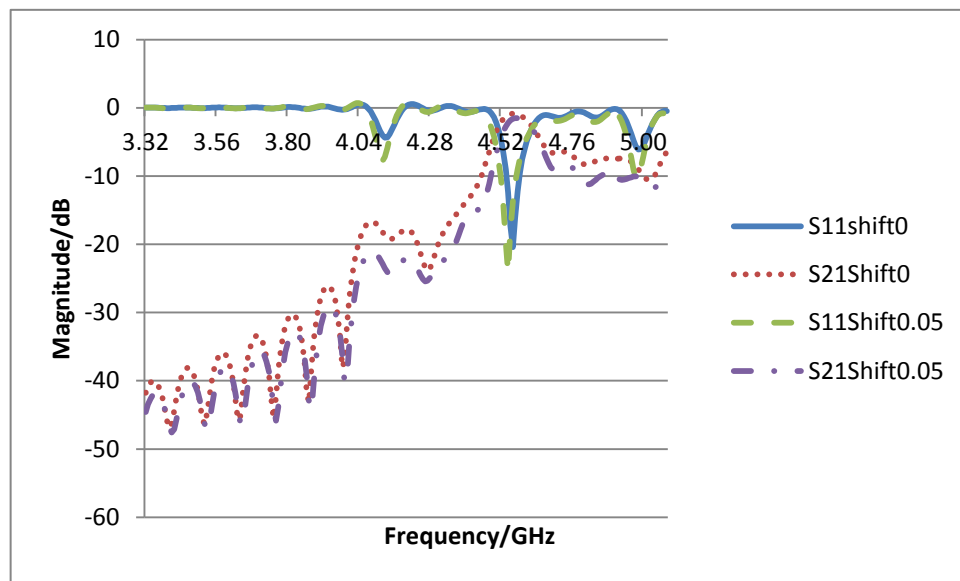


Fig. 5. 8 S11 and S21 magnitude

They are almost overlapped that means changes the position of the cable will not affect the simulation result too much. Left the cable over the edge of the dielectric ring is better than other two solutions.

5.3 Optimization

In this section the model will be changed to get a better result. Previous

resonator will also be compared. For the original paper [15] gave an accurate measured result, their data will be used as standard values to calibrate the result.

In the one ring loaded on substrate model, the ports are extended outside the metal box in version 3. In this section, the cable will be exactly the thickness of the metal box which is 1mm.

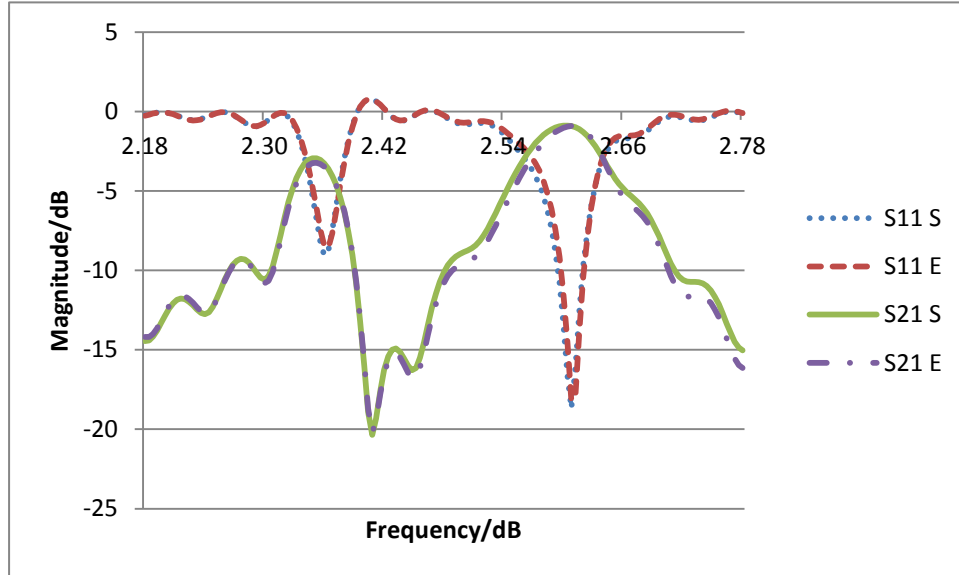


Fig. 5.9 S11 and S21 magnitude for different cable length.

Fig 5.9 shows the 4GHz test of one ring model version 3. S11 S means shortened cable, S11 E means version 3 model. The S11 and S21 magnitude are almost similar. Thus the length of coaxial cable will not change the simulation result significantly for this result. The peak magnitude difference is 0.6dB. When reduce the maximum frequency to 4GHz, the first ripple becomes a passband. The peak frequency of this new pass band is 2.36GHz.

In the two rings model, if the coaxial cable is as thick as the metal box, the 4GHz ripple becomes a passband too. In original paper, the two ring model supposed to have a pass band at 4GHz. In original design, the cable is extended outside the metal box as is shown in Fig. 1.9, so the simulation model has extended cables. The optimized model is shown in Fig. 5.10.

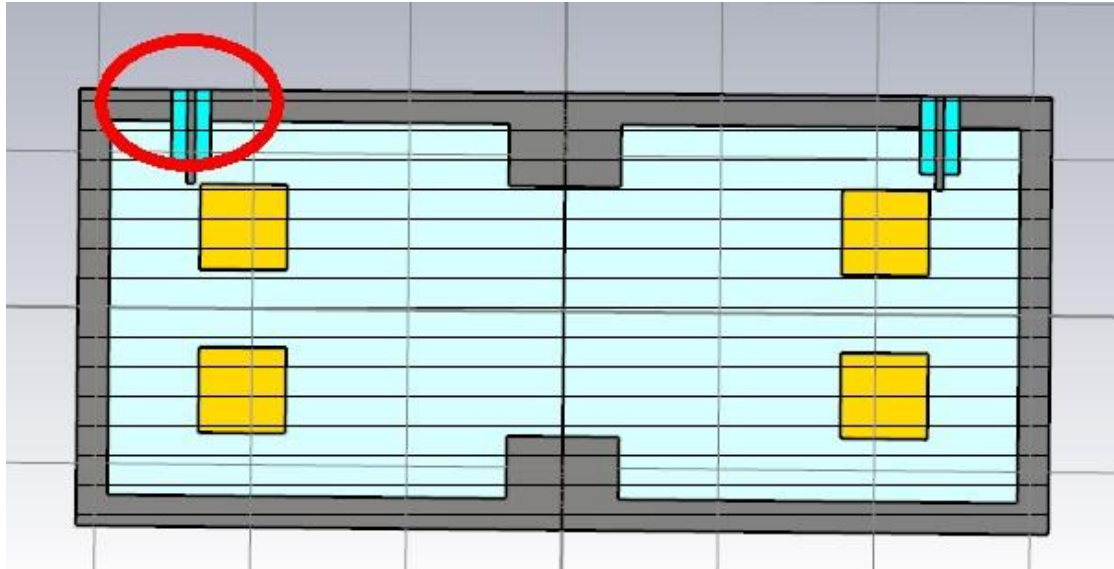


Fig. 5. 10 Cross-section draw of the optimized model.

The cable is as thick as the metal box as is highlighted in Fig. 5.10. Then the adaptive mesh refinement in the time domain solver settings is turned on. That option is tested in the one ring loaded on substrate too, but it took more than 3 days before I stopped the solver. The start CST parameters are set as 45-45-20, after 3 day's calculation the CST parameters changed to 95-95-20 when I stopped the solver. While in the two ring model, the start CST parameters is set as 25-25-10, when the simulation ended automatically the CST parameters increased to 35-35-10. So, all the tests run in this section have CST parameters set as 35-35-10

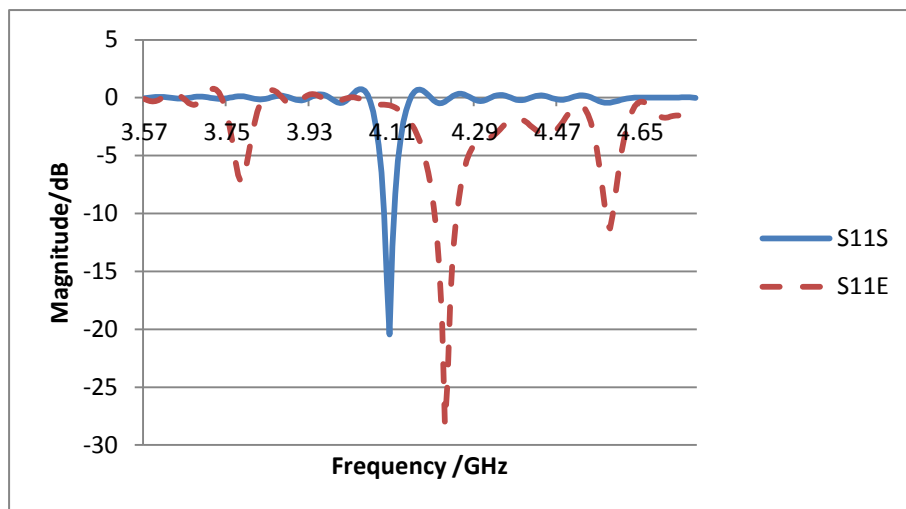


Fig. 5. 11 S11 magnitude for short length and normal length of the cable

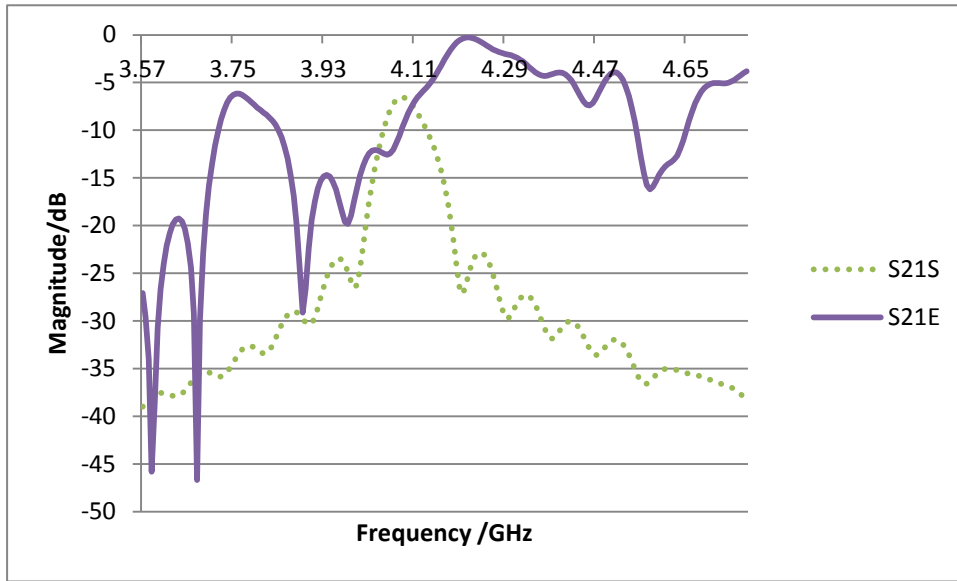


Fig. 5. 12 S11 magnitude for short length and normal length of the cable

Fig. 5.11 and Fig.5.12 proves that if the cable is extended outside the metal box the simulation result would be greatly changed. In both figures, the S suffix means shorter cable, E means extended.

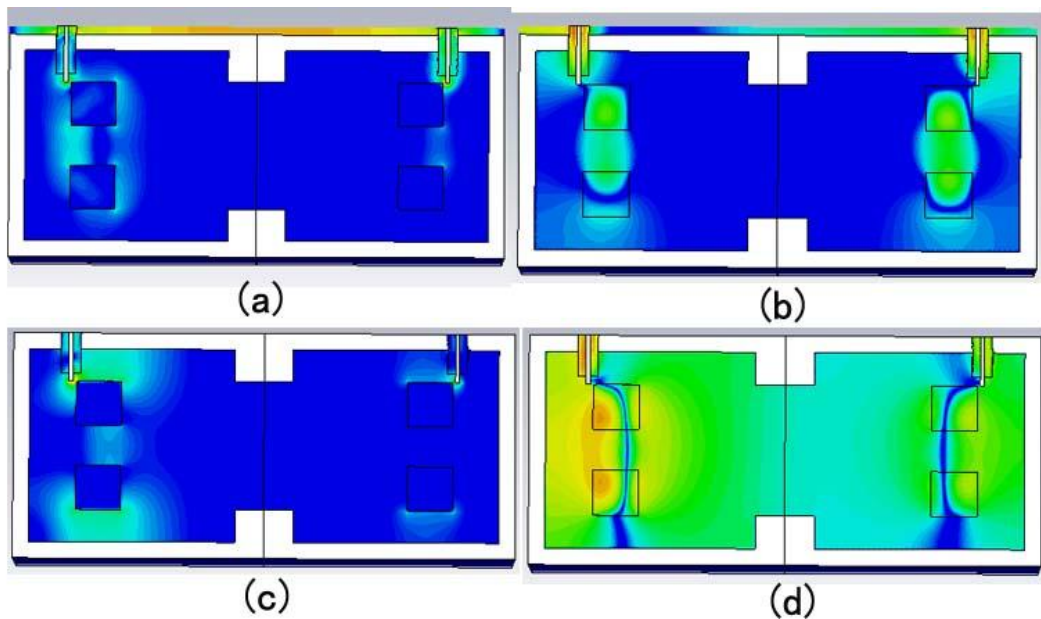


Fig. 5. 13 (a) e-field ($f=4.58\text{GHz}$) of extended model. (b) h-field ($f=4.58\text{GHz}$)of extended model. (c) e-field ($f=4.1\text{GHz}$)of shorter model (d) h-field ($f=4.1\text{GHz}$) of shorter model.

Fig. 5.13 explains the reason why extended model and shorter model have difference. The energy is transmitted through the air outside the metal box. In reality,

the cable has shielding part while in the simulation model the cable's structure is simplified. The shorter model has a peak frequency at around 4GHz (4.04GHz-4.15GHz). The peak frequency difference is caused by changing CST parameters. That is very close to the measured result.

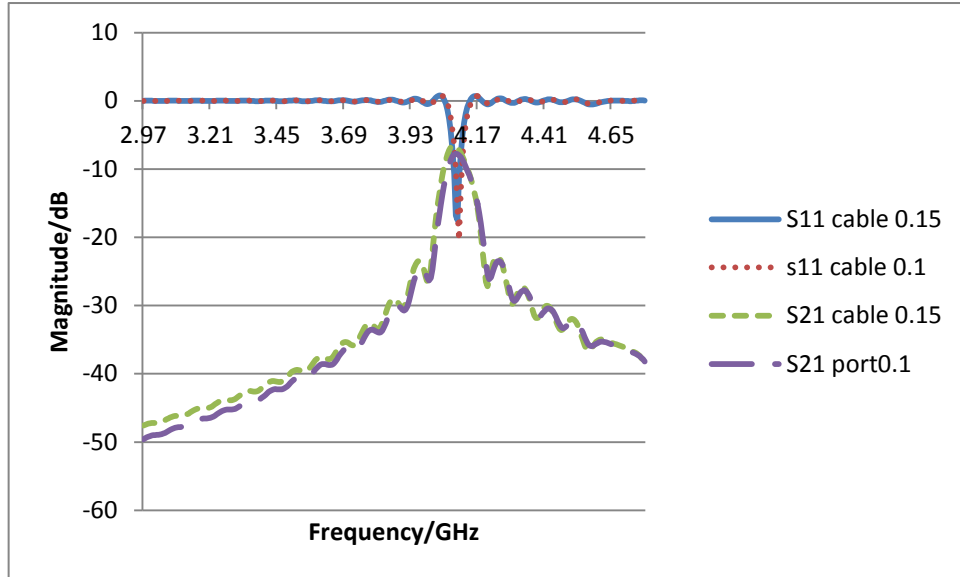


Fig. 5. 14 S11 and S21's magnitude of shorter model with different cable length

As is shown in Fig.5.14 the cable length of the shorter model does not affect result too much as is test in extended model in section 5.2.1. The curves are almost overlapped.

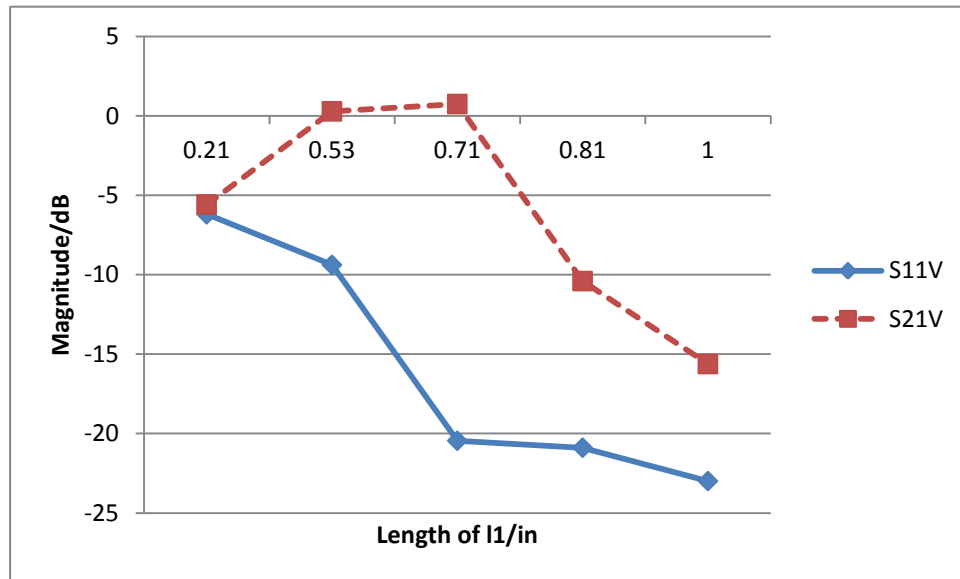


Fig. 5. 15 S11 and S21 magnitude of different length of l1.

Fig. 5.15 shows that when the length of $l_1=0.71$ the simulation result is similar to the measured result. That means shorter model is much accuracy and the CST parameters set as 35-35-10 is high enough for this model, this combination provides good speed and accuracy. When l_1 becomes smaller the S_{11} peak magnitude becomes higher and if l_1 's length increased the peak magnitude of S_{21} becomes lower. That means 0.71in is the best length for l_1 .

Chapter 6 Conclusions

In this chapter several possibilities which might cause errors will be discussed. As is introduced in previous chapters the simulation results are not as good as what they should be.

6.1 Errors caused by maximum frequency

When the maximum frequency is extremely high (more than first peak frequency plus 8GHz), there would be significant simulation error as is shown in Chapter 4.3. In this section, the second model dielectric rings loaded in waveguide is tested.

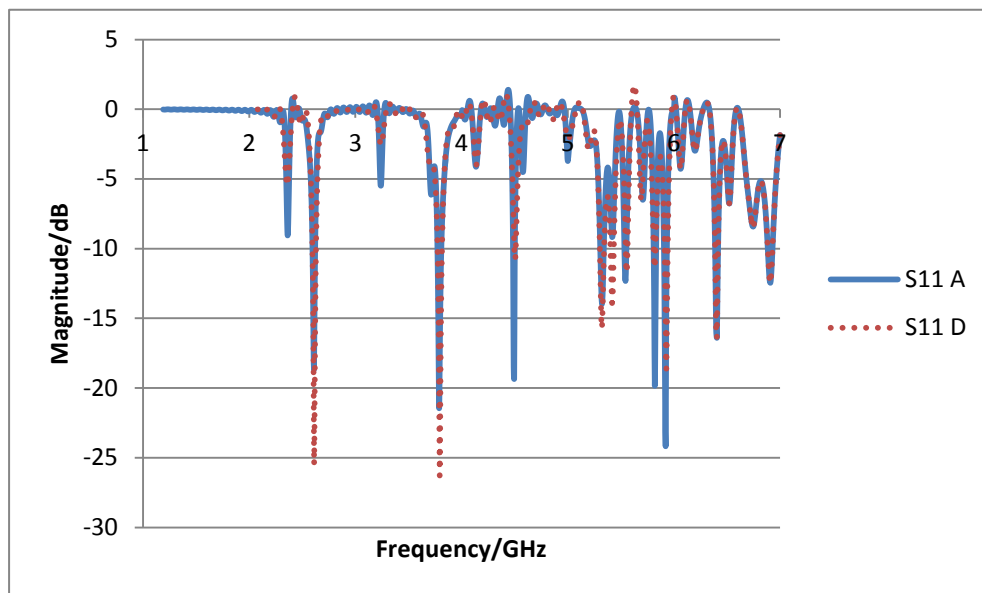


Fig. 6. 1 Accumulated S11 and direct S11 magnitude.

Accumulated S11 in Fig.6.1 means plotted by adding 5 different maximum frequency range tests results together. For 0-3GHz, use the simulation results from maximum frequency=3 test. Then added the 3GHz-4GHz part from 4GHz test result. Use the same way to expend the maximum frequency to 7GHz. Direct means set 7GHz as the maximum frequency then plot only that result. As can be seen from the figure, the accumulated result have different magnitude compared with direct one. But they have same peak frequencies.

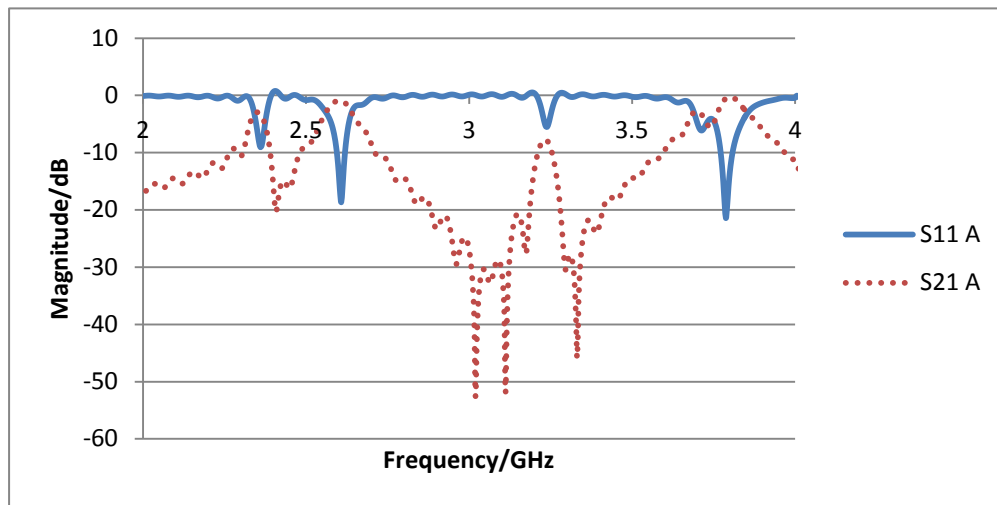


Fig. 6. 2 Accumulated S11 and S21 magnitude.

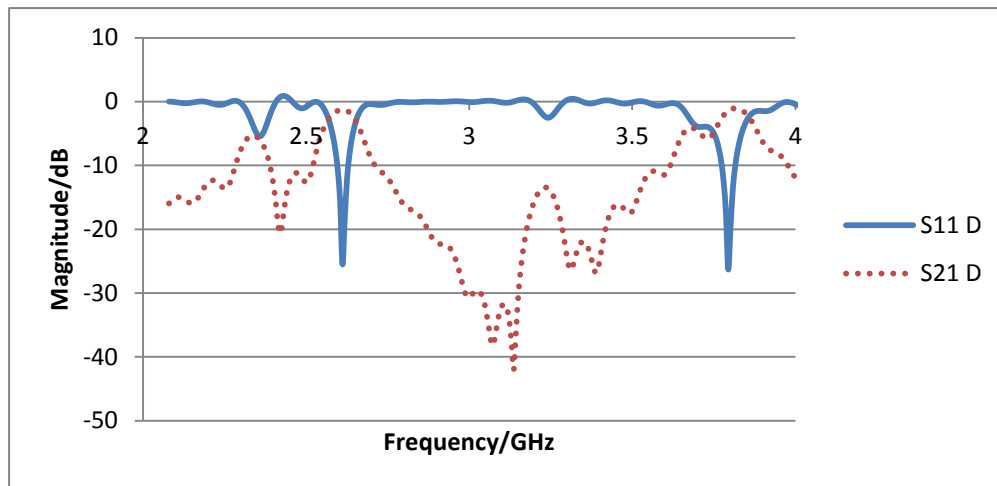


Fig. 6. 3 Direct S11 and S21 magnitude

In Fig. 6.2 there is a pass band at around 2.4GHz while in Fig. 6.3, the pass band disappeared. The peak magnitude is different too, in accumulated model the

magnitude is -18dB, while in direct test, the magnitude become -20dB. Thus high simulation frequency range will cause error in low frequency, but it is uncertain that whether the ripple in low frequency is truly exist or created by simulation algorithm.

If the low frequency ripple is measured in reality, CST software should use accumulated S-parameter. Else CST software should add a recommend lowest frequency range to avoid such errors.

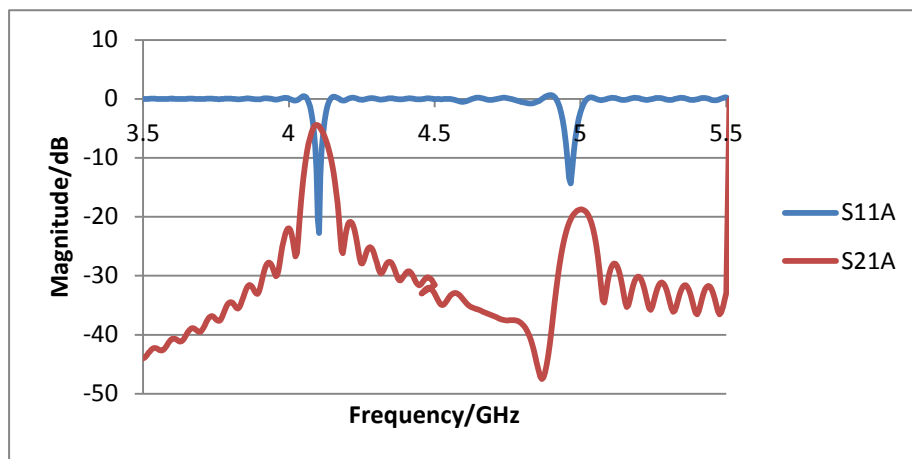


Fig. 6. 4 Accumulated result of two rings model

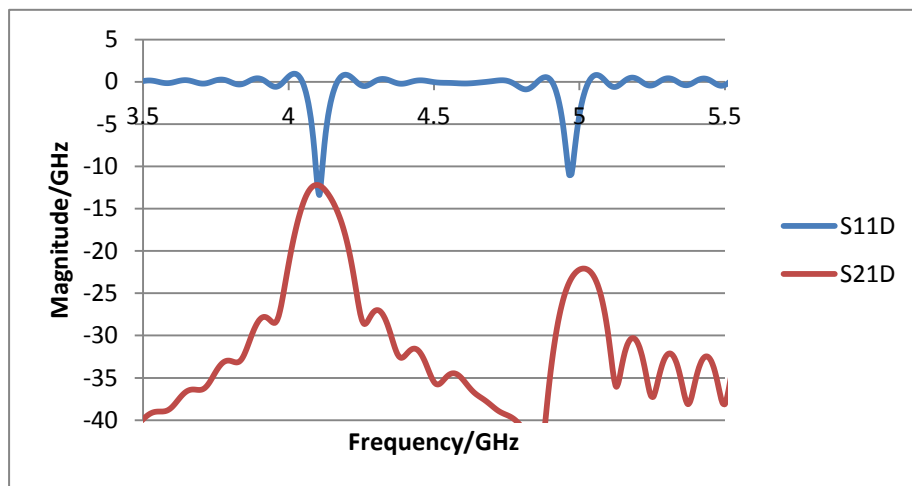


Fig. 6. 5 Direct result of two rings model

Fig. 6.4 and Fig. 6.5 proves that the accumulated result has different magnitude compared with direct high maximum frequency (8GHz) result. The measured result shows that the accumulated result is more accurate.

6.2 PBA and FPBA test.

In this section PBA and FPBA(enhanced accuracy) are tested. They are two main algorithm for the CST time domain solver. In official guide book, FPBA is recommended, but the default setting is using PBA when the mesh number is very large then automatically change to FPBA.

	15-15-10	20-20-10	30-30-20
FPBAS11F	2.64	2.616	2.646
PBAS11F	2.55	2.868	2.646
FPBAS11V	-21.3355	-19.6861	-10.7052
PBAS11V	-0.24721	-0.05106	-10.7052
FPBAS21F	2.616	2.616	2.652
PBAS21F	2.664	2.97	2.652
FPBAS21V	-1.83965	-1.46902	-3.47542
PBAS21V	-25.2153	-61.3876	-3.47542

Table 6. 1 Comparisons of FPBA and PBA

In Table. 6.1, FPBAS11F means the S11 peak frequency using FPBA algorithm. PBAS21V means the peak magnitude of S21 using PBA algorithm. Table. 6.1 shows that the PBA algorithm is not suitable for low mesh density. There is no pass band formed as is shown in Fig 6.3. When the CST parameters increased to 30-30-20 PBA draw same result as FPBA. The h-field patterns are also similar as is shown in Fig. 6.4. That means FPBA can totally replace PBA, so the official guidance should write instruction about their difference.

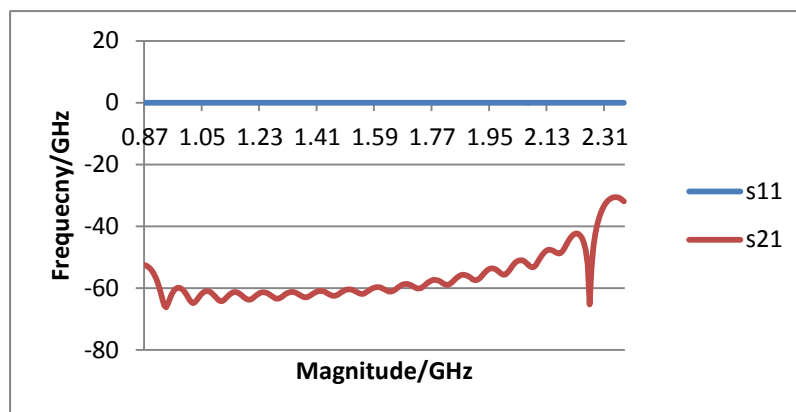


Fig. 6. 6 PBA S-parameters with CST parameters set as 15-15-10.

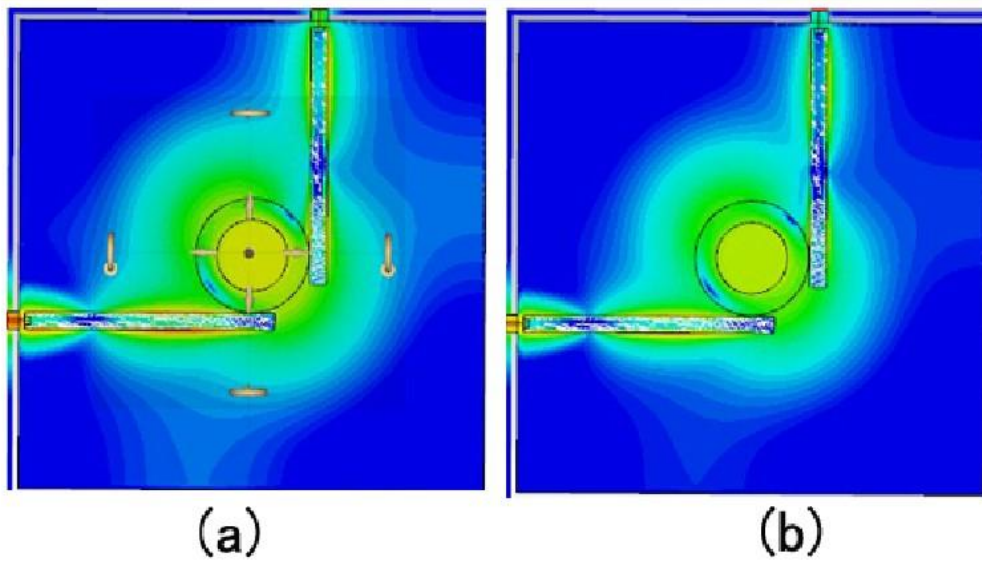


Fig. 6. 7 (a) h-filed $f=2.646\text{GHz}$ using FPBA (b) h-filed $f=2.646\text{GHz}$ using PBA

6.3 A guess for algorithm refinement

CST corporation had refined the CST software package for many years, the solver is much better than previous one. There still have problems: 1. when increasing the mesh density, the magnitude of both S_{11} and S_{12} become unstable. They are not converging to a constant state. 2. The peak frequency seems to have a flat curve, but it still have several gaps. 3. Different maximum frequency will significantly change the simulation result.

If the algorithm and the solver is well developed, all these problems should have been solved. CST software offers several solvers: time domain, frequency domain, eigenmode, integral equation, multilayer and asymptotic. According to official guide book, different solver is suitable for different tasks. That means different solver will draw different simulation results about S-parameters.

As is mentioned in Chapter 4.3.3, the mesh is generator might have problems too. But even under same mesh structure the simulation result can be different. That means the error could be also caused by the FPBA algorithm or the solver. Solver is designed on the theory, after many version's refinement, it should be capable to represent the theory. The theory is well developed and proved to be effective, the

solver is totally based on the theory and has been revised several times, there is possibility that high accuracy calculation requires new theory.

The solver shows that after a flat period, there would be a gap to another flat period. Confined by experimental condition, I don't have any measured data to calibrate the result. I think there should be a maximum value to confine the number of iterations. If an error is calculated too many times, it will lead to an overflow or amplified this error. All algorithm has small error, even using unstructured mesh, that will also introduce errors. The unstructured mesh might have a higher maximum iterations value than FPBA, but it will reach that point if increase the mesh accuracy into a certain level. Thus I think to solve this problem require step revise. That means to find out certain algorithm's error constant. After certain steps, the result will be revised by the error constant. To realize this, there must be calibrate points. Using low accuracy mesh to get certain point which possess similar values as measured one, then refine the mesh without changing those point. Measured data should used as standard when define those calibrate points.

Bibliography

[1] Michael Steer. Microwave and RF Design: A Systems Approach. SciTech Publishing, ISBN-10: 189112188X, ISBN-13: 978-1891121883 April 30, 2010.

[2] Cameron, Richard J. General coupling matrix synthesis methods for Chebyshev filtering functions. Microwave Theory and Techniques, IEEE Transactions on (Volume:47 , Issue: 4)433 - 442

[3] Moo, C.S. ; Dept. of Electr. Eng., Nat. Sun Yat-Sen Univ., Kaohsiung, Taiwan. Designing passive LC filters with contour maps. Power Electronics and Drive Systems, 1997. Proceedings., 1997 International Conference on (Volume:2)

[4] R.A. Kranenburg 1 ; S.A. Long. Microstrip transmission line excitation of dielectric resonator antennas. Electronics Letters, Volume

24, Issue 18, 1 September 1988, p. 1156–1157.

[5] Iulian Rosu. Microstrip, Stripline, and CPW Design. YO3DAC / VA3IUL <http://www.qsl.net/va3iul>

[6] Feng Xu and Ke Wu, Fellow, IEEE. Guided-Wave and Leakage Characteristics of Substrate Integrated Waveguide. IEEE TRANSACTIONS ON MICROWAVE THEORY AND TECHNIQUES, VOL. 53, NO. 1, JANUARY 2005

[7] S. B. Cohn. Microwave bandpass filters high-Q dielectric resonators. IEEE Trans, MTT, 1968, MTT-16(4), 218–227.

[8] James H. Harlow (2004). Electric power transformer engineering. CRC Press. pp. 2 – 216. ISBN 978-0-8493-1704-0.

[9] Michael H. Tooley (2006). Electronic circuits: fundamentals and applications. Newnes. pp. 77 – 78. ISBN 978-0-7506-6923-8.

[10] Pendry, J.B.; Holden, A.J.; Robbins, D.J.; Stewart, W.J. Magnetism from conductors and enhanced nonlinear phenomena. IEEE Trans. Microwave Theory Tech. 1999, 47, 2075–2084.

[11] Smith, D.R.; Padilla, W.J.; Vier, D.C.; Nemat-Nasser, S.C.; Schultz, S. Composite medium with simultaneously negative permeability and permittivity. Phys. Rev. Lett. 2000, 84, 4184–4187

[12] Attie P C, Lahanas A, Tsaoussidis V. Beyond AIMD: Explicit Fair-share Calculation [C]// Proceeding of IEEE ISCC 2003. New York, USA: IEEE CS, 2003, v2: 727–734

[13] Shah Nawaz Burokur, Mohamed Latrach, Serge Toutain. Study of the effect of dielectric split-ring resonators on microstrip-line transmission. Microwave and Optical Technology Letters Volume 44, Issue 5, pages 445 – 448, 5 March 2005

[14] Yohannan, J.; Dept. of Electron., Cochin Univ. of Sci. & Technol., Kochi, India; Vasudevan, K.; Mathew, K.T.; Abdulla, P. Dielectric ring resonator band pass filter for 2.4 GHz WLAN frequencies. Microwave Conference, 2009. APMC 2009. Asia Pacific 7–10 Dec. 2009, 1331 – 1333

[15] Chen, S.-W.; Comsat Syst. Div., Clarksburg, MD, USA; Zaki, K.A. Dielectric ring resonators loaded in waveguide and on

substrate. Microwave Theory and Techniques, IEEE Transactions on (Volume:39 , Issue: 12)Dec 1991. Pages 2069 - 2076.

[16] Peter Schwartz , Michael Barad , Phillip Colella , Terry Ligocki. A Cartesian grid embedded boundary method for the heat equation and Poissons equation in three dimensions, Journal of Computational Physics 211 (2006) 531 - 550.

[17] Hans Johansen and Phillip Colella. A Cartesian Grid Embedded Boundary Method for Poisson' s Equation on Irregular Domains. JOURNAL OF COMPUTATIONAL PHYSICS 147, 60 - 85 (1998)

[18] K. S. Yee. Numerical solution of initial boundary value problems involving Maxwell' s equations in isotropic media. IEEE Trans. Antennas Propagat. Page(s): 302-307, 1966, Volume: AP-14

[19] R. Holland . "Threde: A free-field EMP coupling and scattering code". IEEE Transactions on Nuclear Science 24 (6): 2416 - 2421. (1977)

[20] K. S. Kunz and K. M. Lee . "A three-dimensional finite-difference solution of the external response of an aircraft to a complex transient EM environment". IEEE Transactions on Electromagnetic Compatibility 20 (2): 333 - 341. (1978)

[21] K. R. Umashankar and A. Taflove . "A novel method to analyze electromagnetic scattering of complex objects". IEEE Transactions on Electromagnetic Compatibility 24 (4): 397 - 405. (1982)

[22] Taflove and K. R. Umashankar . "Radar cross section of general three-dimensional scatterers". IEEE Transactions on Electromagnetic Compatibility 25 (4): 433 - 440 (1983)

[23] X. Zhang, J. Fang, K. K. Mei, and Y. Liu . "Calculation of the dispersive characteristics of microstrips by the time-domain finite-difference method". IEEE Transactions on Microwave Theory and Techniques 36 (2): 263 - 267. (1988)

[24] T. Kashiwa and I. Fukai . "A treatment by FDTD method of dispersive characteristics associated with electronic polarization". Microwave and Optical Technology Letters 3 (6): 203 - 205. (1990)

[25] Aidan Chatwin-Davies. Meshing Lakes with Unstructured Cartesian Grids. 2B Mathematical Physics. April 2009.

[26] D.M. Ingram, , D.M. Causon, C.G. Mingham. Developments in Cartesian cut cell methods. Mathematics and Computers in Simulation. Volume 61, Issues 3 - 6, 30 January 2003, Pages 561 - 572.

[27] Charles S. Peskin. The immersed boundary method. Acta Numerica (2002), pp. 479-517

[28] Hans Johansen and Phillip Colella. A Cartesian Grid Embedded Boundary Method for Poisson' s Equation on Irregular Domains. Journal of Computational Physics Volume 147, Issue 1, 20 November 1998, Pages 60 - 85

[29] Kunihiko Taira , Tim Colonius. The immersed boundary method: A projection approach. Journal of Computational Physics 225. (2007) 2118 - 2137.

[30] Gary L. Miller, Dafna Talmor, Shang-Hua, Teng Noel. A Delaunay based numerical method for three dimensions: generation, formulation, and partition. Proceeding STOC '95 Proceedings of the twenty-seventh annual ACM symposium on Theory of computing. (1995) Pages 683-692.

[31] Paul Louis George and Eric Seveno. The advancing-front Mesh Generation method revisited. Internatioanl journal for numetical methods in engineering. Vol 37 (1994), pages: 3605-3619.

[32] F. Anihal Fernandea', Liikasz Kulast. A Simple Finite Difference Approach Using Unstructured Meshes from FEM mesh generators. Microwaves, Radar and Wireless Communications, 2004. MIKON-2004. 15th International Conference on (Volume:2) (2004) Pages: 585-588.

[33] AWR corporation, product introduction [J/OL] property on line, <http://www.awrcorp.com/products/microwave-office> (2013-8-29)

[34] AWR corporation, RF& MICROWAVE DESIGN SOFTWARE FOR MMIC PCB AND MODULES [J/OL] property on line, <http://www.awrcorp.com/products/microwave-office> (2013-8-29)

[35] WIPL-D d. o. o. corporation, product introduction [J/OL] property on line, <http://www.wipl-d.com/products.php?cont=wipl-d-microwave#>

features_by_version (2013-8-29)

[36] ANSYS corporation, product introduction [J/OL] property on line,
<http://www.ansys.com/Products> (2013-8-29)

[37] CST corporation, product introduction [J/OL] property on line,
<http://www.cst.com/Content/Products/Products.aspx> (2013-8-29)

[38] CST corporation, MWS solver introduction [J/OL] property on line,
<http://www.cst.com/Content/Products/MWS/Solvers.aspx> (2013-8-29)

[39] B. Krietenstein, R. Schuhmann, P. Thoma, T. Weiland. THE PERFECT BOUNDARY APPROXIMATION TECHNIQUE FACING THE BIG CHALLENGE OF HIGH PRECISION FIELD COMPUTATION. 19th International Linear Accelerator Conference, Chicago, IL, USA, 23 - 28 Aug 1998, pp. 860